Cellular Toxicity of C_{60} Fullerenes in RAW 264.7 Immortalized Macrophages

by

Kristen Ann Russ

A dissertation submitted in partial fulfillment
of the requirements for the degree of
Doctor of Philosophy
(Toxicology)
In The University of Michigan
2013

Doctoral Committee:

Professor Martin A. Philbert, Co-Chair
Professor Andrew David Maynard, Co-Chair
Professor Craig Harris
Associate Professor Peter Mancuso
Professor Sem H. Phan

Acknowledgments

There are many people without whom this research would not have been completed. First, I must thank my mentor Dr. Martin Philbert who has provided me with much guidance and occasionally a healthy dose of anguish whenever he uttered the words “Go to the board.” Thank you to Dr. Andrew Maynard for taking on the additional responsibility of being committee co-chair and making his considerable knowledge of nanomaterials available to me. Thanks to my committee members Dr. Craig Harris, Dr. Sem Phan, and Dr. Peter Mancuso for the constructive criticisms they have all provided over the course of my research. A big thank you to all of the undergraduate students who worked on this research: Ariel Dews, Brandon Schneider, Myah Ray, Tessa Adzemovic, and Cameron Sawyer. I hope the time they spent in the lab syringe filtering C_{60}s and splitting cells helped to instill a lifelong love of science. I especially owe many thanks and much gratitude to Jennifer Fernandez, whose sense of humor and willingness to help with any task kept me *somewhat* sane during my time in the Philbert Lab. Most importantly, I could not have completed this research without the love and support of my parents who talked me out of moving to a beach somewhere and starting a snorkel tour business countless times during my time as a doctoral student.

This research was funded in part by the NIEHS Training Grant T32-ES007062-26.

Table of Contents

List of Figures

List of Abbreviations

BrdU	5-bromo-2'-deoxyuridine
CL	Cardiolipin
C_{60}	C_{60} Fullerene
DAPI	4',6-diamidino-2-phenylindole
DLS	Dynamic Light Scattering
GPL	Glycerophospholipid
GSH	Glutathione
GSSG	Glutathion Disulfide
LDH	Lactate Dehydrogenase
LPS	Lipopolysaccharide
MTT	(4,5-Dimethylthiazol-2-yl)-2,5-diphenyltetrazolium bromide
MWCNT	Multiwalled Carbon Nanotube
PC	Phophatidylcholine
PE	Phosphatidylethanolamine
PEG	Polyethylene glycol
PG	Phosphatidylglycerol
PI	Phosphatidylinositol
PS	Phosphatidylserine
ROS	Reactive oxygen Species
SWCNT	Singlewalled Carbon Nanotube
TbC_{60}	Terbium Endohedral C_{60} Fullerene
TEM	Transmission Electron Microscopy
THF	Tetrahydrofuran

Abstract

Cellular Toxicity of C_{60} Fullerenes in RAW 264.7 Immortalized Macrophages

C_{60} fullerenes are nanoparticles (~1nm dia.) composed of 60 carbons in a spherical graphene structure. They are hydrophobic, aggregate in aqueous solution and have been associated with cellular toxicity in multiple cell types. The central hypothesis of this thesis is that exposure of peripheral immune cells to C_{60} fullerenes will result in their uptake into the cytosol, membrane-bound intracellular compartments *and* cell membrane(s) resulting in cellular stress and subsequent activation of apoptosis.

Electron-dense terbium endohedral fullerenes were an excellent model for visualizing C_{60} in cells. Transmission electron microscopy on RAW 264.7 immortalized murine macrophages showed that C_{60} was found in endosomes, embedded within lipid membranes and free in the cytosol and nucleoplasm. Endocytosis was found to be mediated by both caveolin and clathrin.

Cell death assays determined that at 24 hours there was no statistically significant occurrence of early or late apoptosis or necrosis. Cells exhibited subtle alterations in cytokine and chemokine gene expression profiles. Examination of the glutathione synthesis pathway showed changes consistent with a mild form of oxidative stress. Cellular proliferation decreased upon exposure to 1 and 4 μg/mL fullerenes and metabolic studies showed alterations in nucleotide catabolism and lipid metabolism.

These studies show that exposure of immune cells to C_{60} fullerenes results in uptake of the nanoparticles and alterations in the normal functions of the cell. The changes in the synthesis of glutathione, nucleotide catabolism, and lipid synthesis do not result in increased cell death at 24 hours; however, alterations to cellular proliferation and mildly altered inflammatory signals suggest that the cell is in the process of trying to resolve damage inflicted by fullerenes. Moreover, at 24 hours, the cells do not show clear signs of mechanisms leading to survival, proliferation or death.

Chapter I

Introduction

Nanotechnology is thought to have started with a talk entitled, “There’s Plenty of Room at the Bottom,” given by the American physicist, Richard Feynman at the 1959 meeting of the American Physical Society at CalTech. This talk was given prior to the use of the commonly used term “*nanotechnology*” or “*nanomaterials*” [1]. Engineered nanomaterials are typically defined as materials with one or more dimensions between 1 and 100 nanometers [2]. The International Organization for Standardization defines nanomaterials as a “material with any external dimension in the nanoscale or having internal structure or surface structure in the nanoscale” [3]. The incorporation of engineered nanomaterials in consumer products has drastically increased over the past decade. It has been projected that by 2015 there will be over 3 trillion dollar’s worth of products containing nanomaterials in the consumer market [4]. For example, titanium dioxide nanoparticles and zinc oxide nanoparticles are used in sunscreens. Nanosilver is incorporated into a number of consumer products, textiles and materials for its antibacterial properties. Silica nanoparticles may be found in oil absorbant cosmetics. Titanium dioxide, magnesium oxide, silicon dioxide, and aluminum oxide are incorporated into textiles to produce self-sterilizing materials and water repellent textiles [5]. Exposure assessments adequate for the development of classical risk assessments have not yet been completed for most nanomaterials [6]. Nevertheless, the USFDA and USEPA consider materials on a “*case by*

case" basis when determining their suitability for use as drugs or for release in the environment respectively [39].

The emergent physical characteristics of nanomaterials make them desirable for a wide (and growing) variety of industrial purposes. Important physical properties are size, shape, surface area, and surface modifications when exposed to biological conditions (protein coronas), charge, aggregation, and stability [7]. However, due to increased surface area of nanomaterials compared to the bulk material, the role of each of these characteristics in isolation or in concert is uncertain with respect to human exposures and environmental health.

It is generally held that the size of the nanomaterial dictates the manner and mechanism of cellular uptake. Small nanomaterials (less than 10 nm) with hydrophobic properties are able to diffuse into the membrane [7]. Nanomaterials larger than 10 nm are likely to either form holes in the membrane or enter via endocytosis [7]. Shape confounds the issue of size. It has also been shown that aspect ratio, the ratio between width and length, can be a determining factor for the rate of cellular uptake [8]. In nanomaterials greater than 100 nm, rod shaped particles tend to be taken up by cells at a faster rate whereas in nanoparticles smaller than 100 nm spheres tend to have a faster uptake rate [9]. Highly hydrophobic nanomaterials are more likely to aggregate in aqueous solution, which results in larger agglomerates and alternate interactions with the cell.

Surface area is another significant factor in the design and use of nanomaterials in industrial applications. The large surface area to size ratio (compared to the bulk material) allows for more interactions between the surface of the nanomaterial and the external

environment, e.g., the biology, solvent, environment, etc. [10]. It is well documented that biological macromolecules tend to form a corona on the surface of nanomaterials. The chemical and physical composition and nature of the corona similarly affects entry methods. For example, a protein corona can form on nanomaterials when the nanomaterial encounters serum proteins. The proteins surround the particles and in turn mask the native charge of the material, which allows (or may prevent) entry into biological systems. This can increase or decrease the half -life of the nanomaterial remains in a biological system [8]. Neutral or negatively charged nanomaterials have increased rates of uptake [8]. Also, negatively charged nanoparticles cause increased gelation of the membrane whereas positively charged particles cause increased fluidity of biological membranes [11]. This alteration of the lipid membrane will result in altered interaction with nanomaterials [8].

A common mechanism of toxicity seen in cells exposed to nanomaterials of many different physical properties is toxicity via oxidative stress [12]. There are multiple definitions of oxidative stress. Helmut Seis first defined oxidative stress as " a disturbance in the pro-oxidant-antioxidant balance in favor of the former" [40]. Dean Jones later redefined oxidative stress as " a disruption of redox signaling and control" [40]. These prior definitions were predicated on exposure to chemicals (of which undoubtedly molecular C_{60} is one – but not aggregates thereof) that could engender shifts in redox capacity. With the more recent understanding that engineered and ambient nanomaterials gain access to cellular compartments other than by diffusion, Li et al. (2008) proposed an oxidative stress paradigm to compare toxicity of nanomaterials [13]. This paradigm suggests at low levels oxidative stress can be resolved utilizing antioxidants and other mechanisms available within the cell; however, high levels of

oxidative stress results in inflammation and cell death (Figure 1.1) [13]. Oxidative stress is a known cellular stressor much like DNA damage. DNA damage and oxidative stress have been observed in cells exposed to nanomaterials such as multiwalled carbon nanotubes and singlewalled nanotubes [14].

C_{60} fullerene, also known as a buckminsterfullerene or "buckyball", has been researched for over 2 decades [15]. C_{60} fullerenes are 60 carbon spheres with a carbon atom located on each vertex and highly stable icosahedron geometry (Figure 1.1) [10, 16]. Individual C_{60} fullerene molecules have a molecular weight of 720.66 g/mol, a diameter of approximately 1 nm, and contain 30 double bonds, which lend themselves to radical scavenging [10]. C_{60} fullerenes have a structure similar to graphite but the pentagonal and hexagonal rings give it a 3 dimensional structure [16, 17]. C_{60} molecules aggregate in water due to their lack of solubility in polar solvents ($< 10^{-9}$ mg/L) [6, 18].

C_{60} fullerenes are naturally produced by combustion in events such as forest fires and volcanic eruptions [19]. Coal fired power plants are also a source of fullerene exposure [10]. Spectroscopic studies have been able to detect a mixture of C_{60} and C_{70} in the soot from hydrocarbon combustion [20]. Due to their unique properties, C_{60}s are being considered for many applications: nanoscale powders and particles for finishing applications, lubricants, polymer modifications, antiwear applications, high density magnetic storage media, thin film organic field-effect transistors, fuel cells, superconductors, photovoltaic cells, batteries, MRI and X-ray radiotracers, cosmetics, skin creams, and drug delivery devices [10, 21]. C_{60}s are currently incorporated in sporting goods such as tennis racquets because they increase stability and decrease weight [10]. They are incorporated in skin creams and cosmetics for their intrinsic

ability to scavenge free radicals [10]. C_{60}s have high electron affinity and easily transport charge, which makes them good candidates for incorporation in solar cells and other similar technologies [21].

Medical applications for C_{60} fullerenes are centered on their "nano" size (<100 nm) and their ability to be functionalized. Functionalization of fullerenes involves the addition of a chemical group to the outside of the fullerene's cage. This is done for many reasons including the ability to improve the solubility of fullerenes in polar solutions or to add a pharmaceutical to a fullerene in order to improve the efficacy of the drug. The addition of 18 carboxylic groups to the outside of the fullerene structure increases its solubility in water to 34 mg/mL [18]. The addition of polyethylene glycol (PEG) to the outer cage of a fullerene or to the end of the drug attached to the fullerene is a commonly used method to increase the solubility of the compound in aqueous solution as well as decrease the rate of opsonization [7, 22]. For example, the chemotherapeutic drug doxorubicin when coupled to a C_{60} fullerene and a PEG group has increased solubility in water as compared to the drug itself [22]. The attachment of a pharmaceutical to the outside of C_{60} fullerenes has been shown to alter the time in which the drug is able to stay in the body. For example, the drug paclitaxel is an effective anti-cancer drug; however, when administered via liposome aerosol it is rapidly cleared from the lungs reducing the drug's efficacy [23]. Covalently bonding paclitaxel to a C_{60} fullerene via a spacer increases the IC_{50} of the drug 1.6 times in comparison to the drug alone [22]. Incorporation of metals to the inside of the C_{60} cage has resulted in contrast agents that can be utilized for scans such as MRI [22].

Due to their low solubility, the biodistribution of pristine fullerenes is an area of fullerene research that lacks enough data to yield a complete view of the distribution of fullerenes once in a biological system. The available data on pristine fullerene distribution is a result of *in vivo* experiments that utilize multiple exposure methods: tail vein injections, injection into jugular cannulas, inhalation, or intratracheal instillation. Experiments utilizing tail vein injection of pristine C_{60} fullerenes in liposomes once a day for 28 days found C_{60} fullerenes in the lungs, spleen, liver, and kidneys of rats on each day of dissection [24]. Brains dissected on days 1 and 7 were found to contain C_{60}; however later dissections did not [24]. Experiments in which rats were injected with $^{14}C_{60}$ via jugular cannulas found that after 1 minute only 1% of the $^{14}C_{60}$ was left in the blood. At 120 minutes after the injection, 90% of $^{14}C_{60}$ were found in the liver and 7% distributed in the spleen, lung and muscle. At 24 hours, there was also $^{14}C_{60}$ in the urine and feces. Five days after a single injection, 95% of the $^{14}C_{60}$ were found in the liver [25].

Intratracheal instillation of C_{60} fullerenes resulted in particles less than 0.2% of the instillation dose in the liver and less than 0.02% of the instillation dose in the brain [26]. After inhalation of C_{60} fullerenes, only the lung contained the particles [26]. The data, while not complete, shows trends between different routes of administration. Routes of administration that directly inject fullerenes into blood result in a fast removal of the particles from the blood along with distribution to more tissues. Intratrachael instillation and inhalation routes of administration show the lungs as the primary target organ with very few other organs receiving any significant amount of fullerenes.

While there appears to be a trend in biodistribution based on these few studies there are limitations. First, the method by which the C_{60} fullerenes were dissolved and the vehicle in

which the fullerenes were administered differ from paper to paper. Second, lack of characterization of the nanomaterials aggregation within the dose to be delivered renders the data difficult to compare among studies. The method used to dissolve the particles, the vehicle in which the particles were administered to the animals, and the aggregation of the particles in the vehicle will all affect the biodistribution of the particles.

In terms of pristine C_{60} fullerene toxicity, localization in the cell, induction of apoptosis/necrosis, changes in gene expression for inflammatory processes, cell proliferation and senescence are of interest. Localization studies of C_{60} fullerene aggregates conducted in human monocyte macrophages found fullerene aggregates in the nucleus, lysosomes, along the plasma membrane, and free in the cytoplasm. The author states the caveat that it was difficult to determine fullerene aggregates against the dark background of the cell. The C_{60}s in this study were dissolved and delivered to the cell in THF, an organic solvent known to be toxic to cells [27].

Cell viability assessments after exposure to multiple concentrations of C_{60} exhibited no change in cell viability in aveolar macrophages (6 hours, MTT assay) , human dermal fibroblasts (6 hours, crystal violet), human liver carcinoma cells (48 hours, MTT assay), and human monocyte macrophages (48 hours, nuclear red) indicating that C_{60} fullerenes are not cytotoxic. However, there was an increase in LDH release in HDF, HEPG2 and mouse fibrosarcoma cells indicating membrane leakage indicative of cytotoxicity [27, 28, 29, 30]. Differences in cell line origins contribute to the inconsistency of these findings. Sayes et al. (2004) states that they observed no LDH release before 30 hours after fullerene exposure, whereas the mouse fibrosarcoma cells showed LDH release at 6 hours [30]. Another question raised by these

experiments is how one set of viability assays (MTT) which assay mitochondrial enzyme function show no changes in viability even though there is LDH release at the same time point. Further research needs to be done to determine that the LDH release is not due to fullerenes punching their way through the lipid membrane to gain entry into the cell as has been seen with other nanomaterials.

The ability of a toxicant to induce inflammatory responses is a key indicator of toxicity. A few studies have been conducted on C_{60} fullerenes to determine if they elicit an immune response via changes in gene expression for inflammatory cytokines and chemokines. Most of the available data has been from C_{60} fullerenes either inhaled or instilled. These studies have determined that fullerenes alter gene expression. Park et al (2010) determined that in BAL fluid there is an increase in IL-1, TNF-α, IL-6, and IL-12 indicating an inflammatory response [31]. These changes were noted one day after instillation and were elevated up to 28 days after instillation [31]. Another study looked at inhalation of C_{60} fullerenes (6hr/day, 5 day/week, for 4 weeks) in rats and determined that there were changes in gene expression for inflammatory response, oxidative stress, apoptosis, metalloendopeptidase activity, and MHC- mediated immunity. These changes could be seen at 3 days and up to one month after exposure [32].

Altered cell proliferation and induction of senescence are major indicators of toxicity. There are very few studies that have focused on this subject after exposure to C_{60} fullerenes. The results of these studies are highly dependent on cell type and amount of fullerenes to which the cells or animals are exposed. Studies that have been conducted on keratinocytes have been contradictory as to whether or not pristine C_{60} fullerenes alter cell proliferation [10].

BAL cells exposed to C_{60} fullerenes by instillation showed an increase in subG1 and G1 arrest that could be indicative of senescence although more specific tests should be utilized [31].

DNA damage and senescence are often viewed in the context of "*cause and effect*", respectively. A number of studies have been done, *in vivo* and *in vitro*, to determine if C_{60} fullerene exposure results in DNA damage. As with many of the other studies, the data is often contradictory which again may be due to the origin or species of cells and/or differences of exposure route/vehicle, or concentration of C_{60} fullerenes. The Ames test results were contradictory – one research group determined that fullerenes did not produce DNA damage while another group determined that after irradiation fullerene produced DNA damage [10]. The Comet assay *in vitro* showed no signs of DNA damage in lung epithelial cells whereas *in vivo* there was an increase in DNA damage at 3 hours in mouse lungs and a decrease in damage after 24 hours. This was determined to be consistent with the activation of DNA damage repair enzymes [10]. Micronucleus tests *in vitro* showed an increase in micronuclei that was dose dependent in human lung carcinoma cells whereas *in vivo* there was no sign of micronuclei formation in the bone marrow of ICR mice after fullerene exposure [10]. No chromosomal aberrations were found *in vitro* in hamster lung cells. *In vivo,* there was elevated 8-oxodG found in the liver and lung indicating oxidative damage with no increase in liver DNA repair as well as gpt mutations in the lung (2 fold increase seen with one dose and 3 fold increase seen with multiple doses of C_{60} fullerenes) [10].

The studies presented in this thesis focus on the cell most likely to make contact with the nanomaterial once it enters the blood stream: the macrophage. Since macrophages have evolved to remove particulate matter from the circulation and to engage in the neutralization,

destruction and removal of that material from the systemic flow, these studies focus on the biological effects elicited by exposure to C_{60} fullerenes and the ultimate disposition of the cell. C_{60} fullerenes are produced naturally through combustion processes such as forest fires, volcanic eruptions and low-temeprature combustion of fossil fuels. Humans are, therefore, most likely to be exposed to C_{60} as a component of ambient air pollution. While inhalation results in deposition in the lung, research has shown that smaller particles able to make it into the lower respiratory tract can translocate into the interstitial space and the blood, which may result in deposition in the liver and spleen as well as contact with immune cells. Additionally, larger nanoparticles that are cleared from the upper respiratory tract by the mucociliary escalator can be deposited in the GI tract where they may be translocated into the circulatory system by gut epithelial cells and potentially result in contact with immune cells and deposition in organs like the liver or spleen [41]. While there are many studies of occupational exposure to fullerenes, there is little available data on exposure from natural sources of fullerenes. It is nonetheless clear that ambient exposure levels are much lower than those likely to be encountered in the occupational setting [10]. The lower end of the likely dose range was chosen to simulate the earliest responses of macrophages to C_{60} exposure.

In addition to human exposure through inhalation, there is a growing body of literature that highlights the utility of C_{60} as a drug carrier [22]. These carriers are most likely to be introduced into the intravascular space and therefore would encounter circulating monocytes almost immediately. Interestingly, as a pulse of C_{60} therapeutic enters the blood stream, the peak circulating concentration is likely to be much higher than that achieved through inhalation. However, over the course of a lifetime, the total amount of nanomaterial entering

the interstitial space of the lung and gaining access to the blood stream is likely to be much higher than through a single injection. These considerations highlight the importance of understanding the pharmacokinetics/pharmacodynamics and toxicokinetics/toxicodynamics.

RAW 264.7 immortalized murine macrophages are commonly utilized in the literature to determine effects of toxicants on immune cells [14, 33, 34, 35, 36,37]. This cell line was utilized in the current study based on current use in the literature as well as use in nanomaterial studies to allow for proper comparison of fullerenes to other nanomaterial's effects on immune cells. The studies presented herein address the following hypothesis and specific aims:

Hypothesis:

Exposure of peripheral immune cells to C_{60} fullerenes will result in their uptake into the cytosol, membrane-bound intracellular compartments *and* cell membrane(s) resulting in cellular stress with subsequent activation of apoptosis at 24 hours.

Specific Aims:

1) **What are C_{60} fullerene methods of entry into RAW 264.7 macrophages?**
2) **Does exposure to C_{60} fullerenes result in altered cellular functions of RAW 264.7 macrophages?**
    a. **Does C_{60} fullerene exposure result in apoptosis at 24 hours?**
    b. **Does C_{60} fullerene exposure increase the inflammatory potential of peripheral macrophages at 24 hours?**

c. **Does C_{60} fullerene exposure cause cellular stress in RAW 264.7 macrophages?**

3) **Does cell stress induced by C_{60} fullerenes alter cellular proliferation?**

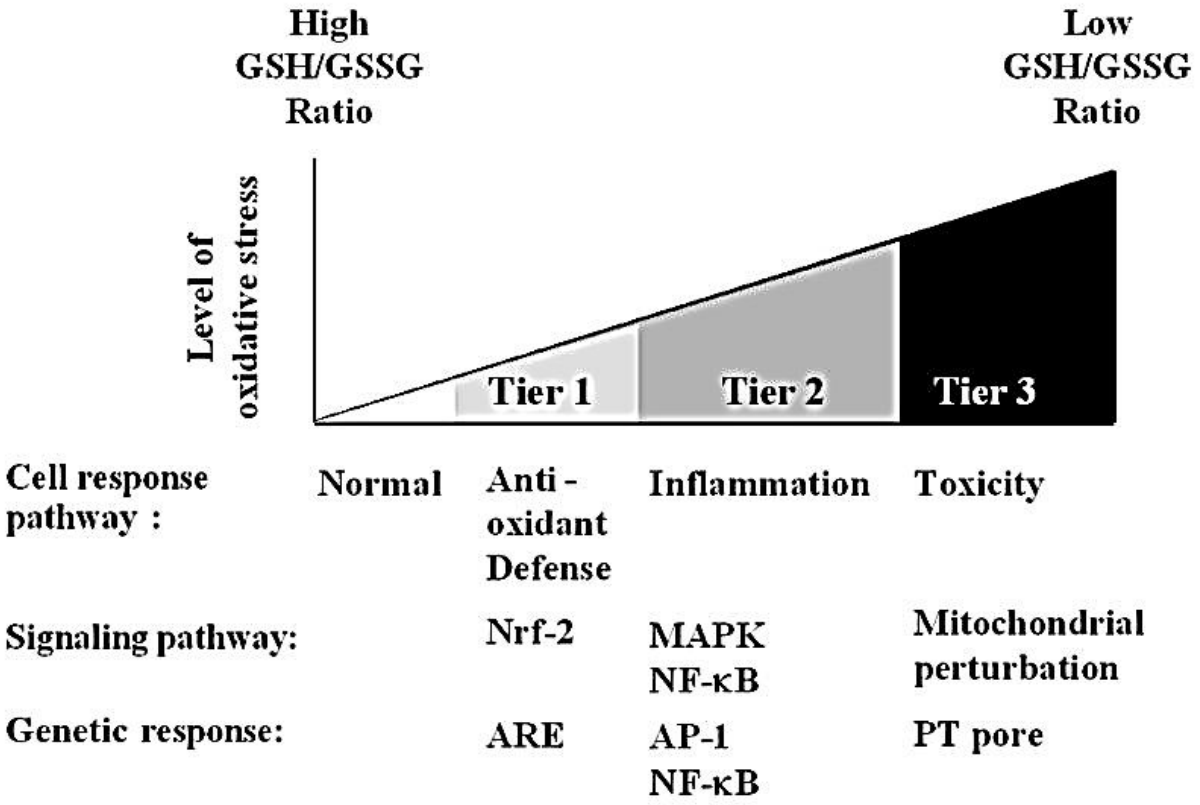

Figure 1.1: Oxidative Stress Paradigm: Oxidative stress has recently been identified as a useful indication of toxicity of nanomaterials. An oxidative stress paradigm was published that describes the different levels of oxidative stress. Tier 1 is mild oxidative stress in which the cell utilizes mechanisms available to combat oxidative stress and is able to resolve the issue. Tier 2 results in inflammation as the mechanisms available to combat oxidative stress are unable to totally resolve the issue. Tier 3 is oxidative stress that the cell is unable to control and results in the activation of cell death pathways [13].

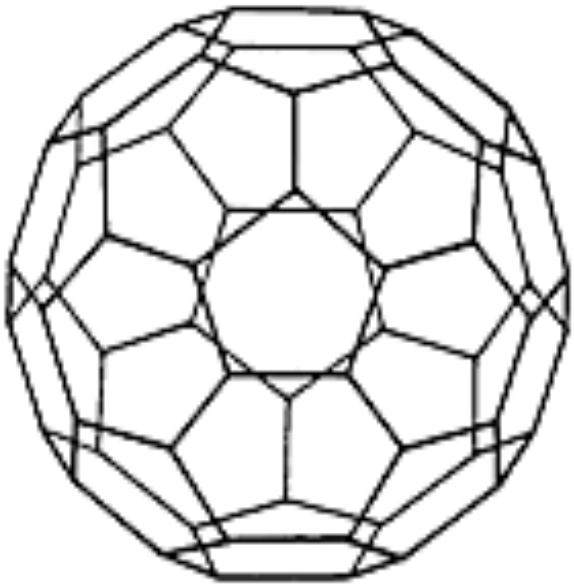

Figure 1.2: Fullerene Structure: C_{60} fullerene molecules contain 60 carbons, 30 double bonds, and have a diameter of approximately 1 nanometer. They are being researched for potential incorporation into consumer products as well as for utilization as drug delivery devices [10, 38].

References

[1] Mirkovic, T.; Zacharia, N. S.; Scholes, G. D.; Ozin, G. A. Fuel for thought: chemically powered nanomotors out-swim natures flagellated bacteria. *ACS Nano.* **4(4)**: 1782-1789; 2010.

[2] Murdock, R. C.; Braydick-Stolle, L.; Schrand, A. M.; Schlager, J. J.; Hussain, S. M. Characterization of nanomaterial dispersion in solution prior to *in vitro* Exposure Using Dynamic Light Scattering Technique. *Tox. Sci.* **101(2)**: 239-253; 2008.

[3] Lovestam, G; Rausher, H; Roebben, G, Kluttgen, B.; Gibson, N; Putard, J-P; Stamm, H; Considerations on a Definition of Nanomaterial for Regulatory Purposes. JRC Reference Reports; 2010.

[4] Turco, R.F.; Bischoff, M.; Tong, Z.H.; Nies, L. Environmental implications of nanomaterials: are we studying the right thing? *Current Opinion in Biotechnology.* **22**:527-532; 2011.

[5] Haase, A.; Tentschert, J.; Luch, A. Nanomaterials: A Challenge for Toxicological Risk Assessment? *EXS.* **101:** 219-50; 2012.

[6] Fortner, J.D.; Lyon, D.Y.; Sayes, C.M.; Boyd, A.M.; Falkner, J.C.; Hotze, E.M.; Alemany, L.B.; Tao, Y.J.; Guo, W.; Ausman, K.D.; Colvin, V.L.; Hughes, J.B. C60 in Water: Nanocrystal Formation and Microbial Response. *Environ. Sci. Technol*. **39:** 4307-4316; 2005.

[7] Zhu, M.; Nie, G.; Meng, H.; Xia, T.; Nel, A.; Zhao, Y. Physicochemical Properties Determine Nanomaterial Cellular Uptake, Transport, and Fate. Accounts of Chemical Research X; A-J; XXXX.

[8] Albanese, A.; Tang, P.S.; Chan, W.C.W. The Effect of Nanoparticle Size, Shape, and Surface Chemistry on Biological Systems. *Annu. Rev. Biomed. Eng.* **14:**1-16; 2012.

[9] Podila, R.; Brown, J.M. Toxicity of Engineered Nanoparticles: A Physicochemical Perspective. *J Biochem. Mol. Toxicol.* **00**:1-6; 2012.

[10] Aschberger, A.; Johnston, H. J.; Stone, V.; Aitken, R. J.; Tran, C. L.; Hankin, S. M.; Peters, S.A.K.; Christensen, F.M. Review of fullerene toxicity and exposure – Appraisal of a human health risk assessment, based on open literature. *Regul. Toxicol. Pharm.* **58**: 455-437; 2010.

[11] Dawson, K.; Salvati, A.; Lynch, I. Nanoparticles reconstruct lipids. *Nature Nanotoxicology.* **4:** 84-85; 2009.

[12] Xia, T.; Kovochich, M.; Brant, J.; Hotze, M.; Sempf, J.; Oberley, T.; Sloutas, C.; Yeh, J. I.; Wiesner, M. R.; Nel, A. E. Comparison of the abilities of ambient and manufactured nanoparticles to induce cellular toxicity according to an oxidative stress paradigm. *Nano Letters*. **6(8):** 1794-1807; 2006.

[13] Li, N.; Xia, T.; Nel, A. The role of oxidative stress in ambient particulate matter-induced lung diseases and its implications in the toxicity of engineered nanoparticles. *Free Radical Bio. Med.* **44**:1689-1699; 2008.

[14] Di Giorgio, M. L.; Di Bucchianico, S.; Ragnelli, A. M.; Aimola, P.; Santucci, S.; Poma, A. Effects of single and multi walled carbon nanotubes on macrophages: Cyto and genotoxicity and electron microscopy. *Mutat. Res.* **722**: 20-31; 2011.

[15] Spohn, P.; Hirsch, C.; Hasler, F.; Bruinink, A.; Krug, H.F.; Wick, P. C_{60} fullerene: A powerful antioxidant or a damaging agent? The importance of an in-depth material characterization prior to toxicity assays. *Environmental Pollution.* **157 (4)**:134-1139; 2009.

[16] Johnston, H.J.; Hutchison, G.R.; Christensen, F.M.; Aschberger, K.; Stone, V. The Biological Mechanisms and Physicochemical Characteristics Responsible for Driving Fullerene Toxicity. *Toxicol. Sci.* **114(2)**: 162-182; 2010.

[17] Aitkin, R.J.; Chaudhry, M.Q.; Boxall, A.B.A.; Hull, M. Manufacture and use of nanomaterials: current status in the UK and global trends. *Occupational Medicine.* **56:** 300-306; 2006.

[18] Bosi, S.; Da Ros, T.; Spalluto, G.; Prato, M. Fullerene derivatives: an attractive tool for biological applications. *Eur. J. Med. Chem.* **38**: 913-923; 2003.

[19] Oberdörster, G.; Oberdörster, E.; Oberdörster, J. Nanotoxicology: An Emerging Discipline Evolving from Studies of Ultrafine Particles. *Environmental Health Perspectives.* **113(7):** 823-839; 2005.

[20] Howard, J.B.; McKinnon,T.; Makarovsky, Y.; LaFleur, A.L.; Johnson, M.E. Fullerenes C60 and C70 in flames. *Nature.* **352**:39-141; 1991.

[21] Nielson, G.D.; Roursgaard, M.; Jensen, K.A.; Poulsen, S.S.; Larsen, S.T. In vivo Biology and Toxicology of Fullerenes and Their Derivatives. *Basic & Clinical Pharmacology & Toxicology.* **103:** 197-208; 2008.

[22] Montellano, A.; DaRos, T.; Bianco, A.; Prato, M. Fullerene C60 as a multifunctional system for drug and gene delivery. *Nanoscale.* **3**:4035- 4041; 2011.

[23] Zakharian, T.; Seryshev, A.; Sitharaman, B.; Gilter, B.E.; Knight, V.; Wilson, L.J. A Fullerene-Paclitaxel Chemotherapeutic: Synthesis, Characterization, and Study of Biological Activity in Tissue Culture. *J. AM. CHEM. SOC.* **127 (36)**: 12508-12509; 2005.

[24] Kubota, R.; Tahara, M.; Shimizu, K.; Sugimoto, N.; Hirose, A.; Nishimura, T. Time-dependent variation in the biodistribution of C60 in rats determined by liquid chromatography-tandem mass spectrometry. *Toxicology Letters.* **206:** 172-177; 2011.

[25] Bullard-Dillard, R.; Creek, K.E.; Scrivens, W.A.; Tour, J.M. Tissue Sites of Uptake of 14C-Labeled C60. *Bioorganic Chemistry.* **24:** 376-385; 1996.

[26] Shinohara, N.; Nakazato, T.; Tamura, M.; Endoh, S.; Fusui, H.; Morimoto, Y.; Myojo, T.; Shimada, M.; Yamamoto, K.; Tao, H.; Yoshida, Y.; Nkanishi, J. Clearance Kinetics of Fullerene C60 Nanoparticles from Rat Lungs after Intratracheal C60 Installation and Inhalation C60 Exposure. *Toxicological Sciences.* **118(2)**: 564-573; 2010.

[27] Porter, E.P.; Muller, K.; Skepper, J.; Midgley, P.; Welland, Mark. Uptake of C60 by human monocyte macrophages, its localization and implications for toxicity: Studied by high resolution electron microscopy and electron tomography. *Acta Biomaterialia*. **2**: 409-419; 2006.

[28] Jia, G.; Wang, H.; Yan, L.; Wang, X.; Pei, R.; Yan, T.; Zhao, Y.; Guo, X. Cytotoxicity of Carbon Nanomaterials: Single-Wall Nanotube, Multi-Wall Nanotube, and Fullerene. *Environmental Science & Technology.* **39(5)**: 1378-1383; 2005.

[29] Isakovic, A.; Markovic, Z.; Todorovic-Markovic, B.; Nikolic, N.; Vranjes-Djuric, S.; Mirkovic, M.; Dramicanin, M.; Harhaji, L.; Raicevic, N.; Nikolic, Z.; Trajkovic, V. Distinct Cytotoxic Mechanisms of Pristine versus Hydroxylated Fullerene. *Toxicological Sciences.* **91(1)**: 173-183; 2006.

[30] Sayes, C.M.; Fortner, J.D.; Guo, W.; Lyon, D.; Boyd, A.M.; Ausman, K.D.; Tao, Y.J.; Sitharaman, B.; Wilson, L.J.; Hughes, J.B.; West, J.L.; Colvin, V.L. The Differential Cytotoxicity of Water-Soluble Fullerenes. *Nano Lett.* **4(10)**: 1881-1887; 2004.

[31] Park, E.; Kim, H.; Kim, Y.; Yi, J.; Choi, K.; Park, K. Carbon fullerenes (C60s) can induce inflammatory responses in the lung of mice. *Toxicology and Applied Pharmacology.* **244:** 226-233; 2010.

[32] Fujita, K.; Morimoto, Y.; Ogami, A.; Myojyo, T.; Tanaka, I.; Shimada, M.; Wang, W.; Endoh, S.; Uchida, K.; Nakazato, T.; Yamamoto, K.; Fukui, H.; Horie, M.; Yoshida, Y.; Iwahashi, H.; Nakanishi, J. Gene expression profiles in rat lung after inhalation exposure to C_{60} fullerene particles. *Toxicology.* **258**: 47-55; 2009.

[33] Wang, W.; Luo, M.; Fu, Y.; Wang, S.; Efferth, T.; Zu,Y.Glycyrrhizic acid nanoparticles inhibit LPS-induced inflammatory mediators in 264.7 mouse macrophages compared with unprocessed glycyrrhizic acid. *Int. J. Nanomedicine.* **8:** 1377-83; 2013.

[34] Di Bucchianico, S.; Fabbrizi, M. R.; Misra, S. K.; Valsami-Jones, E.; Derhanu, D.; Reip, P.; Bergamaschi, E.; Migliore, L. Multiple cytotoxic and genotoxic effects induced in vitro by differently shaped copper oxide nanomaterials. *Mutagenesis*. **28(3)**: 287-99; 2013.

[35] Xia, W.; Song, H. M.; Wei, Q.; Wei, A. Differential response of macrophages to core-shell Fe3O4@Au nanoparticles and nanostars. *Nanoscale.* **4(22)**: 7143-8; 2012.

[36] Rehman, M. U.; Yoshihisa, Y.; Miyamoto, Y.; Shimizu, T. The anti-inflammatory effects of platinum particles on the lipopolysaccharide- induced inflammatory response in RAW 264.7 macrophages. *Inflamm. Res.* **61(11)**: 1177-85; 2012.

[37] Nishanth, R. P.; Jyotsna, R. G.; Schlager, J. J.; Hussain, S. M.; Reddanna, P. Inflammatory responses of RAW 264.7 macrophages upon exposure to nanoparticles: role of ROS NF-κB signaling pathway. *Nanotoxicology*. **5(4)**: 502-16; 2011.

[38] Kroto,H. W.; Allaf, A. W.; Balm, S. P. C_{60}: Buckminsterfullerene. *Chem. Rev.* **91**: 1213-1235; 1991.

[39] Thomas, T.; Thomas, K.; Sadrich, N.; Savage, N.; Adair, P.; Bronaugh, R. Reseach Strategies for Safety Evaluation of Nanomaterials, PVII: Evaluating Consumer Exposure to Nanoscale Materials. *Tox.Sci*. **91(1):** 14-19; 2006.

[40] Jones, D. P. Redefinining Oxidative Stress. *Antioxid. Redox Signaling.* **8 (9 & 10):** 1865-1879; 2006.

[41] Oberorster, G.; Sharp, Z.; Atudorei, V.; Elder, A.; Gelein, R.; Lunts, A.; Kreyling, W.; Cox, C. Extrapulmonary Translocation of Ultrafine Carbon Particles Following Whole-Body Inhalation Exposure of Rats. *J. Toxicol. Environ. Health Part A.* **65 (20)**: 1531-1543; 2011.

Chapter II

Determination of C_{60} Fullerene Methods of Entry in RAW 264.7 Macrophages

Introduction

Lack of solubility in aqueous solution is an issue for most applications of fullerenes especially the highly anticipated medical applications. Due to these issues, several methods of C_{60} preparation have evolved of which most involve the use of solvents such as tetrahydrofuran (THF). The simplest method is to dissolve the particles in solvent only [1]. Another method first dissolves the particles in a solvent such as THF and then uses rotary evaporation to force the fullerenes into water while removing the solvent [2]. Dissolving fullerenes in solvents results in additional toxicity issues resulting from the solvent. In the case of THF, even the solvent to water method results in residual toxicity from tetrahydro-2- furanol and γ-butyrolacetone, as well as peroxides [3]. Spohn et al (2009) and Zhang et al (2009) both determined that washing C_{60} fullerene preparations via centrifugal filtration removes the toxic products of the solvents. Sonication from solvents such as toluene into water has also been utilized [3, 4]. Sonication results in the least chemical complications, but requires weeks to dissolve the fullerenes [5].

The method of preparation of C_{60} fullerenes has a distinct effect on the outcome of biological experiments. Porter et al (2006) showed that fullerenes enter the cell and are found

in the cytosol as well as encapsulated in vesicles. They also found evidence that fullerenes were able to enter the nucleus [1]. Questions arose due to their preparation method of dissolving the particles in THF. There were also difficulties determining C_{60} fullerene location against the background of the cell. The experiments in this section are to determine if particles prepared via THF, rotary evaporation and centrifugal filtration yield similar localization in RAW 264.7 immortalized mouse macrophages to the experiments done by Porter et al (2006). In addition to the altered preparation method, terbium endohedral fullerenes (TbC_{60}) were employed to add electron density to the core of the particle. This was done to increase the ability to differentiate the particles from the background of the cell in the TEM images. Characterization of the zeta potential and aggregate size of the particles was key to determine that the terbium endohedral fullerenes were an adequate substitute for the C_{60} fullerenes.

Materials & Methods

Chemicals

All cell culture supplies were purchased from Gibco (Invitrogen, Carlsbad, CA). Solid C_{60} fullerenes (99.9%) were purchased from MER Corporation (Tucson, AZ). Terbium C_{60} fullerenes were purchased from BuckyUSA (Houston, TX). Tetrahydrofuran was purchased from Acros Organics (Fair Lawn, NJ). Glutaraldehyde was purchased from Electron Microscopy Sciences (Hatfield, PA).

Cell Culture

RAW 264.7 immortalized mouse macrophages were obtained from American Type Culture Collection. They were maintained in Dulbecco's Modified Eagle Medium with 10% fetal

bovine serum and 1% penicillin- streptomycin- glutamate solution. The cells were grown at 37°C and 5% humidity. Cells were utilized until passage 30.

C_{60} Fullerene and Terbium Endohedral Preparation

Fullerenes were prepared via the method of Deguchi et al (2001) and Spohn et al (2009).

Fullerene Size and Charge Analysis

A Malvern Zeta Sizer was used to determine zeta potential and aggregate size. A Nanosight LM 14C was used to determine and compare the aggregate size of terbium particles and fullerenes. C_{60} fullerenes prepared on three separate days were analyzed for charge and aggregate size on each instrument. Due to the precious nature of the terbium endohedral preparations only one preparation was sampled three times.

Transmission Electron Microscopy

RAW 264.7 cells were allowed to attach to the culture dish overnight. Cells were dosed with 0.1 and 0.36 µg/mL terbium endohedral C_{60} fullerenes for 8 hours. They were fixed at 8 hours with glutaraldehyde and sodium phosphate buffer and refrigerated over night. The cells were then processed by the University of Michigan Microscopy and Image Analysis core in preparation for viewing on a Philips CM-100 transmission electron microscope. Terbium endohedral fullerenes in water were dried on a TEM grid and imaged.

Freeze Fracture Transmission Electron Microscopy

RAW 264.7 cells were allowed to attach to culture flasks overnight. Cells were dosed with 0.5 µg/mL terbium endohedral fullerenes for 8 hours. They were fixed with glutaraldehyde and shipped to NanoAnalytical Laboratory for imaging.

Results

C_{60} Fullerene and Terbium Endohedral Fullerene Size and Charge

C_{60} fullerene aggregates have an average size of 91.13 nm based on measurements from the Malvern zeta sizer. Terbium endohedral fullerene aggregate size measured 99.31 nm by the same instrument (Figure 2.1). The Nanosight LM 14C measured the average size of the C_{60} fullerene aggregates to be 55.179 nm with a standard deviation of 34.16 nm and the terbium endohedral fullerenes as 63.765 nm with a standard deviation of 24.46 nm. The Malvern zeta sizer showed the average charge of the C_{60} fullerenes was -44.3 mV. The charge of the terbium endohedral fullerenes was -64.3 mV (Figure 2.1).

Transmission Electron Microscopy of TbC_{60} in RAW 264.7 cells

The TbC_{60} fullerenes entered the RAW 264.7 immortalized macrophages via endocytosis. Figure 2.4 A shows the TbC_{60} fullerene membrane bound within a vesicle. The TbC_{60} fullerenes are able to exist unbound in the cytosol . Figure 2.4 B shows a TbC_{60} aggregate in the cytosol unbound by any membrane and also a TbC_{60} aggregate approaching the plasma membrane without evidence of endocytosis occurring. The TbC_{60} aggregates also entered the nucleus. Figure 2.4 C & D are the same image at different magnifications showing a group of TbC_{60} aggregates in the process of crossing into the nucleus as well as another group of aggregates fully inside the nucleus.

Freeze Fracture Transmission Electron Microscopy of TbC_{60} in RAW 264.7 cells

Freeze Fracture TEM images of RAW 264.7 immortalized mouse macrophages exposed to 0.5 μg/mL TbC_{60} for 8 hours showed aggregates of fullerenes decreasing in size as their proximity to the membrane increased. Also, aggregates were seen in the membrane space.

Discussion

One of the first considerations in a nanomaterials study are the characteristics of the particles. Aggregate size and zeta potential are commonly measured in order to characterize nanomaterials because the zeta potential of the particles reflects the stability of the particles. The stability of the particle is a measure of the repulsion between the particles meaning how likely they are to aggregate. Nanoparticles that have zeta potentials of equivalent sign and strength would have similar repulsive forces between the particles and, therefore, similar zeta potentials are considered to have similar aggregation in solution [6]. Aggregate size in particles under 100 nm is a result of Brownian diffusion that results in particle collisions and Van der Waals forces that hold the particles together. Aggregation in nanomaterials is an important consideration because the size of the particles will have a distinct effect on the reactivity, uptake, and ultimately the toxicity [7].

The zeta potential data measurements demonstrate that C_{60} fullerenes and terbium endohedral fullerenes possess zeta potentials of similar sign and strength. TbC_{60} fullerenes have a slightly stronger zeta potential at -64.3 mV but as compared to the zeta potential of the C_{60} fullerenes -44.3 mV the difference is not large enough to result in major differences in repulsion between fullerenes. Analysis of aggregate size on the Malvern zetasizer showed the average fullerene aggregate size as 91.13 nm and TbC_{60} average aggregate size as 99.31 nm. In

comparison, the data from the nanosight showed the average aggregate size of the C_{60} fullerenes as 57.179 nm and the average TbC_{60} aggregate size as 63.765 nm. Two methods of aggregate size measurement were utilized due to the tendency of DLS to skew the measurements towards larger sized particles. The characterization data show terbium endohedral fullerenes are similar in aggregate size and zeta potential; thus, they are a relatively accurate substitute for determination of C_{60} fullerene localization in cells via TEM.

TEM imaging showed fullerenes have three mechanisms of entry into the cell (Figure 2.4). Endocytosis of the particles appears to be the main method of entry. This has been seen in the literature as a common mechanism for many different types of nanomaterials. Fullerenes also have the ability to enter the cytosol through the membrane as evidenced by the lack of vesicles surrounding aggregates in the cytosol in the TEM images. Whether they enter through the plasma membrane or are endocytosed and have the ability to escape the vesicle is unclear. The fullerene aggregates enter the nucleus through an, as yet, unknown mechanism of entry. While these three mechanisms of entry were previously reported by Porter et al (2006), their method of particle preparation utilized THF as the vehicle for delivery of the C_{60}s and raised questions about THF toxicity affecting their entry into the cells. The particles used in this study have been prepared and washed by the method of Spohn et al. (2009), which results in removal of THF and its oxidized products. This new data agrees with the data of Porter et al (2006) suggesting that the THF does not affect the fullerene entry into cells.

After observing C_{60}s ability to enter the cytosol by passing through either the plasma membrane or vesicle membrane, visualization of C_{60}s in the cell membrane was attempted. Processing of the samples for standard TEM imaging resulted in the membrane being stripped

away due to the chemicals utilized. Therefore, freeze fracture TEM was employed to visualize the plasma membrane in order to determine if the fullerenes were able to sit in the membrane before they make their way into the cytosol. The freeze fracture images of cells exposed to 0.5 μg/mL TbC_{60}s showed that the fullerene aggregates decrease in size as their proximity to the membrane increases and that they are able to enter the membrane space.

In summary, this study shows TbC_{60}s are an acceptable model nanoparticle to utilize in order to increase electron density in localization studies using TEM imaging. Additionally TEM imaging showed that TbC_{60}s in water are endocytosed by RAW 264.7 macrophages, are able to diffuse through the plasma membrane or escape endocytotic vesicles by diffusing through lipids to reside unbound in the cytosol, and are able to enter the nucleus. Finally, freeze fracture TEM determined that fullerenes are able to enter the membrane space.

A.

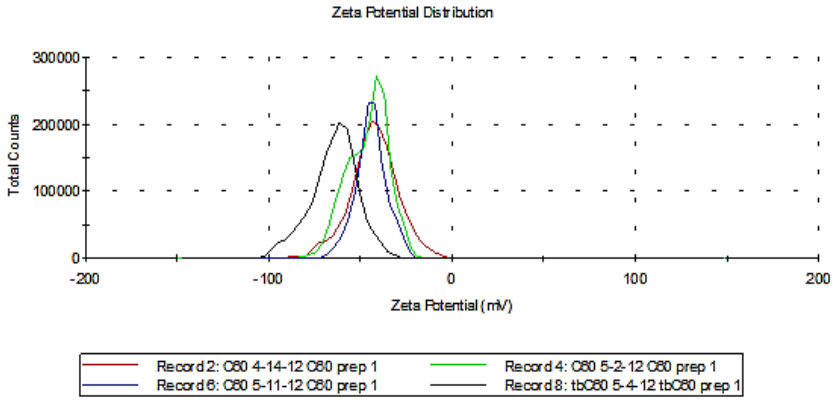

B.

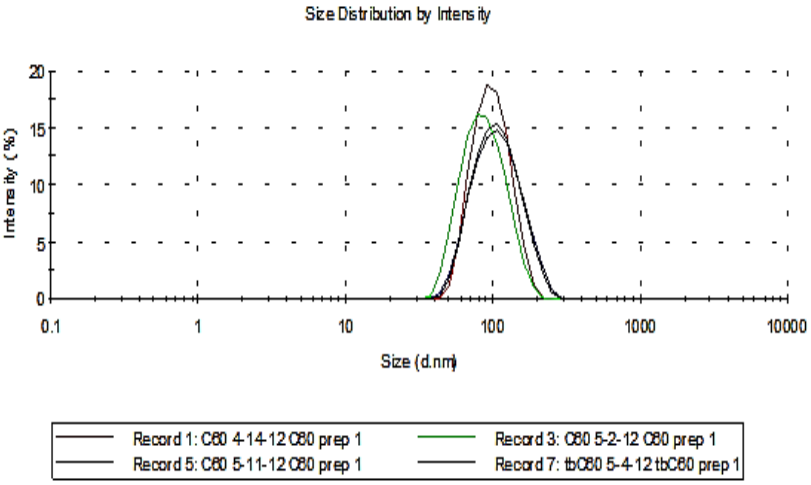

Figure 2.1: Characterization of Terbium Endohedral Fullerenes and C_{60} Fullerenes. A) Zeta Potential of C_{60} fullerenes and terbium endohedral fullerenes. The average zeta potential of the C_{60} fullerenes was -44.3 mV and -64.3 mV for the terbium endohedral fullerenes. The increased zeta potential is the indication of the repulsion between the particles [6]. The similar sign and measurment of the zeta potential predict that the particles behave similarly. B) Size Distribution of C_{60} fullerenes and terbium endohedral fullerenes by the Malvern zeta sizer. The average aggregate size of C_{60} fullerenes was 91.13 nm and 99.31 nm in the terbium endohedral fullerenes.

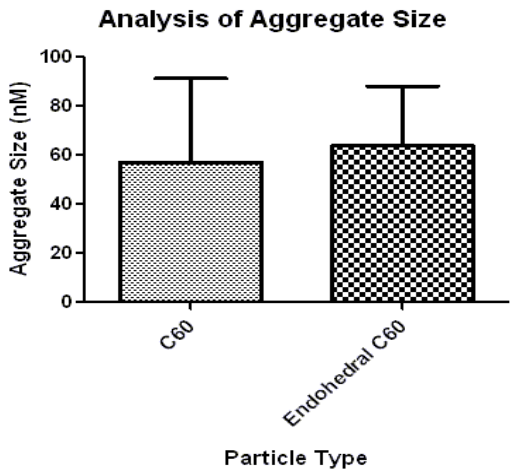

Figure 2.2: Nanosight Analysis of C_{60} Fullerene and Terbium Endohedral Fullerene Aggregate Size: C_{60} fullerene aggregates were approximately 55.179 nm with a standard deviation of 34.16 nm. Terbium endohedral fullerene aggregates were approximately 63.765 nm and had a standard deviation of 24.46 nm.

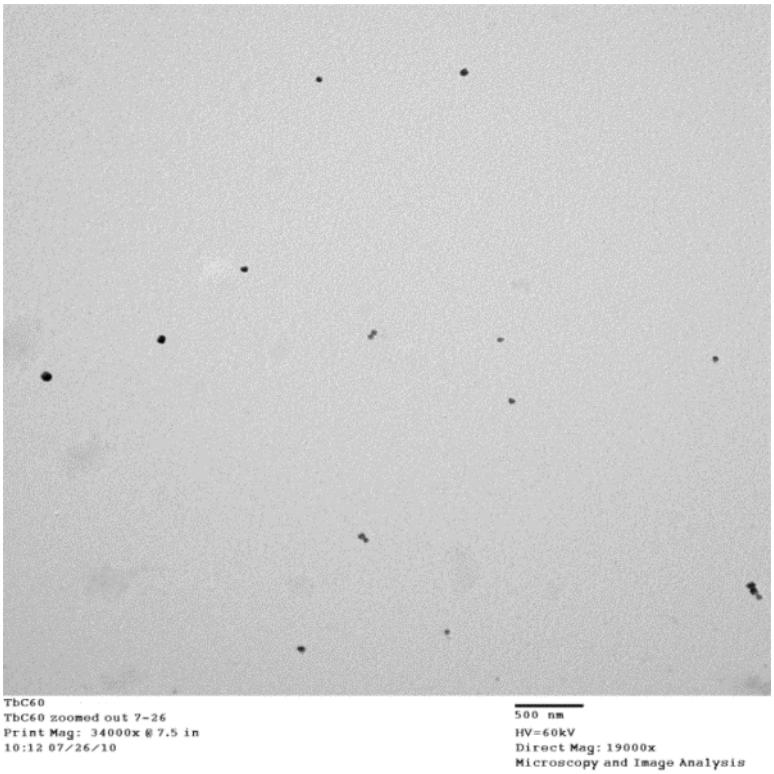

Figure 2.3: Transmission Electron Microscopy Image of Terbium Endohedral Fullerenes: The endohedral fullerenes were dissolved in water and then dried on the TEM grid to obtain this image.

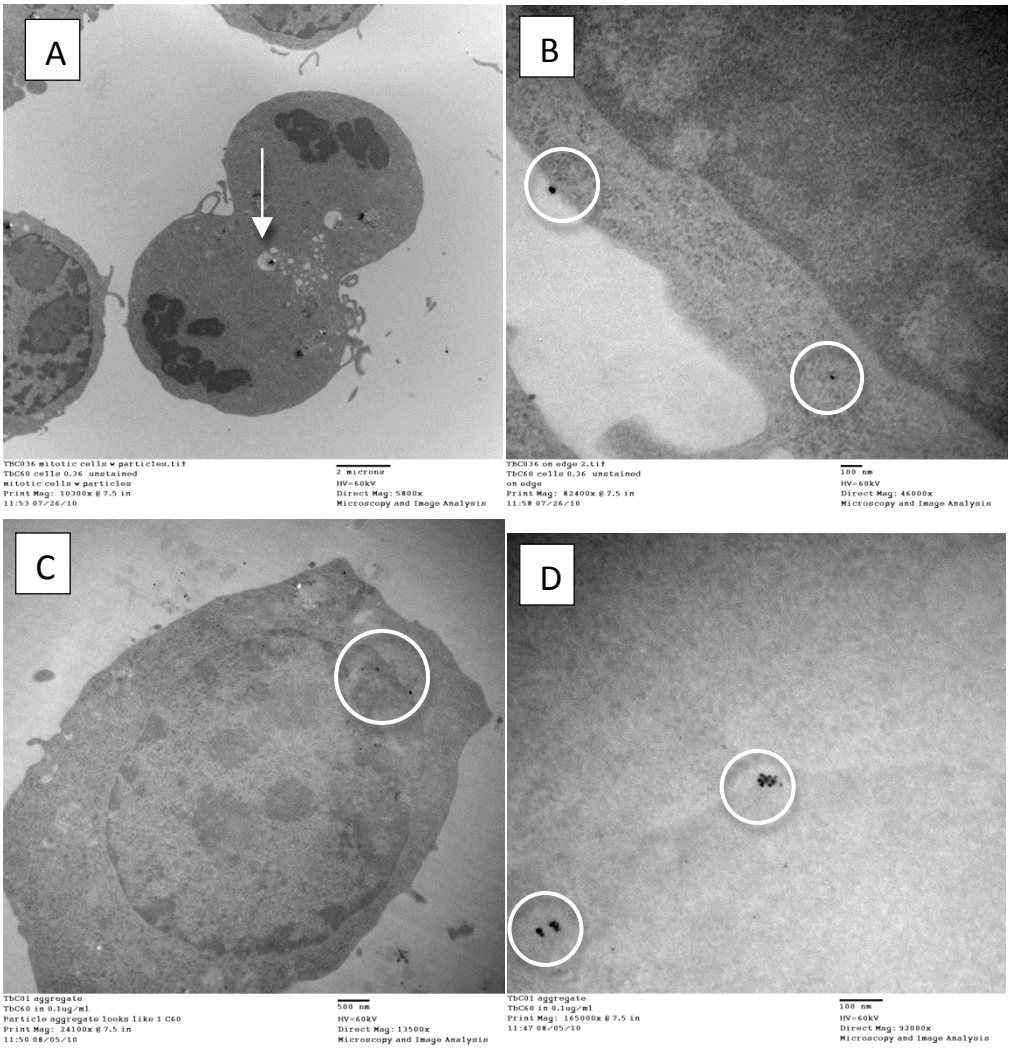

Figure 2.4: Transmission electron microscopy of terbium endohedral fullerenes in RAW 264.7 immortalized macrophages: A) Endocytosis of TbC_{60}s. B) Diffusion though the membrane. C & D) Entry into the nucleus.

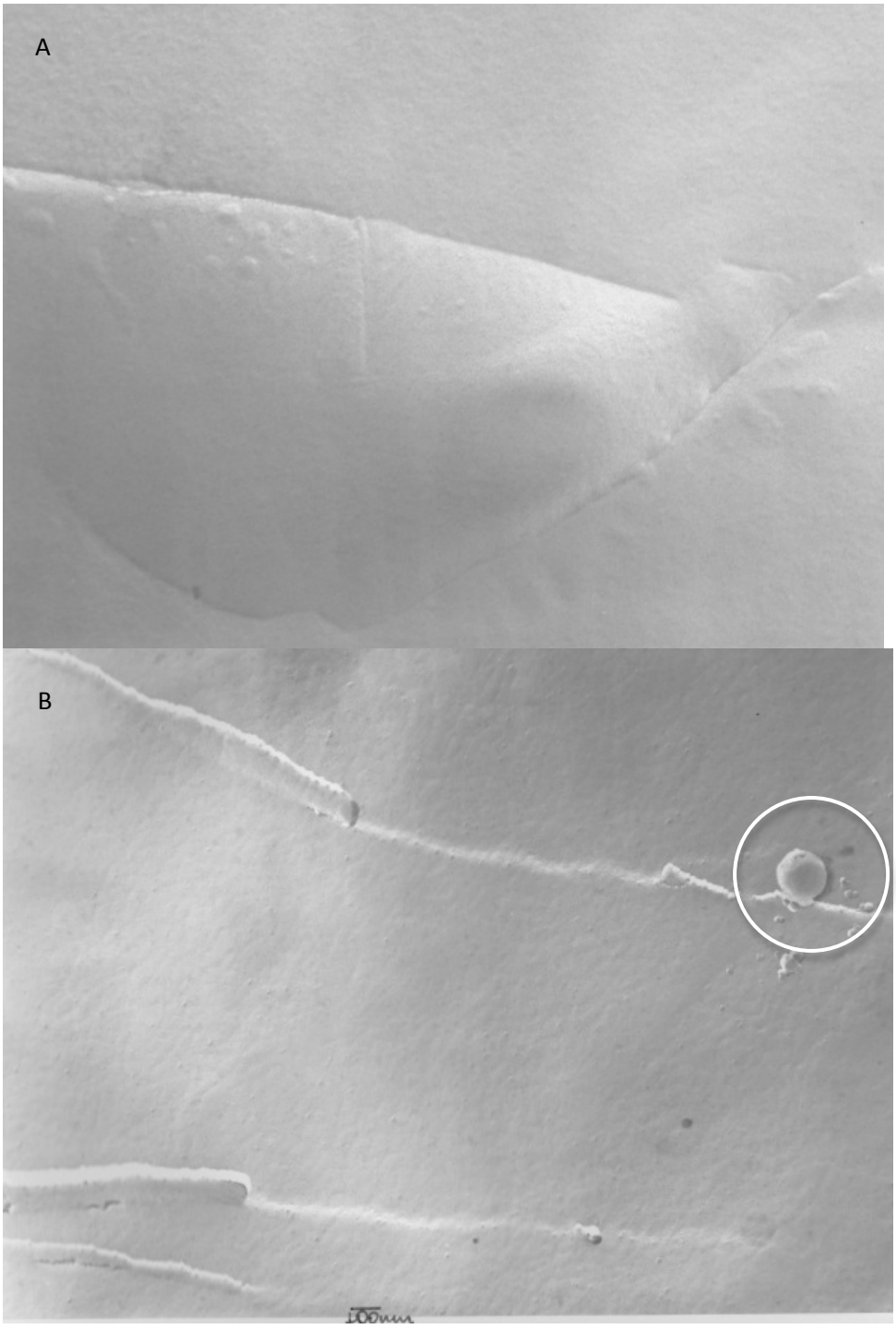

Figure 2.5: Freeze Fracture Transmission Electron Microscopy on RAW 264.7 cells. (A) Control cells, (B) cells exposed to 0.5 µg/mL TbC_{60} (fullerenes entering the membrane space are circled).

References

[1] Porter, E.P.; Muller, K.; Skepper, J.; Midgley, P.; Welland, Mark. Uptake of C60 by human monocyte macrophages, its localization and implications for toxicity: Studied by high resolution electron microscopy and electron tomography. *Acta Biomaterialia.* **2**: 409-419; 2006.

[2] Deguchi, S.; Alargova, R. G.; Tsujii, K. Stable Dispersions of Fullerenes, C60 and C70, in Water. Preparation and Characterization. *Langmuir.* **17:** 6013-6017; 2001.

[3] Zhang, B.; Cho, M.; Fortner, J.D.; Lee, J.; Huang, C. H.; Hughes, J. B.; Kim, J. H. Delineating oxidative processes of aqueous C_{60} preparations: role of THF peroxides. *Env. Sci. Technol.* **43 (1):** 108-113; 2009.

[4] Spohn, P.; Hirsch, C.; Hasler, F.; Bruinink, A.; Krug, H.F.; Wick, P. C_{60} fullerene: A powerful antioxidant or a damaging agent? The importance of an in-depth material characterization prior to toxicity assays. *Environmental Pollution.* **157 (4)**:134-1139; 2009.

[5] Markovic, Z.; Todorovic-Markovic, B.; Kleut, D.; Nikolic, N.; Vranjes-Djuric, S.; Misirkic, M.; Vucicevic, L.; Janjetovic, K.; Isakovic, A.; Harhaji, L.; Babic-Stojic, B.; Dramicanin, M.; Trajkovic, V. The mechanism of cell-damaging reasctive oxygen generation by colloidal fullerenes. *Biomaterials.* **28**: 5437-5448; 2007.

[6] Dougherty, G. M.; Rose, K. A.; Tok, J. B.: Satinderpall, S. P.; Chuang, F. X.; Sha, M. Y.; Chakarora, G; Penn, S. G. The Zeta Potential of Surface-Functionalized Metallic Nanorod Particles in Aqueous Solution. UCRL-JRNL-230853; 2007.

[7] Hotze, E. M.; Phenrat, T.; Lowry, G. V. Nanoparticle Aggregation: Challenges to Understanding Transported Reactivity in the Environment. *J Environ Qual.* **39:** 1909-1924; 2010.

Chapter III

Mechanism of Endocytosis of C_{60} Fullerenes in RAW 264.7 Macrophages

Introduction

There are several methods of endocytosis: Clathrin mediated endocytosis, caveolin mediated endocytosis, marcopinocytosis, and phagocytosis [1, 2]. Clathrin is a protein that has three heavy chains and three light chains that form a "triskeleton". Clathrin polymerizes to form a structure that surrounds vesicles on the cytoplasmic side of the plasma membrane. Clathrin does not bind to the membrane or phospholipids but serves to stabilize the curved area of the membranes by binding proteins that help create the curvature like endophilin or amphiphysin. These proteins also serve to bring in dynamin for vesicle scission at which time the vesicle coatings are removed [2]. The number of coated pits on the membrane is limited to 0.5-2% of the membrane surface [3]. Clathrin coated pits are able to invaginate and form vesicles that are 60-200 nm in diameter [1].

Caveolin is a membrane protein that resides in areas rich in sphingolipids and cholesterol [4]. Caevolae resemble flasks able to take in particles greater than 200 nm [1, 4]. The ability to utilize caveolae mediated endocytosis relies on the availability of membrane cholesterol [4]. This form of endocytosis requires actin depolymerization resulting in disruption

of the cytoskeleton that can be initiated by various signaling cascades, which then recruit dynamin II to the site to finish the process [4].

Macropinocytosis results in the engulfment of large amounts of extracellular fluid resulting in a macropinosome of 0.2 to 10 micrometer in size [5]. Macropinocytosis requires actin remodeling after membrane ruffling occurs. Membrane ruffling results in the folding of the ruffle onto the plasma membrane and formation of a vacuole filled with fluid [2].

Phagocytosis is utilized for cargo that is greater than 0.5 μM and requires actin polymerization. Opsonized particles come into contact with receptors on the outside of the cell and activate FcϒR signaling that results in actin polymerization. Once the opsonized particles are engulfed, actin must breakdown to allow the entry of the phagocytotic vesicle into the cell [2]. The size of the nanomaterial or aggregates of nanomaterial and their affinity for lipids will dictate the method of entry into the cell.

The results of the TEM images in Chapter II showed endocytosis as a main mechanism of fullerene entry into the macrophages. In order to assess the utilization of different types of endocytosis, cells were pre-incubated with inhibitors of endocytosis before exposure to C_{60} fullerenes. Genistein was utilized to inhibit receptor associated tyrosine-specific kinases that will interrupt caveolae mediated endocytosis. Chlorpromazine HCl inhibits clathrin disassembly and receptor signaling. Cytochalasin A disrupts F-actin polymerization, which inhibits macropinocytosis and phagocytosis [1]. This may also affect cavolae mediated endocytosis and clathrin mediated endocytosis if the vehicle is causing any osmotic differences in the cell membrane [2].

Materials & Methods

Chemicals

All cell culture supplies were purchased from Gibco (Invitrogen, Carlsbad, CA). Solid C_{60} fullerenes (99.9%) were purchased from MER Corporation (Tucson, AZ). Fullerene antibody and Clathrin secondary antibody were purchased from Santa Cruz Biotech (Santa Cruz, CA). Primary Clathrin antibody was purchased from Abcam (Cambridge, MA). DMSO, Paraformaldehyde, Chlorpromazine HCl, Cytochalasin A, and Genistein were purchased from Sigma Aldrich (St. Louis, MO). Dylight 594 labeling kit was purchased from Pierce (Rockford, IL). DAPI was purchased from Invitrogen (Grand Island, NY).

Fullerene Preparation

Fullerenes were prepared via the method of Deguchi et al (2001) and Spohn et al (2009).

Cell Culture and Dosing

RAW 264.7 immortalized mouse macrophages were cultured in Matek glass bottom plates overnight. They were maintained in Dulbecco's Modified Eagle Medium with 10% fetal bovine serum and 1% penicillin- streptomycin- glutamate solution. The cells were grown at 37°C and 5% humidity. Cells were utilized until passage 30. Cells were preincubated for 30 minutes with 200 µM genistein, 10 µg/mL chlorpromazine hydrochloride, or 5 µg/mL cytochalasin A. C_{60}s were added at a concentration of 4 µg/mL and incubated for 3 hours.

Immunocytochemistry

Cells were fixed with 4% paraformaldehyde and stained with DAPI and antibodies against fullerenes and clathrin. The fullerene antibody was conjugated to Dylight 594. The

Clathrin secondary antibody was conjugated to FITC. Wide field microscopy was performed on an Olympus IX-81 Disk Scanning Biological Microscope.

Image Analysis

ImageJ with RGB plugin was utilized to quantitate the amount of fullerene aggregates in the images. Fullerene aggregates were counted in 4 images of each inhibitor and 4 images of control cells exposed to only fullerenes. In each image, 7 cells were assessed and the mean amount of red pixels in the images was calculated.

Results

At 24 hours, fullerenes were visualized in RAW 264.7 macrophages. Cells exposed for 3 hours to 4 μg/mL resulted in an average red pixel value of 51.58. Pre-incubation with genistein before fullerene exposure resulted in an average red pixel value of 45.35. Pre-incubation with chlorpromazine HCl before fullerene exposure resulted in an average red pixel value of 45.69. Preincubation with cytochalasin A resulted in an average red pixel value of 34.45 (Figure 3.3)

Discussion

Immunocytochemistry utilizing an anti-fullerene fluorescently labeled antibody on RAW 264.7 cells exposed to 4 μg/mL C_{60} fullerenes allowed visualization of fullerene aggregates in the cell (Figure 3.1). Pre- incubating the cells with endocytosis inhibitors prior to C_{60} exposure allows characterization of the mechanisms of endocytosis utilized by the cell when exposed to fullerenes. Two main pathways of endocytosis were studied. Clathrin mediated endocytosis was inhibited by chlorpromazine hydrochloride. Cells pre-incubated with chlorpromazine hydrochloride demonstrated a decreased uptake of fullerene aggregates when the number of

red pixels in the image was analyzed and compared to cells exposed to only C_{60} fullerenes (Figure 3.3 and 3.4).

Caveolae mediated endocytosis was assessed by pre-incubating cells with genistein. These cells showed a decrease in the amount of red pixels in the image as compared to cells exposed to only fullerenes. Both caveolae mediated and clathrin mediated endocytosis resulted in a decrease of approximately 11.7 % of red pixel value compared to cells exposed to fullerenes. In order to further inhibit forms of endocytosis, cells were pre-incubated with cytochalasin A, an actin inhibitor, prior to fullerene exposure. As expected, there was a greater decrease (33% decrease) in red pixels in the image as compared to the image of cells exposed only to fullerenes as well as cells exposed to inhibitors for caveolae and clathrin mediated endocytosis. Although the changes were not statistically significant, this data supports that C_{60} fullerenes are taken up by the cell utilizing caveolae mediated endocytosis and clathrin mediated endocytosis equivalently. The actin inhibition will have an effect upon any type of endocytosis that utilized actin (caveolae mediated, macropincytosis, and phagocytosis). As mentioned previously, actin inhibition can even have an effect on clathrin mediated endocytosis if there are alterations to the osmolarity of the membrane, which is possible since the vehicle for the fullerenes is water.

The inhibitor study had some intrinsic difficulties. The images had to be taken at 3 hours after exposure to fullerenes to ensure that the inhibitors were working. This led to increased background in the images due to the limited time that the particles had to enter the cell resulting in low signal. All of the images have this same increased background so the pixel calculations are valid.

In summary, this study showed that C_{60} fullerenes are able to be tracked in cells utilizing immunocytochemistry with a fluorescently labeled antibody against fullerenes. Use of inhibitors allowed the elucidation of the endocytotic mechanisms utilized by the cell upon exposure to fullerenes. Inhibition of clathrin and caveolae mediated endocytosis resulted in approximately the same level of decreased endocytosis. Cytochalasin A disrupted all forms of endocytosis and suggested that the vehicle did have an effect on the mechanism of clathrin-mediated endocytosis. Additional studies should be undertaken to determine the role of scavenger receptors in C_{60} fullerene entry since clathrin and caveolin mediated endocytosis only account for a small percentage of fullerene entry at 3 hours.

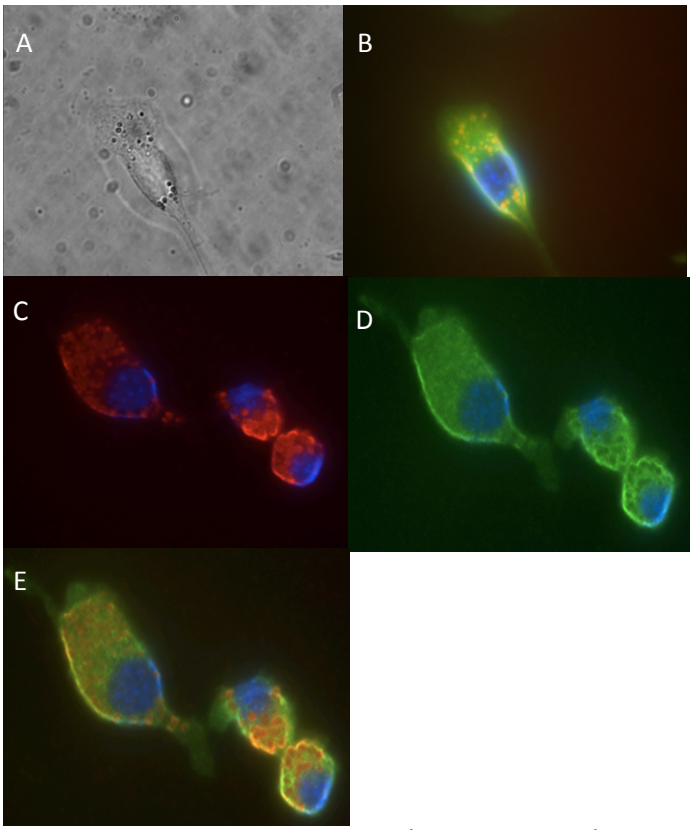

Figure 3.1: RAW 264.7 Macrophages exposed to 4 ug/mL C_{60} fullerenes for 24 hours. A) Brightfield image, B-E) Cells stained with antibodies against fullerenes (red) & clathrin (green) and DAPI (blue).

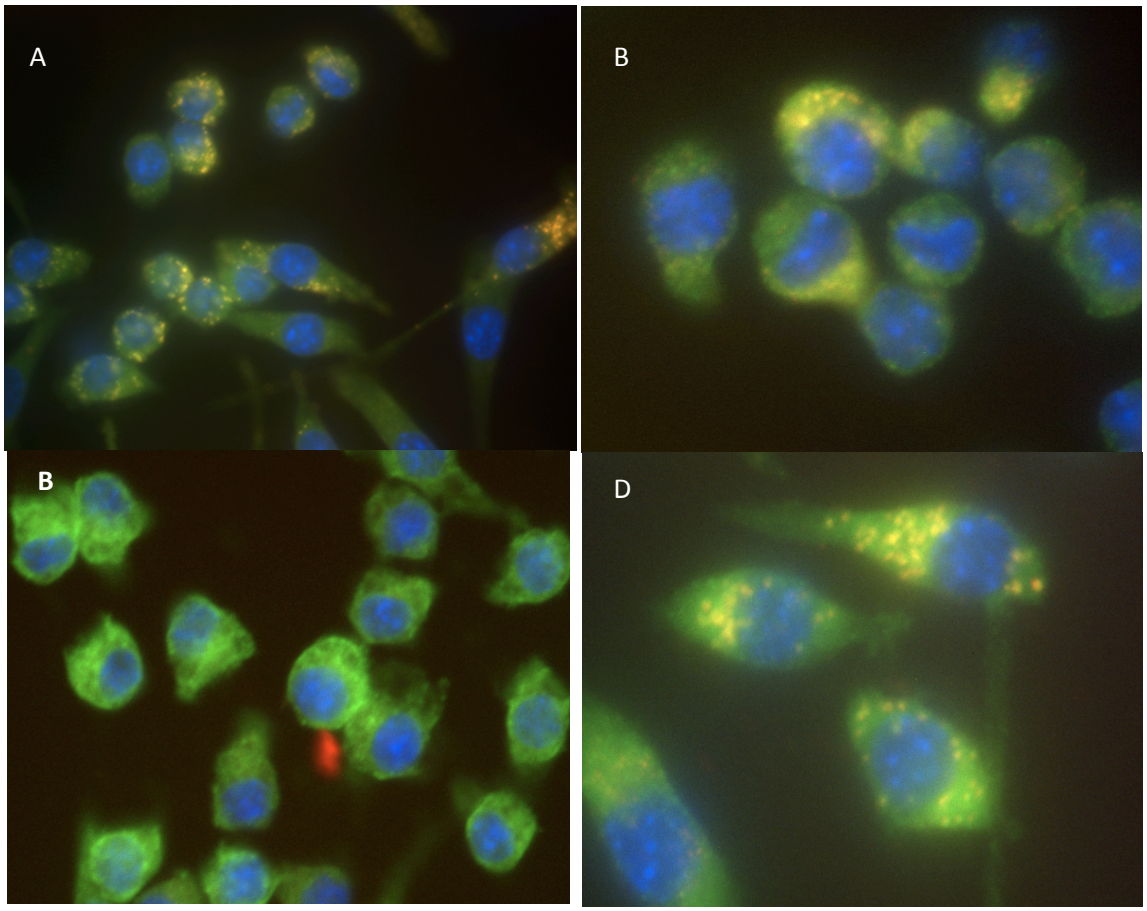

Figure 3.2: RAW 264.7 Immortalized Macrophages Endocytosis Inhibition Study. Figure A)Cells exposed to fullerenes for 3 hours, B) Chlorpromazine and fullerenes- pharmacological inhibition of clathrin mediated endocytois, C) Cytochalasin A and fullerenes- pharmacological inhibition of F-actin polymerization (caveolin mediated endocytosis, macropinocytosis, phagocytosis, and potentially clathrin mediated endocytosis if there are osmolarity differences that require utilization of actin), D) Genistein and fullerenes- pharmacological inhibition of caveolin mediated endocytosis.

	C_{60} Fullerenes	Chlorpromazine HCl + Fullerenes	Genistein + Fullerenes	Cytochalasin A + Fullerenes
Average	51.58075	45.69575	45.3595	34.452
Standard Dev.	7.485148111	12.48690982	16.52164916	9.972901717

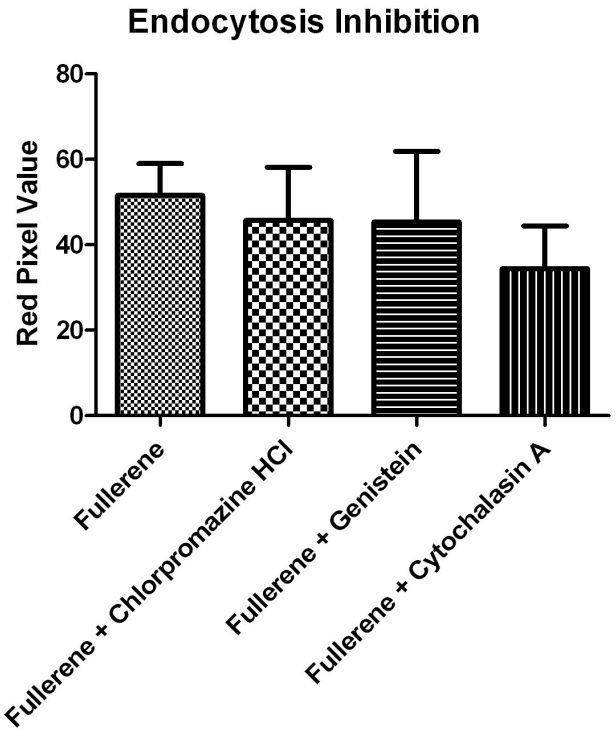

Figure 3.3: Measurement of pixels in representative images. Clathrin and caveolin mediated endocytosis appear to contribute approximately equally to endocytosis of the fullerenes however, there was no statistical significance shown in comparison to the control cells exposed only to fullerenes.

References

[1] dos Santos, T.; Varela, J.; Lynch, I.; Slavati, A.; Dawson, K.A. Effects of Transport Inhibitors on the Cellular Uptake of Carboxylated Polystyrene Nanoparticles in Different Cell Lines. *Plos ONE.* **6(9)**: e24438; 2011.

[2] Bohdanowicz, M.; Grinstein, S. Role of Phospholipids in Endocytosis, Phagocytosis, and Macropinocytosis. *Physiol Rev.* **93**: 69-106; 2013.

[3] Mousavi, S.A.; Malerod, L.; Berg, T.; Kjenken, R. Clathrin-dependent endocytosis. *Biochem J.* **377**: 1-16; 2004.

[4] Nabi, I. R.; Le, P. U. Caveolae/ raft dependent endocytosis. *JCB.* **161(4)**:673-677; 2003.

[5] Kumari, S.; MG, S.; Mayor, S. Endocytosis unplugged: multiple ways to enter the cell. *Cell Research.* **20:** 256-275; 2010.

Chapter IV

RAW 264.7 Macrophage Stress Response to C_{60} Fullerene Exposure

Introduction

Previous chapters have shown that fullerene aggregates can enter the cell through various methods: endocytosis, diffusion through the membrane, and an as yet undetermined method of entry into the nucleus. In addition to entering the cell, they are able to reside in the membrane as shown by the freeze fracture imaging in chapter II. In support of this data, Bortolous et al (2011) showed via computational modeling and EPR studies on model membranes that C_{60} fullerenes are able to reside in the lipid bilayer as single particles [1].

The ability of fullerenes to pass through as well as reside in the membrane suggests that fullerenes may have increased interactions with cellular components that could result in altered signaling and cellular function. This raises the following question: Do C_{60} fullerenes induce a stress response in macrophages at 24 hours? In order to assess the state of the cell, assays were performed to examine the inflammatory potential of the macrophages, examine metabolites that indicate oxidative stress, and observe the possible outcome of cell death (necrosis or apoptosis) after 24-hour exposure to fullerenes.

Materials & Methods

Chemicals

All cell culture supplies were purchased from Gibco (Invitrogen, Carlsbad, CA). Solid C_{60} fullerene (99.9%) were purchased from MER Corporation (Tucson, AZ). Apoptotic DNA ladder assay was purchased from Roche Applied Science (Indianapolis, IN). Caspase-Glo 3/7, Caspase-Glo 8, and Cytotox-Glo Assays were purchased from Promega (Madison, WI). PCR arrays were purchased from SA Biosciences (Valencia, CA). Annexin V and propidium iodide staining kit was purchased from Abcam (Cambridge, MA).

Fullerene Preparation

Fullerenes were prepared via the method of Deguchi et al (2001) and Spohn et al (2009).

Caspase-Glo 3/7, 8 Assays

RAW 264.7 cells were plated at 5000 cells per well in an opaque 96 well plate and allowed to adhere overnight. They were maintained in Dulbecco's Modified Eagle Medium with 10% fetal bovine serum and 1% penicillin- streptomycin- glutamate solution. The cells were grown at 37°C and 5% humidity. Cells were dosed with 0.1, 0.2, 0.5, 0.76, 1, and 4 μg/mL C_{60}s for 24 hours. Control cells were exposed to the same volume of deionized water as the 4 μg/mL cells. Positive control for the caspase 3/7 assay was staurosporine. Positive control for the caspase 8 assay was IFN-γ. Promega's protocols for these assays were followed.

Cytotox-Glo Assay

RAW 264.7 cells were plated at 5000 cells per well in an opaque 96 well plate and allowed to adhere overnight. They were maintained in Dulbecco's Modified Eagle Medium with

10% fetal bovine serum and 1% penicillin- streptomycin- glutamate solution. The cells were grown at 37°C and 5% humidity. Cells were dosed with 0.1, 0.2, 0.5, 0.76, 1, and 4 μg/mL C_{60}s for 24 hours. Control cells were exposed to the same volume of deionized water as the 4 μg/mL cells. The positive control was the lysis buffer included with the reagents. The protocol provided by Promega was followed.

Apoptotic DNA Ladder Assay

RAW 264.7 cells were allowed to adhere to flasks overnight. They were maintained in Dulbecco's Modified Eagle Medium with 10% fetal bovine serum and 1% penicillin-streptomycin- glutamate solution. The cells were grown at 37°C and 5% humidity. Flasks were dosed with 0.1, 0.2, 0.5, 0.76, 1, and 4 μg/mL C_{60}s for 24 hours. The control flask contained fresh media. The vehicle control flask contained a volume of deionized water equivalent to the volume of 4 μg/mL C_{60}s added. The positive control was lyophilized apoptotic cells supplied by Roche. The protocol provided by Roche Applied Sciences was followed.

Flow Cytometry

RAW 264.7 cells were allowed to adhere to flasks overnight. They were maintained in Dulbecco's Modified Eagle Medium with 10% fetal bovine serum and 1% penicillin-streptomycin- glutamate solution. The cells were grown at 37°C and 5% humidity. Flasks were dosed with 0.1 and 4 μg/mL C_{60}s for 24 hours. The control flask contained fresh media. The vehicle control flask contained a volume of deionized water equivalent to the volume of 4 μg/mL C_{60}s. The positive control was 500 μM hydrogen peroxide. At 24 hours, the cells were scraped and counted. 5×10^5 cells were placed in buffer supplied by Abcam. The cells were stained with annexin-FITC and propidium iodide. Flow cytometry controls were cells with no

dye, cells with only propidium iodide, and cells with only annexin. Assays were performed in the University of Michigan Flow Cytometry core. The protocol for preparation of cells was supplied by Abcam.

PCR Arrays

RAW 264.7 cells were allowed to adhere to flasks overnight. They were maintained in Dulbecco's Modified Eagle Medium with 10% fetal bovine serum and 1% penicillin-streptomycin- glutamate solution. The cells were grown at 37°C and 5% humidity. Flasks were dosed with 0.1 and 4 μg/mL C_{60}s for 24 hours. Control cells were in fresh media and positive control cells contained LPS. RNA was isolated from cells at 24 hours with an RNeasy minikit. cDNA was produced utilizing the reagents supplied by SA Biosciences. PCR arrays were prepared and run by the University of Michigan PCR array core.

Metabolic Analysis

RAW 264.7 cells were allowed to adhere to flasks overnight. They were maintained in Dulbecco's Modified Eagle Medium with 10% fetal bovine serum and 1% penicillin-streptomycin- glutamate solution. The cells were grown at 37°C and 5% humidity. Flasks were exposed to 1 and 4 μg/mL C_{60} fullerenes for 24 hours. Control cells were in fresh media. Vehicle control cells were exposed to the same volume of deionized water as was present in the 4 μg/mL C_{60} samples. Cells were removed from flasks, centrifuged at 4 °C to allow media removal, and flash frozen in liquid nitrogen. Samples collected were kept at -80°C until analysis. Samples had to be pooled to reach the necessary packed cell volume. Analysis by GC/MS, LC/MS, or LC/MS/MS was performed by Metabolon.

Statistical Analysis

Statistical analysis of Caspase 8-Glo, Caspase 3/7-Glo, and Cyotox-Glo assays were done using Levene's Statistic, Welches Test, and the Games-Howell Test. Analysis of flow cytometry data was done with ANOVA and Tukey's Test. Analysis of PCR array data was done utilizing the online software provided by SA Biosciences. Analysis of metabolic data was done utilizing Welches Test.

Results

PCR Arrays

PCR arrays showed no statistically significant changes in gene expression of inflammatory cytokines or chemokines in cells exposed to 0.1 μg/mL C_{60}s. However, cells exposed to 4 μg/mL C_{60} fullerenes showed statistically significant changes in gene expression of IL10ra, CCL4, CX3CR1, and MyD88. CX3CR1, IL10ra, and MyD88 gene expression was decreased significantly. CCL4 exhibited a significant increase in gene expression (Figure 4.1).

Analysis of Metabolic Stress

Analysis of glutathione metabolism pathways showed that exposure to 1 μg/mL C_{60} resulted in a statistically significant increase in glycine, cysteinylglycine, 2-aminobuytrate, opthalmate, and taurine. Exposure to 4 μg/mL C_{60} resulted in a statistically significant increase in cysteine and 2-aminobutyrate. Elevated levels of homocysteine, hypotaurine, cysteine-glutathione disulfide, glutathione and oxidized glutathione were observed. Decreased levels of γ-glutamyl amino acids were observed (Figure 4.2 B & C).

Analysis of Cell Death

A statistically significiant increase in caspase 8 activation was seen in cells exposed to 0.1 and 0.5 μg/mL C_{60} fullerenes. No statistically significant changes in caspase 3/7 activation or cell membrane leakage were observed in cells exposed to C_{60} fullerenes. Similarly, no DNA fragmentation was seen in cells exposed to any exposure level of fullerenes. Flow cytometry data showed no signs of statistically significant necrosis or apoptosis (early or late) in cells exposed to 0.1 or 4 μg/mL C_{60} fullerenes as compared to the control or vehicle control cells. No membrane leakage was observed at any exposure level in the luminescent cytotoxcity assay (Figures 4.3-4.7).

Discussion

Previous chapters have shown fullerenes are able to enter the cell via three mechanisms as well as enter the membrane. The membrane contains many signaling receptors and proteins that could potentially be affected by the fullerene presence within the membrane. Fullerenes could also cause direct toxicity within the cytosol. Therefore, several endpoints were assayed to determine the level of metabolic stress such as inflammation, oxidative stress and cell death.

Macrophages are specialized cells that are tasked with being the first line of defense against invading bacteria or foreign objects as well as clean up of cellular debris. As such, they secrete cytokines and chemokines, which are signaling molecules that result in recruitment of more immune competent cells to the site of the foreign material. In order to determine the extent to which the macrophages responded to the presence of fullerenes, gene arrays were utilized to monitor changes in gene expression of chemokine and inflammatory cytokines.

At 24 hours, the 0.1 μg/mL C_{60} exposed macrophages exhibited no change in gene expression for inflammatory cytokines and chemokines as compared to control cells. However, at the same time point the 4 μg/mL C_{60} exposed macrophages did show altered gene expression. MyD88 showed a statistically significant decrease in gene expression. MyD88 is involved in toll-like receptor signaling as well as interleukin signaling. The decrease in gene expression of this protein is indicative of a decrease in inflammatory processes [1].

The gene expression of CX3CR1 was decreased as well. CX3CR1 is involved in several signaling pathways such as protein kinase C, phosphatidylinositide 3 kinase, MAPK, and NF-κB. CX3CL1 binding and activation of MAPK lead to cell growth and differentiation. The decrease in CX3CR1 gene expression may be indicative of decreased cell growth. In addition, CX3CR1 activation is involved in the production of pro-inflammatory factors TNF-α and IL-8. The decrease in gene expression of CX3CR1 may be indicative of decreased inflammation [2].

A decrease in IL10ra gene expression was also observed. IL10 is an anti-inflammatory cytokine that functions through the JAK pathway [3]. The decrease in expression of IL10ra will lead to a decrease in anti-inflammatory signals. Finally, the gene expression of CCL4 was increased. CCL4 is a member of the macrophage inflammatory protein 1 family and leads to increased macrophage presence in the area of secretion. Interestingly, IL10 has been seen to down regulate the expression of CCL4 thus the finding of decreased IL10ra and increased CCL4 is consistent with the literature [4]. When taken together the data suggests that the decreased MyD88 and CX3CR1 expression leads to a decrease in inflammatory signals; however the decrease in IL10ra effectively becomes a pro-inflammatory signal, as is the increase in CCL4 (Figure 4.1).

In order to assess the effect of fullerenes on the oxidative state of the cell, metabolic analysis of the glutathione production pathways were performed. This analysis showed an increase in homocysteine levels as well as cysteine, taurine, cysteine gluthatione disulfide, oxidized glutathione and cysteinylglycine (Figure 4.2). These increases in metabolites are indicative of increases in oxidative stress. Increased cysteine levels can result in shuttling of cysteine into the taurine pathway as indicated by increased levels of taurine. The increase in taurine was statistically significant at 1 μg/mL fullerene exposure but was also extremely high at 4 μg/mL as well. Taurine is well known for protection against oxidative damage. Taurine reacts with HOCl to form Taurine-Cl which is able to suppress O_2^-, NO, TNF-α, IL-β, IL-2, IL-6, IL-8, IL-10, PGE_2, MIP-2, and MCP-1 & 2 in phagocytic cells [5].

GSH/ GSSG ratio deviations are indicative of oxidative stress. GSH reacts with hydroxyl radicals, peroxynitrite, superoxide, hydrogen peroxide, and lipid peroxides and shifts the ratio toward GSSG [6]. Alterations in GSH/GSSG can be reflected in the metabolic precursors of GSH. Figure 4.2A shows the metabolites utilized in the production of glutathione. Metabolic analysis of the glutathione metabolism pathway showed cells exposed to 1 μg/mL fullerenes had statistically significant increases in glycine, cysteinyl glycine, 2-aminobutyrate, and taurine as well as a decrease in opthalmate. Cells exposed to 4 μg/mL fullerenes showed a statistically significant increase in cysteine and 2- aminobutyrate. While these changes reflect an increase in glutathione metabolic intermediates and are potentially indicative of oxidative stress, it is necessary to look at the changes in the pathway as a whole to interpret the whole effect of fullerenes.

At both dose levels, there was an increased fold change in homocysteine levels, a precursor to cysteine. Cysteine is part of the mechanism for maintaining the levels of GSH. Typically the levels of cysteine are lower than glutamate and glycine, which are the other precursor amino acids involved in synthesis of GSH. Cysteine is often the limiting factor in GSH synthesis [6, 7]. Cysteine was elevated in 1 μg/mL C_{60} exposed cells and had a statistically significant increase at 4 μg/mL fullerenes. Glycine, another precursor to GSH, showed a statistically significant increase at 1 μg/mL and slightly elevated levels at 4 μg/mL. High levels of two out of three precursor amino acids is highly suggestive of increased GSH utilization. Elevated levels of glutathione and GSSG were observed which potentially denotes oxidative stress. Additionally, increases in cysteine glutathione disulfide at 4 μg/mL suggest increase protein GSH interaction which occurs during oxidative stress. A statistically significant increase at 1 μg/mL C_{60} and elevated levels at 4 μg/mL C_{60} in cysteinyl glycine suggest an increase in breakdown of glutathione. The overall assessment of the glutathione metabolism pathway (Figure 4.2) suggests that the cells may potentially be undergoing oxidative stress.

Future experiments should explore relationships between alterations to glutathione metabolism produced by nanomaterals and the effects of those changes on Nrf-2 activation of the antoxidant response element (ARE). Activation of ARE by Nrf-2 is one of the major mechanisms by which the cells respond to changes in oxidative stress [11]. Other cell lines show changes in expression of Nrf-2 protein levels at 1 hour and up to 48 hours after exposure to nanoparticles [12, 13, 14]. In future work, Nrf-2 protein expression should be monitored at 1, 8, 16, and 24 hours after exposure to C_{60} fullerenes via westernblot of cytosolic and nuclear fractions of RAW 264.7 immortalized macrophages.

Cell death is an excellent indicator of the extent of toxicity. There are two forms of cell death: apoptosis and necrosis. Apoptosis is tightly regulated programmed cell death that ultimately ends in the disassembly of the cell without inflammation. This process can be mitochondria dependent or independent. In mitochondrial independent apoptosis, a ligand interacts with death receptors in the membrane of the cell such as TNF or Fas. These receptors become activated and oligomerize with other TNF or Fas receptors to start the signaling that results in activation of caspase 8 that in turn activates caspases 3 and 7. Caspases 3 and 7 then result in DNA fragmentation. Mitochondria dependent apoptosis starts with the release of cytochrome C from the mitochondria resulting in activation of caspase 9 which in turn activates caspase 3. Caspase 3 then causes DNA fragmentation [9]. The result is rounding of cells, pyknosis, karyorrhexis, membrane blebbing and uptake by macrophages [10].

In order to assess apoptosis, caspase 8 and 3/7 activation was assayed (Figure 4.3 & 4.4). Caspases 3 and 7 are considered the executioner caspases as they are part of the process deemed late apoptosis and result in the direct activation of apoptosis, whereas caspase 8 is considered early apoptosis. In this study, caspase 8 was seen to have increased activation in the 0.1 and 0.5 µg/mL C_{60} exposed macrophages. No caspase 3/7 activation was seen. This suggests that at 24 hours, the C_{60}s are just starting to induce the caspase activation that will ultimately result in apoptosis. In order to support this data DNA fragmentation assays were performed. DNA fragmentation, or the breakdown of DNA by endonucleases in the nucleus, only occurs upon caspase 3/7 activation in late apoptosis. There was no DNA fragmentation occurring in the macrophages in any exposure group; therefore the results are consistent with the caspase activation assays (Figure 4.6). As further confirmation of the effects of C_{60} fullerenes on RAW

264.7 macrophages, flow cytometry was performed on annexin V-FITC and propidium iodide stained cells (Figure 4.7). This assay showed no significant differences in the amount of apoptotic or necrotic cells versus the control and vehicle control in 0.1 and 4 μg/mL C_{60} fullerene exposed cells. This confirms the results of the caspase 3/7 assay and the DNA fragmentation assay. The caspase 8 assay and the results of the flow cytometry are at odds. The high standard deviations in the caspase 8 assay suggest that the results of the caspase 8 assay are unreliable. This could be due to an interaction between the fullerenes and the assay reagents.

Another form of cellular death is necrosis. Where apoptosis is controlled and the breakdown of the cell is contained, necrosis is uncontrolled. Necrosis is not controlled by any receptors within the cell. It is characterized by the swelling of organelles, dilation of the nuclear membrane, chromatin condensation, oncosis, and breaking open of the plasma membrane which result in the release of organelles such as intact nuclei. The debris from this death pathway is released into the extra cellular space [10].

Necrosis was assayed by monitoring membrane leakage that results in leakage of enzymes in to the well plate (Figure 4.5). This assay showed no increases in membrane leakage as compared to the control. Flow cytometry data confirms that necrosis was not increased in comparison to the control and vehicle control in either the 0.1 or 4 μg/mL C_{60} fullerene exposed cells (Figure 4.7).

In summary, RAW 264.7 macrophages exposed to C_{60} fullerenes exhibit changes in gene expression of MyD88, IL-10ra, CCL4 and CX3CR1 signaling metabolic stress. The GSH/GSSG ratio, as well as the increase in cysteine, taurine, cysteine glutathione disulfide, and cysteinylglycine

suggests the cells may potentially experience increased oxidative stress upon exposure to C_{60} fullerenes. The caspase 8 luminescent assay showed increased expression of caspase 8 at 0.1 and 0.5 µg/mL C_{60} exposure; however, flow cytometry with annexin-FITC and propidium iodide showed no statistically significant changes in the amount of cells in early apoptosis. Caspase 3/7 luminescent assays, DNA fragmentation assays, and flow cytometry data all show no increase in cells undergoing late apoptosis. Both the luminescent assay for membrane leakage and the flow cytometery with propidium iodide agree that there is no increase in cells undergoing necrosis. This data suggests that while the cells are experiencing metabolic stress, this stress does not result in cell death at 24 hours.

A)

Inflammatory Cytokines & Receptors

Chemokines & Receptors

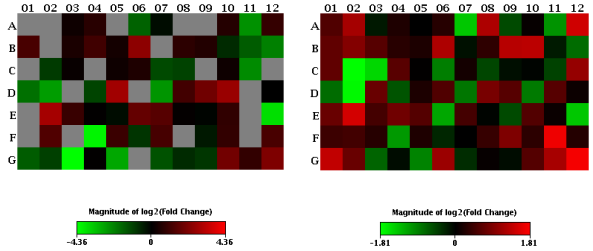

0.1 ug/mL C_{60}

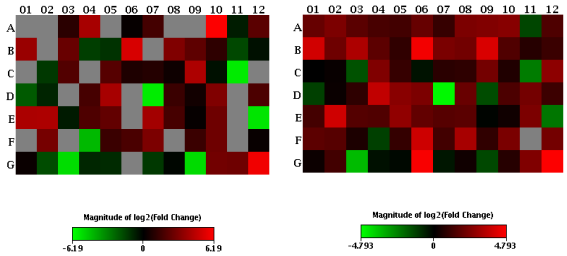

4 ug/mL C_{60}

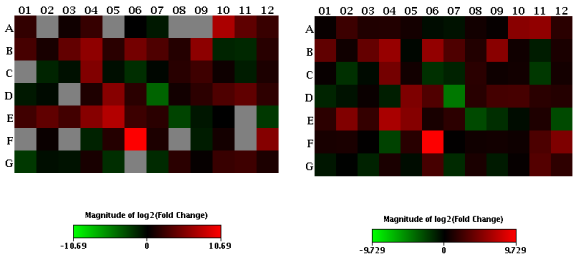

LPS

B)

	Low Dose (0.1 µg/mL)	*High Dose (4 µg/mL)*	*Positive Control LPS*
Cytokines & Receptors	*None*	*IL10ra, CCL4*	*IL1b, IL1a, IL10, CCR1, CCL2, CCL5, CXCL5*
Chemokines & Receptors	*None*	*CX3CR1, MyD88, CCL4*	*CX3CR1, CCL2, CCL4, CCL9, CCL17, CCR1, CXCL1*

Figure 4.1: Gene expression changes in RAW 264.7 immortalized macrophages exposed to 0.1 or 4 µg/mL C_{60} fullerenes (n=3). A) Heat maps showing changes in gene expression as compared to the control. B) Table of genes that had gene expression changes.

A)

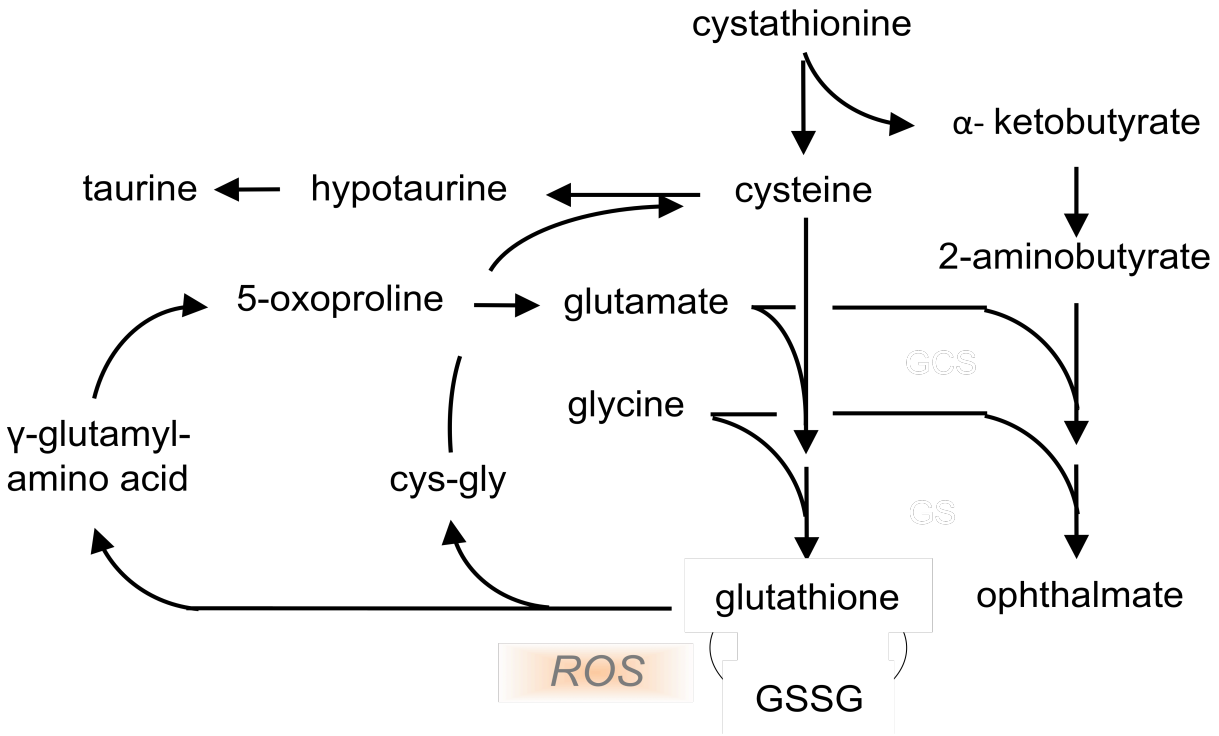

Figure 4.2 A: Glutathione Synthesis Pathway

B)

Comparison mean values significantly different: p ≤ 0.05, fold of change ≥ 1.00; p ≤ 0.05, fold of change < 1.00

Comparison mean values approaching significance: 0.05 < p < 0.10, fold of change ≥ 1.00; 0.05 < p < 0.10, fold of change < 1.00

	Welch's Two-Sample t-Test			Welch's Two-Sample t-Test					
	Vehicle	1 µg/mL C60	4 µg/mL C60	Vehicle / Untreated		1 µg/mL C60 / Vehicle		4 µg/mL C60 / Vehicle	
	Un-treated	Vehicle	Vehicle	*p*-value	*q*-value	*p*-value	*q*-value	*p*-value	*q*-value
glutathione, reduced (GSH)	0.80	1.27	1.11	0.0926	0.3331	0.1220	0.3690	0.6868	0.5710
S-methylglutathione	0.78	1.39	0.89	0.3459	0.5786	0.0617	0.3092	0.3526	0.4714
5-oxoproline	0.78	1.05	1.14	0.3681	0.6002	0.7774	0.6841	0.6437	0.5579
glutathione, oxidized (GSSG)	1.00	1.18	1.27	0.8249	0.8552	0.4364	0.5864	0.3282	0.4714
cysteine-glutathione disulfide	0.83	0.72	2.69	0.9867	0.8799	0.2375	0.4856	0.0729	0.3519
ophthalmate	0.33	1.98	0.69	0.0004	0.0215	0.0301	0.2289	0.1430	0.3971
S-lactoylglutathione	1.82	0.57	0.47	0.3854	0.6166	0.4196	0.5862	0.2078	0.4382
Cysteine	0.70	1.90	2.14	0.0983	0.3332	0.1096	0.3593	0.0302	0.3519
hypotaurine	0.52	1.92	1.03	0.0961	0.3331	0.1129	0.3645	0.7614	0.6034
Taurine	0.02	206.98	88.12	0.0296	0.1955	0.0277	0.2289	0.1748	0.4303
homocysteine	0.64	1.56	1.33	0.1473	0.3786	0.2584	0.4856	0.4758	0.5048
2-aminobutyrate	0.40	1.94	1.44	0.0005	0.0215	0.0044	0.1169	0.0773	0.3519
cysteinylglycine	0.71	1.88	1.26	0.1773	0.3912	0.0108	0.1917	0.2509	0.4382
gamma-glutamylvaline	0.72	1.08	0.71	0.0517	0.2464	0.7881	0.6841	0.0716	0.3519
gamma-glutamylleucine	0.77	1.07	0.74	0.1188	0.3437	0.7652	0.6841	0.0888	0.3519
gamma-glutamylisoleucine*	0.70	1.15	0.74	0.0721	0.2917	0.4209	0.5862	0.0626	0.3519
gamma-glutamylglutamate	1.04	0.79	1.13	0.6599	0.7726	0.0302	0.2289	0.3624	0.4745
gamma-glutamylphenylalanine	0.71	1.07	1.23	0.1055	0.3351	0.5755	0.6245	0.3901	0.4831
gamma-glutamylthreonine*	0.36	1.78	0.80	0.0003	0.0215	0.0194	0.2139	0.2486	0.4382
Glycine	0.47	1.96	1.08	0.0186	0.1455	0.0221	0.2144	0.8573	0.6235
glutamate	1.03	0.94	0.97	0.8581	0.8634	0.5713	0.6245	0.7817	0.6039

Figure 4.2 B: Metabolic Analysis of Glutathione Synthesis Pathway (n=6). Non-targeted metabolic analysis of glutathione synthesis pathway showed that exposure to C_{60} fullerenes resulted in alterations to metabolites of glutathione synthesis.

C)

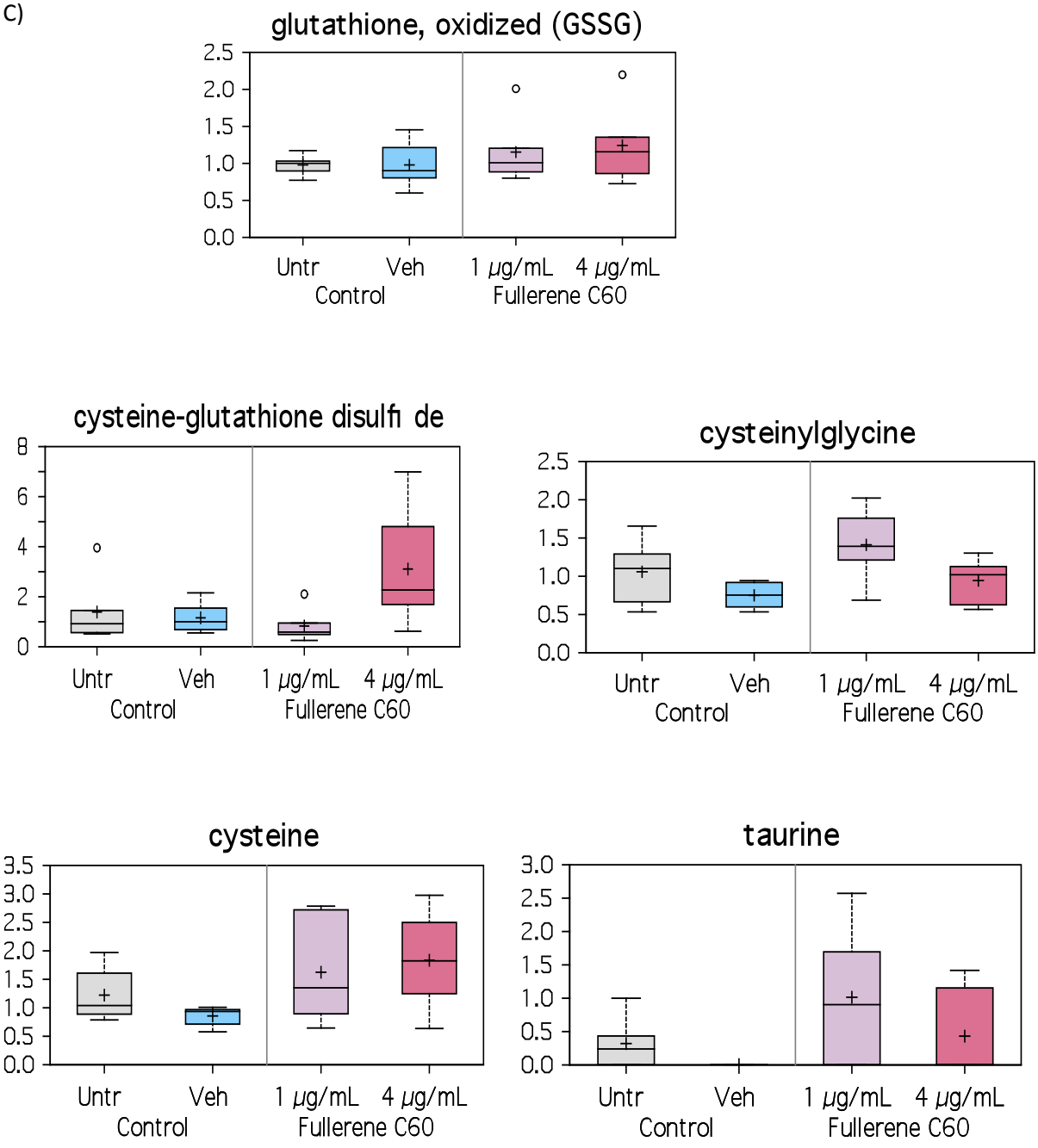

Figure 4.2 C: Analysis of Metabolites Indicative of Potential Oxidative Stress: Boxplots showing the changes in metabolites seen via non-targeted metabolic analysis of the glutathione synthesis pathway.

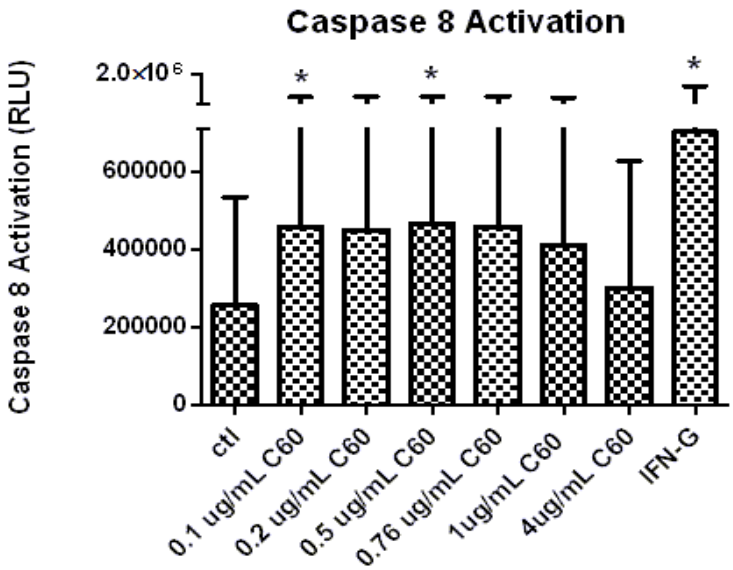

Figure 4.3: Caspase 8 activation at 24 hours in RAW 264.7 immortalized mouse macrophages. P values for 0.1 µg/mL, 0.5 µg/mL and IFN-G are 0.043, 0.042 and 0.000 respectively ($n \geq 3$). Caspase 8 is activated during the early stages of apoptosis. The high standard deviations suggest that the fullerenes interfere with this assay; therefore no conclusions can be drawn from this data.

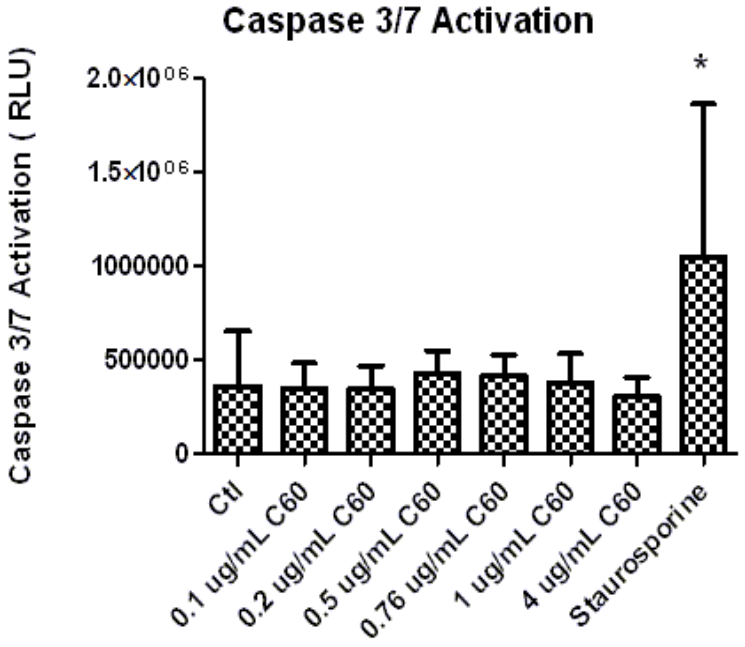

Figure 4.4: Caspase 3/7 Activation at 24 hours in RAW 264.7 macrophages ($n \geq 3$). There were no statistically significant changes in casapse 3/7 activation except for the positive control. This data suggests that the cells are not in the late apoptotic stage at 24 hours.

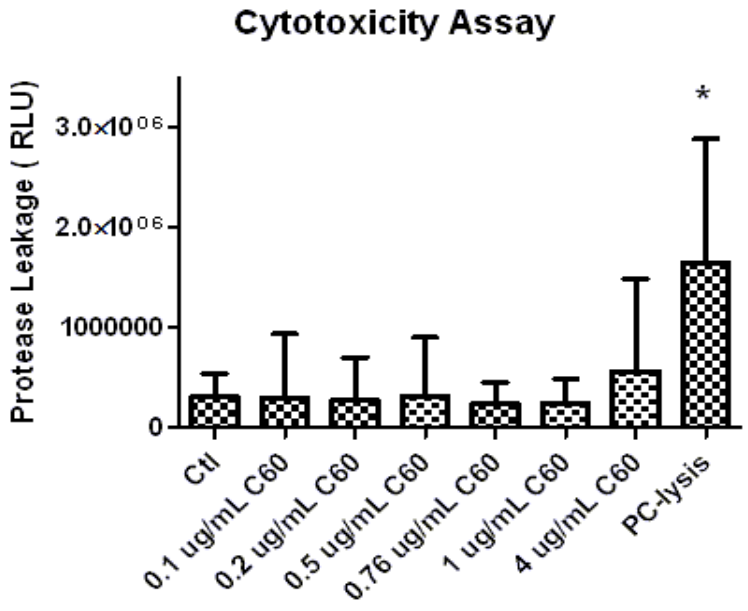

Figure 4.5: Cytotoxicity assay measuring protease leakage from the cells at 24 hours in RAW 264.7 macrophages($n \geq 3$). Cells undergoing necrotic cell death have leaky membranes that allow the leakage of intracellular contents into the extracellular space. This assay showed no statistically significant changes at any of the C_{60} fullerene doses examined suggesting that the fullerenes do not induce necrosis at 24 hours.

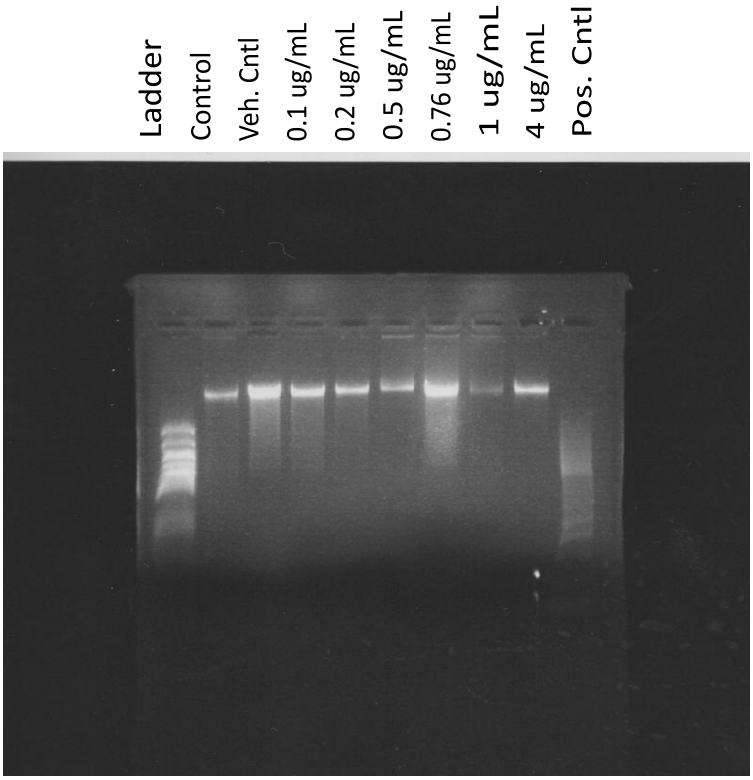

Figure 4.6: DNA fragmentation assay in DNA from RAW 264.7 immortalized macrophages isolated at 24 hours (n=3). DNA fragmentation occurs as part of late apoptosis. Comparision of the DNA from fullerene exposed cells to the positive control for DNA fragmentation show that at 24 hours the cells do not appear to be undergoing DNA fragmentation. This data agrees with the caspase 3/7 that exposure to fullerenes for 24 hours at any of the doses ranges examined does not appear to lead to apoptosis.

A

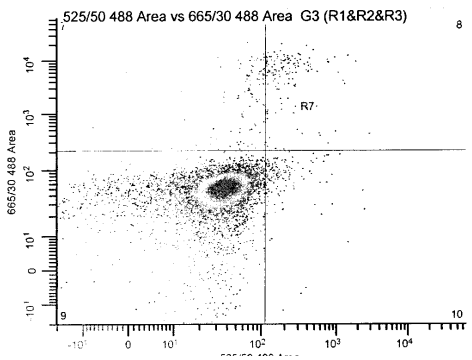
525/50 488 Area vs 665/30 488 Area G3 (R1&R2&R3)
R7
665/30 488 Area

B

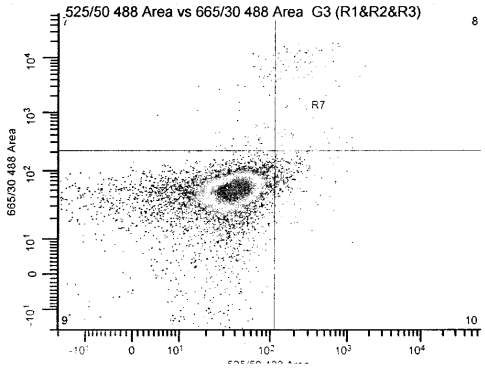
525/50 488 Area vs 665/30 488 Area G3 (R1&R2&R3)
R7
665/30 488 Area

C

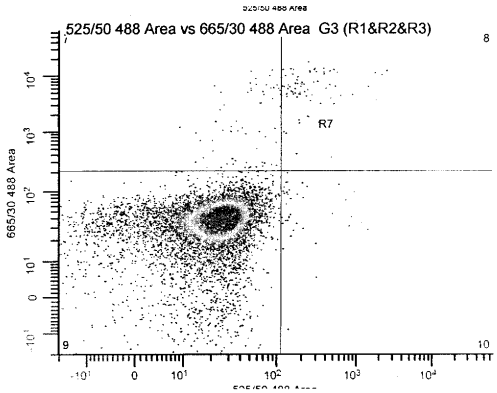
525/50 488 Area vs 665/30 488 Area G3 (R1&R2&R3)
R7
665/30 488 Area

D

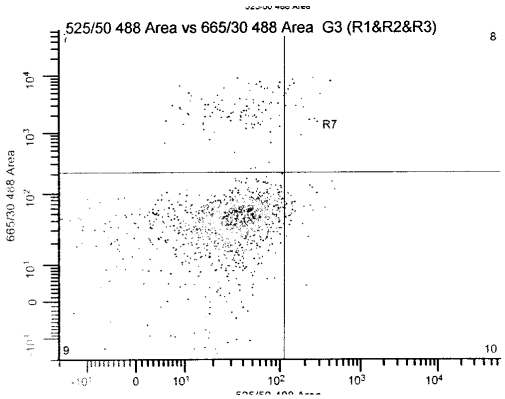
525/50 488 Area vs 665/30 488 Area G3 (R1&R2&R3)
R7

E

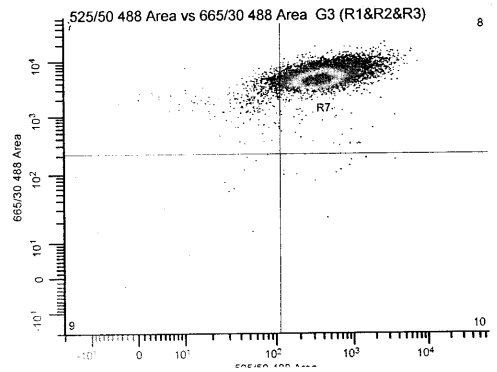
525/50 488 Area vs 665/30 488 Area G3 (R1&R2&R3)
R7
665/30 488 Area

F)

	Control	*Veh.Control*	*0.1 µg/mL*	*4 µg/mL*	*H_2O_2*
Live	*71.853*	*83.223*	*83.443*	*71.43*	*5.257*
Necrotic	*8.027*	*3.623*	*23.14*	*13.24*	*16.233*
Early Apoptotic	*7.583*	*4.46*	*6.06*	*4.287*	*0.093*
Late Apoptotic	*12.533*	*8.693*	*20.46*	*11.077*	*78.413*

G)

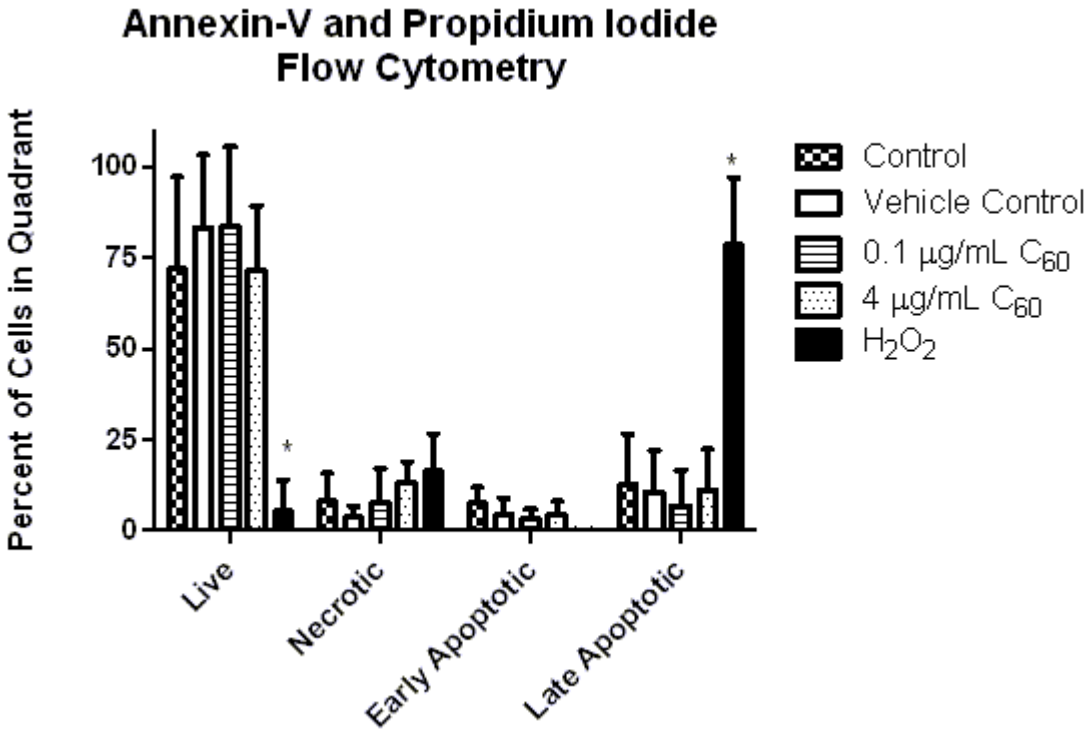

Figure 4.7: Flow cytometry plots on Annexin-FITC and propidium iodide stained cells after 24 hour incubation with fullerenes. A) Control cell, B) Vehicle Control, C) 0.1 µg/mL C_{60} fullerenes, D) 4 µg/mL C_{60} fullerenes, E) Hydrogen Peroxide, F) Average percentage of cells in each quadrant (n=3) G) Statistical Analysis and Graph. The flow cytometry data verifies the results seen in the caspase 3/7, DNA fragmentation, and membrane leakage assays. No signs of apoptosis or necrosis were seen at 24 hours in RAW 264.7 macrophages exposed to the low or high dose of fullerenes.

References

[1] Bortolus, M.; Parisio, G.; Maniero, A. L.; Ferrarini, A. Monomeric Fullerenes in Lipid Membranes: Effects of Molecular Shape and Polarity. *Langmuir*. **27:** 12860-12568; 2011.

[2] Stievano, L.; Provan, E.; Amadori, A. C and CX_3C Chemokines: Cell Sources and Physiopathalogical Implications. *Crit Rev in Immunol*. **24 (3)**: 205-228; 2004.

[3] Riley, J. K.; Takeda, K.; Akira, S; Schreiber, R. D. Interleukin-10 receptor signaling through the JAK-STAT pathway. Requirement for two distinct receptor-derived signals for anti-inflammatory action. *J. Biol. Chem.* **274 (23)**: 16513-21; 1999.

[4] Maurer, M; von Stebut, E. *Macrophage Inflammatory Protein-1*. Int J Biochem Cell Bio. **36 (10)**: 1882-7; 2004.

[5] Kim, C; Cha. Y-N. Production of Reactive Oxygen and Nitrogen Species in Phagocytes is Regulated by Taurine Chloramine. *Adv. Exp. Med. Biol.* **643:** 463-72; 2009.

[6] Griffith, O. W. *Biologic and Pharmacologic Regulation of Mammalian Glutathione Synthesis.* Free Radical Biology & Medicine. **27 (9/10)**: 922-925; 1999.

[7] Wu, G; Fang, Y-Z; Yang, S; Lupton, J; Turner, N. D. *Glutathione Metabolism and Its Implications for Health*. Journal of Nutrition. **134**: 489-492; 2004.

[8] Circu, M. L; Aw, T. Y. *Glutathione and Modulation of Cell Apoptosis*. Biochemica et Biophysica Acta. **1823:** 1767-1777; 2012

[9] Shultz, D. R.; Harrington, W. J. Apoptosis: Programmed Cell Death at a Molecular Level. *Semin Arthritis Rheu*. **32 (6)**: 345-369; 2003.

[10] Vandenabeele, P. I.; Galluzzi, L.; Berghi, T. V.; Kroemer, G. Molecular mechanisms of necroptosis: an ordered cellular explosion. *Nature*. **11:** 700-714; 2010.

[11] Niture, S. K.; Khatri, R.; Jaiswal, A. K. Regulation of Nrf-2- an update. *Free Radic. Biol. Med.* Epub ahead of print; 2013.

[12] Diabate, S.; Bergfeldt, B.; Plaumann, D.; Ubel, C.; Weiss, C. Anti-oxidative and inflammatory responses induced by fly ash and carbon black in ung epithelial cells, *Anal. Bioanal. Chem.* **401**: 3197-3212; 2011.

[13] Berg, J.M.; Romoser, A. A.; Figueroa, D. E.; West, C.S.; Sayes, C. M. Comparative cytological responses of lung epithelial and pleural mesothelial cells following *in vitro* exposure to nanoscale SiO_2. *Toxicol. In vitro.* **27**: 24-33; 2013.

[14] Piret, J-P. Jacques, D.; Audinot, J-N.; Mejia, J.; Boilan, E.; Noel, F.; Fransslet, M.; Demazy, C.; Lucas, S.; Saout, C.; Toussaint, O. Copper (II) oxide nanoparticles penetrate into HepG2 cells, exert cytotoxicity via oxidative stress and induce proinflammatory response. *Nanoscale.* **4**: 7168-7184; 2012.

Chapter V

Analysis of Cell Proliferation Alterations in RAW 264.7 Macrophages after C_{60} Fullerene Exposure

Introduction

In previous chapters it was determined that fullerenes induce cellular stress. Cellular stress can result in cell survival or cell death. Cellular stress occurs and then the cell must respond to the stress. Cell survival occurs if the cellular response to the stress resolves the issue. If the problem is persistent, the cell activates death pathways [1]. In this study, the cellular stressors are C_{60} fullerenes. In the previous chapter it was determined that at 24 hours the cell is stressed, but cell death does not occur. This suggests that the cell is in the process of trying to repair the cell.

During cellular stress, homeostasis within the cell is disrupted. Cellular processes such as cell proliferation may be altered [1]. For cell proliferation to occur, the cell requires a number of metabolic processes to provide the building blocks (Figure 5.1). Among these important metabolic processes are nucleotide synthesis and lipid synthesis [2]. Interestingly, computational modeling already in the literature suggests that fullerenes are able to form complexes with dsDNA and cause alterations in DNA structure [3, 4]. In order to elucidate the effect of fullerenes on RAW 264.7 immortalized macrophages, cell proliferation assays were

utilized as well as metabolic analysis of pathways relied upon in cell proliferation such as nucleotide catabolism and lipid metabolism pathways.

Materials & Methods

Chemicals

All cell culture supplies were purchased from Gibco (Invitrogen, Carlsbad, CA). Solid C_{60} fullerenes (99.9%) were purchased from MER Corporation (Tucson, AZ). BrdU assay was purchased from Roche Applied Science (Indianapolis, IN).

Fullerene Preparation

Fullerenes were prepared via the method of Deguchi et al (2001) and Spohn et al (2009).

Cell Proliferation Assay

RAW 264.7 cells were plated at 5000 cells per well in a 96 well plate. Cells were given time to adhere to the plate. At the time of dosing (0 hours) BrdU was added to the well. Control cells contain fresh media and BrdU. Vechicle control cells contain media, filtered deionized water in the same volume as the 4 µg/mL fullerenes, and BrdU. Cells were exposed to 0.1, 0.2, 0.5, 0.76, 1, and 4 µg/mL C_{60} fullerenes in water, media, and BrdU. Positive control was LPS and IFN-γ. The protocol supplied by Roche Applied Sciences was followed.

Metabolic Analysis

RAW 264.7 cells were allowed to adhere to flasks overnight. Flasks were exposed to 1 and 4 µg/mL C_{60} fullerenes for 24 hours. Control cells were in fresh media. Vehicle control cells were exposed to the same volume of deionized water as was present in the 4 µg/mL C_{60}

samples. Cells were removed from flasks, centrifuged at 4 °C to allow media removal, and flash frozen in liquid nitrogen. Samples collected were kept at -80°C until analysis. Samples had to be pooled to reach the necessary packed cell volume. Analysis by GC/MS, LC/MS, or LC/MS/MS was performed by Metabolon.

Statistical Analysis

Statistical analysis of BrdU data was done utilizing Levene's Statistic, Welches Test, and the Games-Howell Test. Analysis of metabolic data was done utilizing Welches Test.

Results

Cell Proliferation

BrdU Assays showed a statistically significant decrease in RAW 264.7 immortalized macrophages exposed to 1 and 4 μg/mL C_{60} fullerenes for 24 hours (Figure 5.2).

Nucelotide Catabolism Analysis

Metabolic analysis of the nucleic acid catabolism pathway showed that after exposure to 4 μg/mL C_{60} fullerenes there were statistically significant increases in adenine, urate, allantoin, cytidine 5'-monophosphate (5'-CMP) as compared to the vehicle control. Additional nonsignificant increases in uridine 5'-monophosphate, uridine, adenosine 5'-monophosophate, cytidine, and guanosine 5'-monophosphate were observed. Non-significant decreases seen were inosine, hypoxanthine, xanthosine, xanthine, guanosine, and uracil. 1 μg/mL C_{60} exposure resulted in a statistically significant increase in adenine and decrease in uracil in comparison to the vehicle control. Nonsignificant increases were observed in urate and allantoin. Nonsignificant decreases were detected in uridine 5'-monophosphate, guanosine 5'-

monophosphate, cytidine 5'-monophosphate (5'-CMP), cytidine, adenosine, adenylosuccinate, inosine, hypoxanthine, xanthosine, xanthine, and guanosine (Figure 5.3).

Lipid Metabolism Analysis

Metabolic analysis of lipid metabolism pathways showed that at 1 μg/mL C_{60} fullerene exposure resulted in a statistically significant alteration in 2-oleoylglycerophosphoinositol, 2-stearoylglycerophosphocholine, myo-inositol, glycerol, 1,3-dipalmitoylglycerol, 4-hydroxybutyrate, 7-dehydrocholesterol, glycerol-3-phosphate, propionylcarnitine, butyrylcarnitine, 3-dehydrocarnitine, acetyl carnitine, glycerophosphorylcholine, and oleoylglycerol. Additional alterations at this exposure level with $0.05<p< 0.1$ were palmitoylcarnitine, scyllo-inositol, 1-palmitoylglycerol, docosatrienoate, and deoxycarnitine. Exposure to 4 μg/mL fullerenes resulted in statistically significant alterations in 2-oleoylglycerophosphoinositol, 2-stearoylglycerophosphocholine, myo-inositol, glycerol, 1,3-dipalmitoylglycerol, 4-hydroxybutyrate, 7-dihydrocholesterol, 1-myristoglycerol, 1-palmitoylglycerol, 1-stearoylglycerol, phosphoethanolamine, linolenate (α or γ), myristate, palmitoleate, and 10-heptadecenoate. Additional alterations at this exposure level with $0.05<p< 0.1$ were glycerol-3-phosphate, linoleate, dihomolinolenate, myristoleate, palmitate, nonadecanoate, 15-methylpalmitate, inositol-1-phosphate, 1-palmitoylglycerophosphoinositol, 7-dehydrocholesterol, and choline phosphate (Figure 5.4).

Discussion

In previous chapters it was shown that fullerenes alter inflammatory response and GSH metabolism; however, no signs of cell death were seen at 24 hours. This may indicate that

fullerenes are seen by the cell as stressors. Cellular stress can result in changes in the cell such as DNA damage or oxidative stress. The result of the stressor must be repaired. If the cell is successful it is able to survive, if not the cell activates cell death pathways [1].

DNA damage is a classical form of cellular stress. If the cell senses single or double strand breaks, repair mechanisms are activated which in turn activate p53. P53 then either results in p21 activation and quiescence, which would result in a decrease in cell proliferation or activation of apoptosis [1]. Another classical form of cellular stress is oxidative stress. The cell may respond to this stressor by utilizing common radical scavengers or antioxidants such as GSH, taurine, or urate.

In order to investigate the effect of fullerenes as a cellular stressor cell proliferation was assayed. In addition, metabolic analysis was conducted on nucleotide catabolism and lipid metabolism in an effort to further determine the role of stress created by C_{60} fullerenes. The results of cell proliferation assays performed on RAW 264.7 macrophages showed a statistically significant decrease in cell proliferation at 24 hours in the two highest doses, 1 and 4 μg/mL C_{60} fullerenes. These results may be indicative of DNA damage that results in quiescence and/or alterations in important metabolic pathways necessary to promote cell growth and survival.

In addition to the possible cellular quiescence due to cellular stress, computational simulations in the literature have shown that DNA in solution exposed to individual C_{60} fullerenes forms energetically stable structures specifically with the free ends and minor grooves of dsDNA [1]. The study found that B-form DNA was not as affected as A-form DNA in which fullerenes were able to deform the stacking angles as well as penetrate the DNA from the free end and force the base pairs apart [3]. Interestingly, the fullerene models showed that a

fullerene is the correct size to enter the position of a missing base pair and form a stable structure [3]. A more recent study confirmed the ability of C_{60} fullerenes to position itself in the minor groove via computational modeling. This study found that fullerenes prefer GC pairs to AT pairs [4]. It was determined that the fullerenes were also able to bind to the major groove of RNA and preferred GC rich sections [4]. In both studies, the binding of the fullerenes to DNA could potentially alter the proliferation and DNA repair mechanisms of the cell. Therefore, in an effort to elucidate the mechanism behind the decrease in proliferation, a metabolic analysis of the nucleotide catabolism pathway was conducted.

Analysis of nucleic acid catabolism showed a statistically significant decrease in uracil in the 1 μg/mL fullerene exposed cells. The 4 μg/mL exposed cells had a statistically significant increase in CMP, urate, and allantoin. Statistically significant accumulation of adenine in both 1 and 4 μg/mL C_{60} exposed cells occurred. In the 1 μg/mL exposed cells, there was a non-significant increase in urate and allantoin that agrees with the statistically significant findings of the 4 μg/mL samples. In addition, 1 μg/mL fullerene exposed cells had non-significantly decreased amounts of UMP, CMP, cytidine, adenosine, adenyl succinate, and GMP. The 4 μg/mL fullerene exposed cells exhibited a non-significant decrease in uracil. Additionally, in both 1 and 4 μg/mL C_{60} exposed cells there was a general non-statistically significant trending decrease in inosine, hypoxanthine, xanthine, xanthosine, and guanosine as compared to the vehicle control (Figure 5.3).

The decrease in the amounts of inosine, hypoxanthine, xanthine, xanthosine, guanosine appear to be the result of increased production of urate and allantoin. These alterations were observed in both the 1 and 4 μg/mL C_{60} fullerene exposure. The higher concentration of

fullerenes resulted in a statistically significant increase in urate and allantoin suggesting that that this is a dose dependent increase. The reaction between radicals and urate results in the production of allantoin, a commonly utilized marker for oxidative stress in biological samples like urine or blood [5]. Therefore, the exposure of cells to C_{60} fullerenes and the resulting increase in allantoin is indicative of an increased production of potential oxidative stress[5].

The increased urate and allantoin may be the cause of the decreased proliferation. Catabolism of purines to guanine, adenine, and hypoxanthine are able to be recycled and reincorporated into purine production. Once the purines are broken down to xanthine and urate, they are no longer able to be recycled thus the cell expends energy to replace the purines for nucleotide synthesis [6].

As previously mentioned, lipids are necessary for cellular proliferation. Lipids and glycerophospholipids (GPL) have many roles in signaling as well as membrane structure. Glycerophospholipids such as phosphatidylcholine (PC), phosphatidylethanolamine (PE), phosphatidylserine (PS), and cardiolipin (CL) are among the most abundant lipids found in cellular membranes as key components of their structure. In addition to structural components, GPL are involved in eicosanoid formation and signaling by production of arachadonic acid and phosphatidylinositol (PI) is known to mediate protein association in the membrane [7]. Additionally, GPLs are involved in ceramide and sphingomeylin signaling which is known to regulate cell proliferation and death outcomes. [8].

Figure 5.4 shows the lipid metabolism pathways that result in PI, CL, PC, PE, PS, and the ceramide pathway. Glycerol-3-phosphate (G-3-P) leads to the production of phosphatidic acid (PA), which is converted to CL, PI, or PG via CDP-diacylglycerol. PA can also be converted to

diacylglycerol (DAG) and then to PC and PE, which can result in PS [7]. Ceramide is produced from serine and palmitate and can be metabolized to sphingosine and broken down to a final product hexadecenal and phosphoethanolamine [8]. Ceramide metabolism is well known for control of cell survival. Ceramide and sphingosine can lead to decreased proliferation and apoptotic signaling whereas metabolism of sphingosine to sphingosine-1-phosphate leads to cell proliferation and survival pathways [8].

In order to elucidate if alterations in lipid metabolism were resulting in altered growth, RAW 264.7 macrophages were exposed to 1 or 4 μg/mL fullerenes for 24 hours and lipid metabolism was investigated. The results of the lipid metabolism study show increases in 1, 3-dipalmitoylglycerol, glycerol-3-phosphate, and glycerophosphorylcholine at 1 μg/mL fullerene exposure. These increases suggest that there is a breakdown in glycerophospholipids resulting in increased pools of these metabololites utilized in producing glycerophospholipids. At 4 μg/mL fullerene exposure, an increase in 1,3-dipalmitoylglycerol, phosphoethanolamine, and glycerol-3-phosphate as well as a decrease in choline phosphate was seen. This also suggests that there is a breakdown of glycerophospholipids. Additionally, the increase in phosphoethanolamine signals that ceramide may have increased break down which would have implications on cell proliferation and survival. Ceramide concentrations have been linked to DNA damage within the cell and are a known response to cellular stress [8].

Phosphatidylinositol (PI) is a metabolite of CDP-DAG as seen in Figure 5.4. In the cell, phosphatidylinositol is a major signaling lipid. Myo-inositol is a key component of PI. In both 1 and 4 μg/mL fullerene exposure there was an increase in myo-inositol suggesting a breakdown

of phosphatidylinositol. These results taken together with the other GPL alterations show that exposure to fullerenes alters GPL signaling and composition within the cellular membrane.

Consistent with the changes in GPL, there was an increase in the metabolites linolenate (α or γ), linoleate, and dihomolinolenate after exposure to 4 μg/mL C_{60} fullerenes. These metabolites are the precursors to eicosanoids such as arachidonic acid which in turn lead to prostaglandins and promote inflammation (Figure 5.4) [9]. The increase in precursors of eicosanoids suggest changes to the structure of the membrane since they are a result of the cleavage of GPLs [10].

β-oxidation in the mitochondria results in funneling of acetyl-CoA into the TCA cycle. Production of acetyl-CoA is another critical regulator of cell proliferation [2]. In order for this to occur, free fatty acids are converted to acyl-CoA in the cytosol, which is transported by carnitine into the mitochondria at which point acetyl-CoA is produced. In addition to being necessary for transport of acyl-CoA into the mitochondria, carnitine is also a good antioxidant [11]. Cells exposed to 1 μg/mL fullerenes showed an increase in propionylcarnitine, butyrylcarnitine, 3-dehydrocarnitine, acetyl carnitine, palmitoylcarnitine, and a decrease in deoxycarnitine. In comparison to the fold changes exhibited by the cells exposed to 4 μg/mL fullerenes and the change exhibited by the vehicle control versus the control cells it appears that the vehicle has skewed the results due to the fact that the 1 μg/mL exposure contains less water than the vehicle control. The vehicle control is water in a volume equivalent to the volume received by the cells in the 4 μg/mL fullerene exposure. In most cases like the BrdU assay and flow cytometry data for example, the control (cells containing only media) and the

vehicle control behave similarly. Figure 5.2 shows that at 24 hours the vehicle and the control have the same level of growth and the growth curves maintain the same overall shape. The metabolic study, however, shows at that level there is more of a vehicle effect at 24 hours. In the metabolism data changes induced by the vehicle are not usually statistically significant when compared to the control. The results of the metabolic data in control cells and vehicle control cells, as well as the fullerene exposed cells, allow a determination of how much of the significance in the exposed cells is driven by the vehicle. In the case of lipid metabolism, the vehicle had an effect on the significance of the carnitine pathway that resulted in opposing trends in the 1 μg/mL and 4μg/mL exposed cells. This is due to the fact that the 1 μg/mL fullerene dose contains less water; however, because there is a large observable change in the vehicle to untreated comparison it is obvious that in this case the difference in the amount of water in the vehicle is driving most of the effect. The 4 μg/mL exposed cells had a decrease in carnitine metabolites but the effect was small ($p>0.1$). Additionally, the nucleotide catabolism pathway showed opposing effects in UMP, CMP, cytidine, and GMP. The opposing effects were a result of the same cause as in the lipid metabolism results. There was an increase in fold change between the vehicle and control showing that the vehicle was driving the change and a comparison of the vehicle control to 1 μg/mL exposed cells was not a proper comparison. However, the change exhibited in the 4 μg/mL sample was driven by the fullerenes because it is being compared to an equivalent amount of vehicle. Comparison of the vehicle control to the 4 μg/mL fullerene exposed cells highlights the fact that while the vehicle may be driving some of the response, in most cases the fullerenes exposure results in an increased or decreased response over that of the vehicle.

In summary, C_{60} fullerenes are able to cause statistically significant decreases in proliferation at 1 and 4 µg/mL. An increase in nucleotide catabolism was detected as well as an increase in urate and allantoin, which suggests that fullerenes are potentially increasing oxidative stress and the cells are degrading a larger portion of nucleotides than normal to produce urate, which can act as a radical scavenger. This is confirmed by the production of allantoin from urate. This catabolism to urate depletes the pathway of nucleotides that are normally recycled and leads to usage of increased energy, which may potentially lead to the decreased levels of proliferation seen in this study. Additionally it was determined that fullerene exposure alters lipid metabolism of key structural and signaling lipids in the membrane such as the ceramide pathway that is known for activation in times of cellular stress and having an effect on cellular survival.

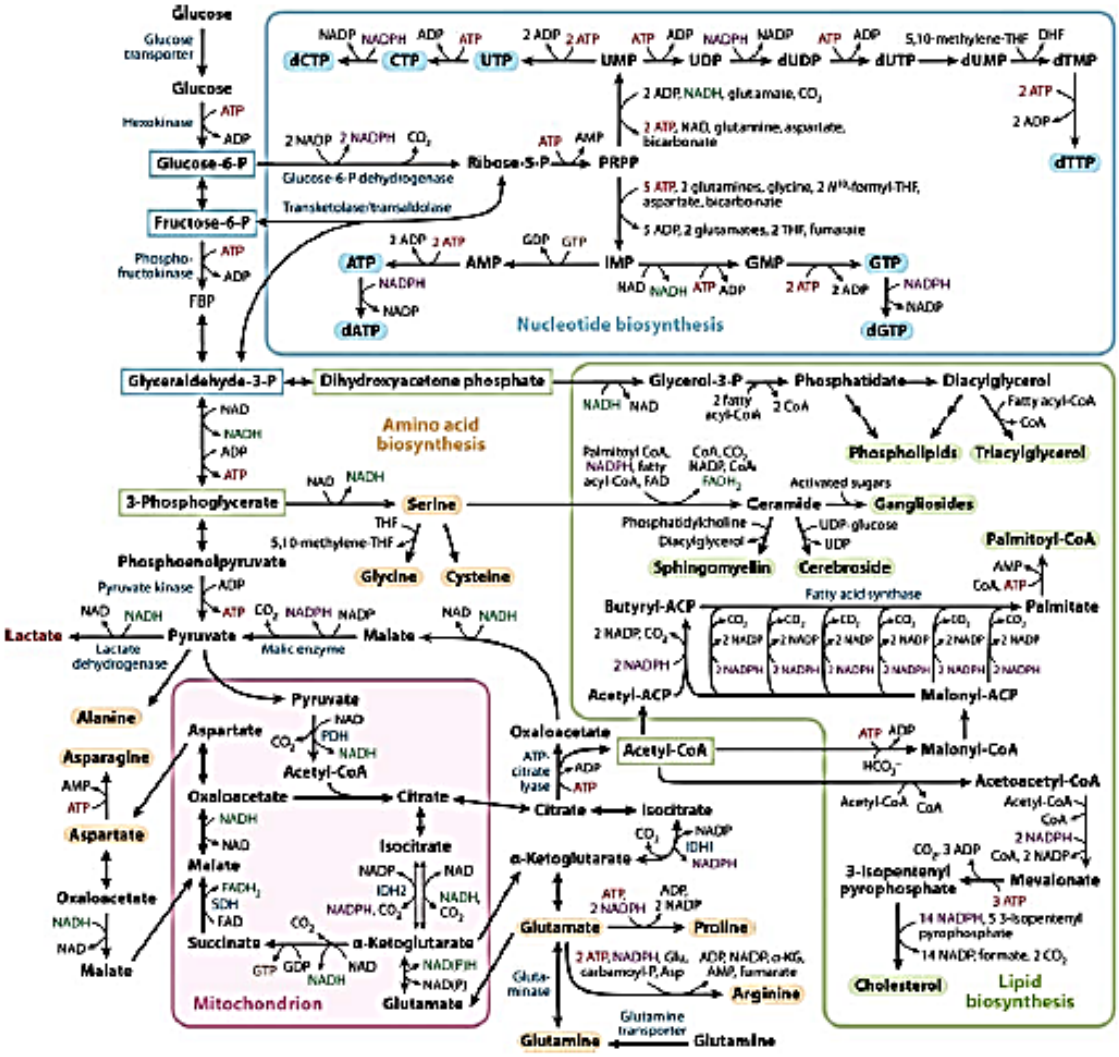

Figure 5.1: Cellular metabolism pathways in which alterations occur during proliferation [2]. Pathways of interest in this thesis are the lipid synthesis pathway as well as the nucleotide catabolism pathway.

A.

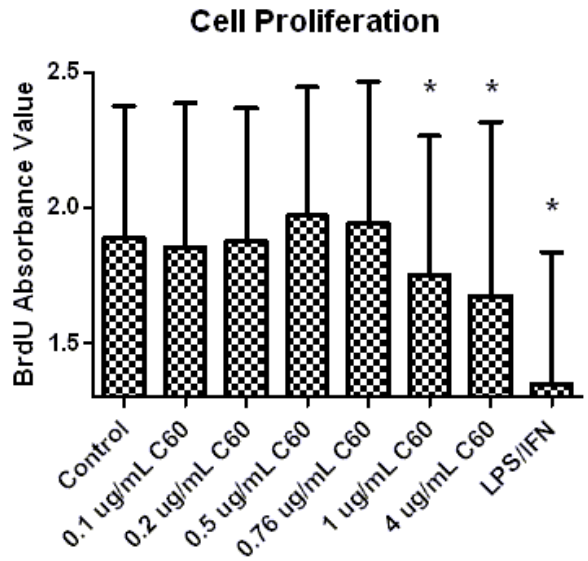

B.

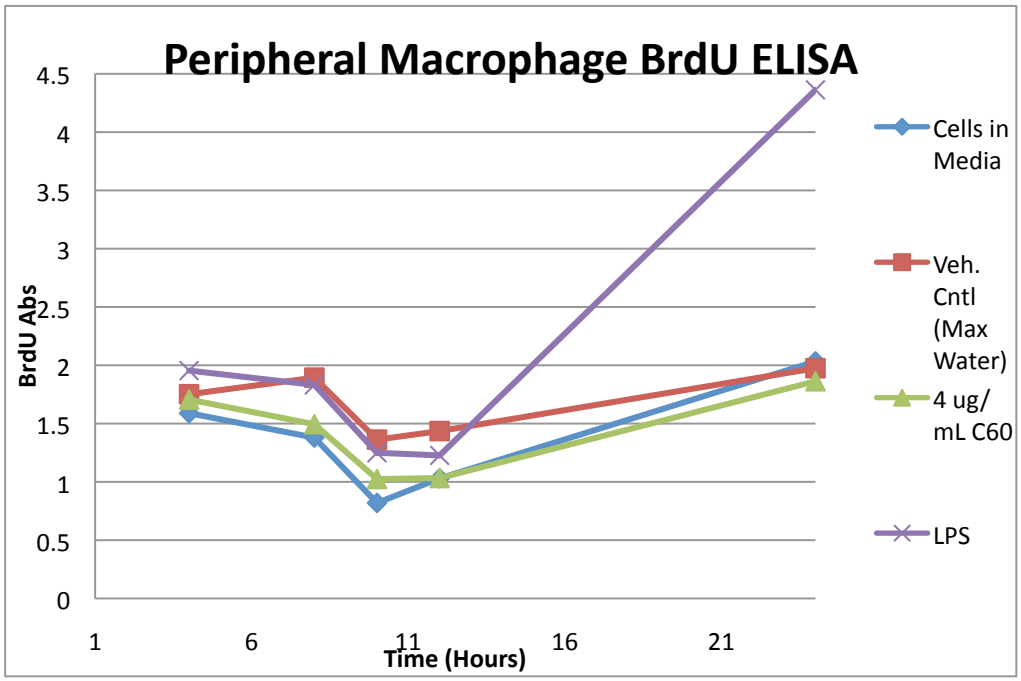

Figure 5.2: Analysis of cell proliferation by BrdU ElISA. A) Cell proliferation at 24 hours. P values for 1 µg/mL and 4 µg/mL are 0.03 and 0.01 respectively ($n \geq 3$). B) Cell growth curve over the course of 24 hours. Decreased cellular proliferation was observed at the two highest concentrations of C_{60} fullerene exposure in this study. A cellular growth curve was obtained to determine that the vehicle did not result in the decreased proliferation seen in figure 5.2A.

A)

Comparison mean values significantly different:
$p \leq 0.05$, fold of change ≥ 1.00
$p \leq 0.05$, fold of change < 1.00

Comparison mean values approaching significance
$0.05 < p < 0.10$, fold of change ≥ 1.00
$0.05 < p < 0.10$, fold of change < 1.00

Biochemical Name	Fold of Change			Statistical Values					
	Welch's Two-Sample t-Test			Welch's Two-Sample t-Test					
	Vehicle Un-treated	1 µg/mL C60 Vehicle	4 µg/mL C60 Vehicle	Vehicle / Untreated		1 µg/mL C60 / Vehicle		4 µg/mL C60 / Vehicle	
				p-value	*q*-value	*p*-value	*q*-value	*p*-value	*q*-value
xanthine	1.11	0.82	0.92	0.5716	0.7209	0.2714	0.4943	0.7046	0.5770
xanthosine	0.94	0.91	0.77	0.5625	0.7173	0.5867	0.6270	0.1951	0.4382
hypoxanthine	1.03	0.80	0.99	0.8750	0.8635	0.2598	0.4856	0.9302	0.6334
inosine	1.32	0.79	0.90	0.6794	0.7778	0.5591	0.6245	0.9660	0.6441
adenine	0.67	1.50	1.27	0.0033	0.0613	0.0156	0.2072	0.0423	0.3519
adenosine	1.28	0.91	1.12	0.5570	0.7138	0.9621	0.7244	0.6285	0.5561
adenosine 3'-monophosphate (3'-AMP)	1.48	0.66	1.06	0.0370	0.2131	0.0199	0.2139	0.8766	0.6235
adenosine 5'-monophosphate (AMP)	1.02	1.06	1.96	0.8693	0.8635	0.7159	0.6604	0.0771	0.3519
adenosine 5'-diphosphate (ADP)	1.18	0.90	1.09	0.3393	0.5713	0.5104	0.6025	0.8744	0.6235
adenylosuccinate	1.55	0.89	1.08	0.2158	0.4399	0.8195	0.6841	0.6016	0.5502
guanosine	1.37	0.96	0.82	0.6786	0.7778	0.9811	0.7244	0.9294	0.6334
guanosine 5'- monophosphate (5'-GMP)	1.17	0.86	2.24	0.8376	0.8552	0.8534	0.6865	0.0526	0.3519
guanosine 5'-diphospho-fucose	1.19	0.82	0.91	0.1008	0.3351	0.0781	0.3146	0.4198	0.4986
urate	0.72	1.18	1.54	0.1649	0.3912	0.2576	0.4856	0.0339	0.3519
allantoin	0.65	1.26	1.47	0.1245	0.3492	0.1571	0.4032	0.0398	0.3519
cytidine	2.21	0.54	1.24	0.0960	0.3331	0.1542	0.4008	0.5109	0.5227
cytidine 5'-monophosphate (5'-CMP)	1.21	0.79	1.67	0.4902	0.6901	0.3397	0.5314	0.0287	0.3519
orotate	0.73	1.78	1.47	0.9255	0.8797	0.2327	0.4852	0.4509	0.4992
thymidine	1.10	1.15	1.00	0.9226	0.8797	0.5049	0.6025	0.8641	0.6235
thymidine 5'-monophosphate	1.20	0.95	1.15	0.7230	0.8168	0.9675	0.7244	0.3349	0.4714
uracil	0.94	0.75	0.92	0.8433	0.8552	0.0434	0.2570	0.5527	0.5360
uridine	1.46	0.68	1.12	0.2107	0.4399	0.1994	0.4569	0.6184	0.5561
pseudouridine	0.83	1.06	1.24	0.2677	0.4961	0.3134	0.5099	0.0923	0.3519
2'-deoxyuridine	1.12	1.14	1.06	0.5283	0.7030	0.3077	0.5083	0.5955	0.5498
uridine monophosphate (5' or 3')	1.43	0.87	2.15	0.6543	0.7726	0.9862	0.7244	0.0906	0.3519
uridine 5'-triphosphate (UTP)	1.64	0.72	0.37	0.1845	0.3992	0.2955	0.5027	0.0479	0.3519
methylphosphate	0.84	1.21	1.01	0.3019	0.5290	0.2307	0.4852	0.8489	0.6235

B)

	1 µg/mL C_{60}	4 µg/mL C_{60}
Statistically Significant	↓ Uracil ↑ Adenine	↑ CMP ↑ Adenine ↑ Urate ↑ Allantoin
Statistically Non-Significant	↑ Urate ↑ Allantoin ↓ UMP ↓ CMP ↓ Cytidine ↓ Adenosine ↓ Adenylo-Succinate ↓ Inosine ↓ Hypoxanthine ↓ Xanthosine ↓ Xanthine ↓ GMP ↓ Guanosine	↑ UMP ↑ Uridine ↑ Cytidine ↑ AMP ↑ GMP ↓ Inosine ↓ Hypoxanthine ↓Xanthosine ↓ Xanthine ↓ Uracil

c)

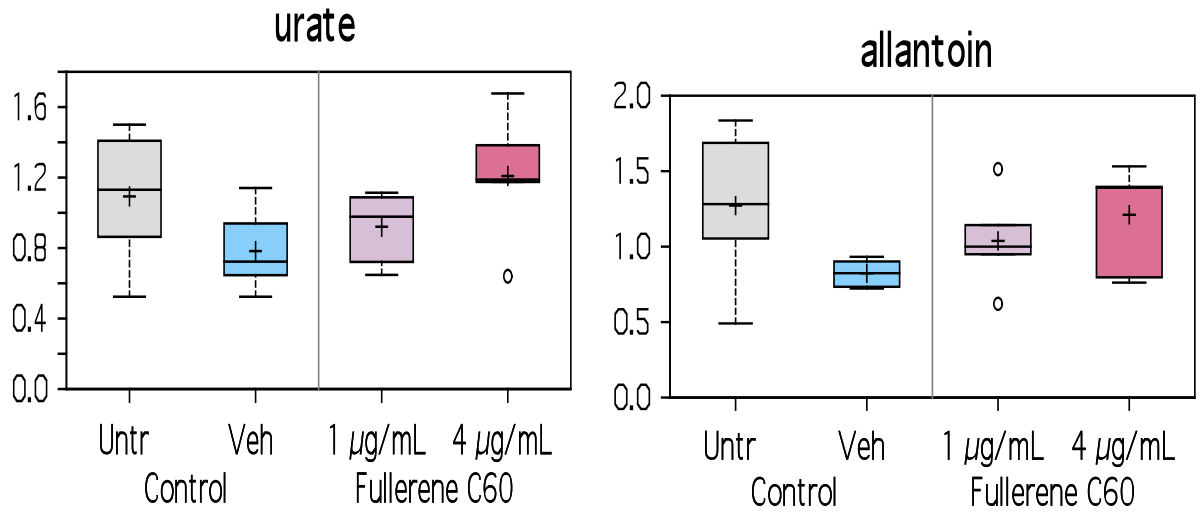
urate
1.6
1.2
0.8
0.4
0.0
Untr
Veh
1 µg/mL
4 µg/mL
Control
Fullerene C60
allantoin
2.0
1.5
1.0
0.5
0.0
Untr
Veh
1 µg/mL
4 µg/mL
Control
Fullerene C60

D)

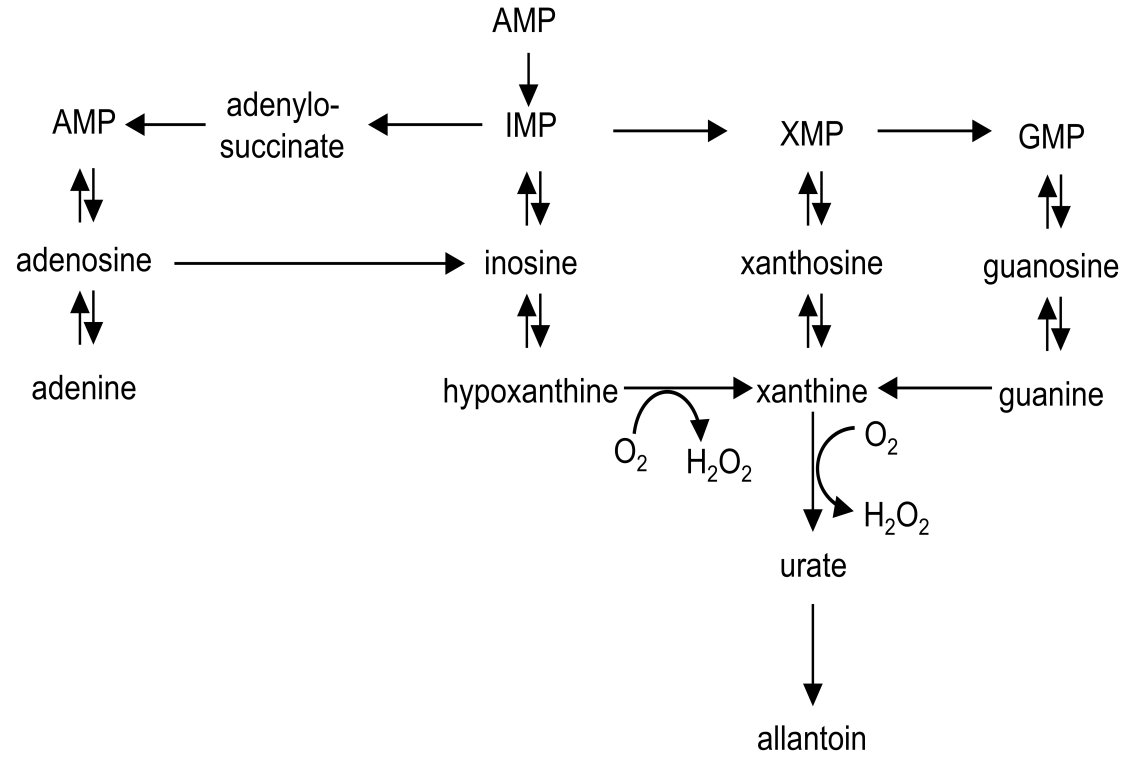

Figure 5.3: Alterations to DNA nucleotide catabolism: A) Nontargeted metabolomics data for the nucleotide catabolism pathway (n=6). B) Results of the metabolomics data showing purines that exhibited altered catabolism by organized by dose and statistical significance C) Boxplot of important alterations in nucelotide catabolism D) Nucleotide catabolism pathway diagram. The results of this study showed decreased amounts of purines that lead to the production of urate and increasing amounts of urates conversion to allantoin. Allantoin is utilized in the literature as a marker of oxidative stress [5]

A)

Comparison mean values significantly different:
- $p \leq 0.05$, fold of change ≥ 1.00
- $p \leq 0.05$, fold of change < 1.00

Comparison mean values approaching significance:
- $0.05 < p < 0.10$, fold of change ≥ 1.00
- $0.05 < p < 0.10$, fold of change < 1.00

	Fold of Change			Statistical Values					
	Welch's Two-Sample t-Test			Welch's Two-Sample t-Test					
Biochemical Name	Vehicle Untreated	1 µg/mL C60 Vehicle	4 µg/mL C60 Vehicle	Vehicle / Untreated		1 µg/mL C60 / Vehicle		4 µg/mL C60 / Vehicle	
				p-value	*q*-value	*p*-value	*q*-value	*p*-value	*q*-value
linoleate (18:2n6)	1.04	1.04	2.30	0.6750	0.7778	0.8792	0.6914	0.0532	0.3519
linolenate [alpha or gamma; (18:3n3 or 6)]	1.03	1.01	2.23	0.7781	0.8447	0.9787	0.7244	0.0469	0.3519
dihomo-linolenate (20:3n3 or n6)	1.05	0.97	1.81	0.7569	0.8447	0.8694	0.6902	0.0643	0.3519
eicosapentaenoate (EPA; 20:5n3)	0.89	0.92	1.57	0.8164	0.8552	0.8745	0.6902	0.3052	0.4579
docosapentaenoate (n3 DPA; 22:5n3)	0.96	0.99	1.15	0.9544	0.8799	0.9414	0.7216	0.3807	0.4799
docosapentaenoate (n6 DPA; 22:5n6)	1.10	0.84	0.90	0.9501	0.8799	0.8388	0.6865	0.9281	0.6334
docosahexaenoate (DHA; 22:6n3)	0.89	1.02	1.17	0.6502	0.7718	0.8038	0.6841	0.3297	0.4714
caproate (6:0)	1.05	0.83	0.70	0.8719	0.8635	0.5721	0.6245	0.2565	0.4382
pelargonate (9:0)	0.96	0.92	1.16	0.9916	0.8799	0.6512	0.6379	0.8041	0.6070
caprate (10:0)	1.15	0.87	1.21	0.4863	0.6901	0.5112	0.6025	0.5881	0.5456
myristate (14:0)	1.01	1.01	1.38	0.9486	0.8799	0.8569	0.6865	0.0363	0.3519
myristoleate (14:1n5)	1.09	0.94	1.47	0.4820	0.6901	0.6212	0.6320	0.0667	0.3519
pentadecanoate (15:0)	1.04	1.09	1.01	0.7674	0.8447	0.6354	0.6320	0.9843	0.6462
palmitate (16:0)	1.10	0.99	1.32	0.3920	0.6233	0.8481	0.6865	0.0520	0.3519
palmitoleate (16:1n7)	1.01	1.00	1.74	0.8340	0.8552	0.9087	0.7042	0.0263	0.3519
margarate (17:0)	1.09	0.93	1.18	0.5404	0.7030	0.6118	0.6304	0.2619	0.4382
10-heptadecenoate (17:1n7)	1.14	0.98	1.60	0.4320	0.6584	0.9063	0.7042	0.0295	0.3519
stearate (18:0)	1.04	0.97	1.15	0.7619	0.8447	0.8268	0.6841	0.2755	0.4382
oleate (18:1n9)	0.98	0.96	1.14	0.7854	0.8447	0.3919	0.5665	0.3353	0.4714
cis-vaccenate (18:1n7)	0.97	0.96	1.00	0.6488	0.7718	0.5355	0.6219	0.8460	0.6235
13-octadecenoate (18:1n5)	0.87	1.21	1.02	0.4541	0.6819	0.4760	0.5980	0.9808	0.6462
nonadecanoate (19:0)	0.86	0.97	1.38	0.4553	0.6819	0.8283	0.6841	0.0943	0.3519
10-nonadecenoate (19:1n9)	1.10	0.92	1.09	0.1540	0.3890	0.1513	0.3979	0.5055	0.5219
eicosenoate (20:1n9 or 11)	1.08	0.89	1.09	0.5498	0.7083	0.2685	0.4943	0.4234	0.4988
dihomo-linoleate (20:2n6)	1.11	0.89	1.13	0.4303	0.6584	0.3531	0.5414	0.2463	0.4382
mead acid (20:3n9)	1.08	0.91	1.14	0.8174	0.8552	0.8170	0.6841	0.4291	0.4992
arachidonate (20:4n6)	1.04	1.06	1.68	0.9419	0.8799	0.6372	0.6320	0.1508	0.4022
erucate (22:1n9)	1.00	1.10	1.00	0.9447	0.8799	0.5747	0.6245	0.8846	0.6239

docosatrienoate (22:3n3)	1.03	0.85	0.96	0.6631	0.7729	0.0681	0.3134	0.6300	0.5561
adrenate (22:4n6)	1.12	0.73	0.78	0.7805	0.8447	0.3728	0.5556	0.4549	0.4992
4-hydroxybutyrate (GHB)	0.60	5.38	20.11	0.0148	0.1408	0.0018	0.0781	0.0013	0.1652
2-hydroxystearate	0.81	1.00	0.98	0.1454	0.3786	0.9957	0.7244	0.8724	0.6235
2-hydroxypalmitate	0.88	0.84	0.88	0.2346	0.4597	0.2838	0.5027	0.4393	0.4992
2-hydroxyglutarate	1.14	0.74	2.12	0.3138	0.5352	0.1160	0.3688	0.1102	0.3852
oleamide	1.76	1.00	1.46	0.4171	0.6511	0.6989	0.6549	0.2532	0.4382
palmitic amide	1.62	0.75	1.01	0.9074	0.8787	0.9270	0.7143	0.7672	0.6036
stearamide	1.58	0.80	0.79	0.5125	0.7022	0.9945	0.7244	0.8441	0.6235
15-methylpalmitate (isobar with 2-methylpalmitate)	1.23	0.88	1.31	0.2356	0.4597	0.4540	0.5864	0.0849	0.3519
17-methylstearate	0.77	1.02	1.29	0.1589	0.3912	0.8154	0.6841	0.1342	0.3906
prostaglandin D2	2.38	0.60	1.44	0.2134	0.4399	0.6395	0.6320	0.2518	0.4382
propionylcarnitine	0.60	1.73	0.77	0.0359	0.2131	0.0434	0.2570	0.3290	0.4714
butyrylcarnitine	0.26	3.12	1.15	0.0011	0.0365	0.0035	0.1080	0.8454	0.6235
isovalerate	1.41	0.80	1.87	0.0062	0.0870	0.1257	0.3690	0.2043	0.4382
deoxycarnitine	0.56	1.34	1.03	0.0064	0.0870	0.0518	0.2865	0.8019	0.6070
carnitine	0.75	1.23	0.83	0.1557	0.3894	0.2589	0.4856	0.2693	0.4382
3-dehydrocarnitine*	0.61	1.37	0.93	0.0062	0.0870	0.0410	0.2570	0.7041	0.5770
acetylcarnitine	0.57	1.56	0.68	0.0106	0.1246	0.0271	0.2289	0.1206	0.3852
palmitoylcarnitine	0.49	1.74	0.63	0.0372	0.2131	0.0750	0.3146	0.2564	0.4382
oleoylcarnitine	0.48	1.76	0.62	0.0827	0.3088	0.1388	0.3791	0.1314	0.3883
choline phosphate	1.47	0.69	0.65	0.1083	0.3351	0.1277	0.3690	0.0936	0.3519
ethanolamine	0.91	0.98	1.00	0.4868	0.6901	0.6715	0.6417	0.8870	0.6239
phosphoethanolamine	0.57	1.22	3.03	0.0541	0.2472	0.3491	0.5390	0.0327	0.3519
glycerol	0.84	3.34	8.62	0.8401	0.8552	0.0205	0.2139	0.0074	0.3519
choline	1.16	0.83	0.98	0.6187	0.7589	0.5951	0.6270	0.9858	0.6462
glycerol 3-phosphate (G3P)	0.43	1.81	2.15	0.0014	0.0412	0.0140	0.2059	0.0736	0.3519
glycerophosphorylcholine (GPC)	0.36	1.96	1.20	0.0134	0.1382	0.0277	0.2289	0.5420	0.5322
cytidine 5'-diphosphocholine	1.10	1.33	1.48	0.5697	0.7209	0.4995	0.6025	0.2864	0.4436
cytidine-5'-diphosphoethanolamine	1.27	0.80	1.23	0.2334	0.4597	0.2532	0.4856	0.8683	0.6235
myo-inositol	0.46	1.43	1.20	0.0006	0.0215	0.0419	0.2570	0.0258	0.3519
inositol 1-phosphate (I1P)	1.13	1.02	0.77	0.4013	0.6341	0.9960	0.7244	0.0860	0.3519
scyllo-inositol	0.26	1.88	1.40	0.0002	0.0215	0.0524	0.2865	0.1153	0.3852
1-palmitoylglycerophosphoethanolamine	1.67	0.90	1.16	0.1210	0.3463	0.8556	0.6865	0.4398	0.4992
2-palmitoylglycerophosphoethanolamine*	2.26	0.95	1.60	0.0220	0.1664	0.7814	0.6841	0.2581	0.4382
1-stearoylglycerophosphoethanolamine	1.77	0.82	0.99	0.1728	0.3912	0.7764	0.6841	0.7769	0.6039
1-oleoylglycerophosphoethanolamine	1.66	0.91	1.35	0.0718	0.2917	0.7808	0.6841	0.3734	0.4799
2-oleoylglycerophosphoethanolamine*	1.39	1.04	1.51	0.2656	0.4958	0.8966	0.6999	0.1559	0.4051

1-arachidonoylglycerophosphoethanolamine*	1.36	1.39	1.57	0.1722	0.3912	0.4445	0.5864	0.1561	0.4051
2-arachidonoylglycerophosphoethanolamine*	1.34	0.96	0.77	0.8748	0.8635	0.5665	0.6245	0.7889	0.6060
2-docosapentaenoylglycerophosphoethanolamine*	1.49	1.04	1.00	0.5207	0.7022	0.6526	0.6379	0.7636	0.6034
2-docosahexaenoylglycerophosphoethanolamine*	1.32	1.07	0.83	0.7702	0.8447	0.4539	0.5864	0.6989	0.5770
1-stearoylglycerophosphoglycerol	1.20	1.03	0.93	0.2512	0.4792	0.9682	0.7244	0.6853	0.5710
2-stearoylglycerophosphoglycerol*	1.31	0.96	0.73	0.2041	0.4346	0.6710	0.6417	0.1441	0.3971
1-myristoylglycerophosphocholine	1.77	1.12	0.75	0.2532	0.4795	0.5630	0.6245	0.5762	0.5449
2-myristoylglycerophosphocholine*	0.95	1.47	1.15	0.9944	0.8799	0.1837	0.4399	0.4107	0.4930
1-palmitoylglycerophosphocholine	1.14	1.40	1.58	0.4142	0.6506	0.3563	0.5414	0.1801	0.4377
2-palmitoylglycerophosphocholine*	1.80	1.52	1.29	0.5129	0.7022	0.3344	0.5279	0.3632	0.4745
1-palmitoleoylglycerophosphocholine*	1.90	1.09	0.83	0.5196	0.7022	0.6646	0.6417	0.9860	0.6462
2-palmitoleoylglycerophosphocholine*	1.29	1.20	0.78	0.6739	0.7778	0.4099	0.5784	0.5135	0.5227
1-stearoylglycerophosphocholine	1.21	1.29	1.10	0.8731	0.8635	0.4360	0.5864	0.4848	0.5087
2-stearoylglycerophosphocholine*	**0.51**	**3.28**	**3.07**	0.0506	0.2459	0.0055	0.1235	0.0086	0.3519
1-oleoylglycerophosphocholine	1.13	1.10	1.35	0.5385	0.7030	0.4399	0.5864	0.2526	0.4382
2-oleoylglycerophosphocholine*	1.36	1.06	1.27	0.9696	0.8799	0.6406	0.6320	0.5164	0.5227
2-arachidonoylglycerophosphocholine*	1.24	1.22	0.73	0.8124	0.8552	0.4708	0.5980	0.5554	0.5360
1-docosapentaenoylglycerophosphocholine*	1.54	1.34	1.51	0.6104	0.7559	0.4024	0.5755	0.3013	0.4577
2-docosapentaenoylglycerophosphocholine*	1.37	1.22	1.02	0.6246	0.7625	0.4295	0.5864	0.9524	0.6418
2-docosahexaenoylglycerophosphocholine*	1.24	1.32	0.79	0.8879	0.8663	0.3260	0.5217	0.6107	0.5559
1-palmitoylglycerophosphoinositol*	0.99	1.51	**2.69**	0.7871	0.8447	0.2244	0.4844	0.0812	0.3519
1-stearoylglycerophosphoinositol	1.42	1.21	1.85	0.1744	0.3912	0.6241	0.6320	0.2773	0.4382
2-stearoylglycerophosphoinositol*	**1.69**	1.28	2.02	0.0531	0.2472	0.6184	0.6320	0.3427	0.4714
1-oleoylglycerophosphoinositol*	**1.47**	1.08	1.78	0.0741	0.2917	0.5900	0.6270	0.2784	0.4382
1-arachidonoylglycerophosphoin	1.37	1.52	2.10	0.3788	0.6097	0.4236	0.5862	0.2763	0.4382

ositol*									
2-oleoylglycerophosphoinositol*	0.88	1.43	1.99	0.3105	0.5336	0.0386	0.2569	0.0105	0.3519
1-palmitoylplasmenylethanolamine*	1.76	1.02	1.15	0.1167	0.3417	0.7912	0.6841	0.5990	0.5502
2-eicosapentaenoylglycerophosphoethanolamine*	1.21	0.86	0.74	0.8919	0.8669	0.9463	0.7228	0.4361	0.4992
1-myristoylglycerol (1-monomyristin)	0.87	1.11	1.67	0.5386	0.7030	0.7094	0.6602	0.0141	0.3519
1-palmitoylglycerol (1-monopalmitin)	0.84	1.32	1.64	0.2739	0.5004	0.0984	0.3459	0.0240	0.3519
2-palmitoylglycerol (2-monopalmitin)	1.12	1.09	1.27	0.4882	0.6901	0.6344	0.6320	0.3750	0.4799
1-stearoylglycerol (1-monostearin)	0.88	1.14	1.30	0.3705	0.6002	0.3281	0.5217	0.0293	0.3519
1-oleoylglycerol (1-monoolein)	1.01	1.43	1.45	0.5766	0.7209	0.0333	0.2289	0.3809	0.4799
2-oleoylglycerol (2-monoolein)	1.78	0.87	0.87	0.1613	0.3912	0.6948	0.6549	0.6667	0.5691
1-linoleoylglycerol (1-monolinolein)	0.99	0.99	2.66	0.9935	0.8799	0.9853	0.7244	0.1214	0.3852
2-linoleoylglycerol (2-monolinolein)	0.98	0.93	1.71	0.9803	0.8799	0.9714	0.7244	0.3104	0.4621
1-arachidonylglycerol	0.81	0.97	1.37	0.4852	0.6901	0.9884	0.7244	0.3823	0.4799
2-arachidonoyl glycerol	0.90	0.93	0.96	0.6015	0.7485	0.8030	0.6841	0.6814	0.5710
1-dihomo-linolenyl-glycerol (1-monoeicosatrienoin)	1.93	0.70	1.07	0.9118	0.8792	0.6111	0.6304	0.7701	0.6036
1-docosahexaenoylglycerol (1-monodocosahexaenoin)	0.80	0.91	1.71	0.4809	0.6901	0.5399	0.6219	0.2525	0.4382
1,2-dipalmitoylglycerol	0.92	1.32	1.03	0.7730	0.8447	0.1383	0.3791	0.7969	0.6070
1,3-dipalmitoylglycerol	0.59	2.19	1.70	0.1712	0.3912	0.0001	0.0228	0.0195	0.3519
sphinganine	0.87	1.45	1.14	0.4789	0.6901	0.1260	0.3690	0.6868	0.5710
sphingosine	1.01	1.06	0.89	0.9758	0.8799	0.8514	0.6865	0.5432	0.5322
palmitoyl sphingomyelin	0.97	1.03	0.93	0.7552	0.8447	0.7007	0.6549	0.5516	0.5360
stearoyl sphingomyelin	0.97	1.08	1.36	0.9877	0.8799	0.6661	0.6417	0.1275	0.3852
cholesterol	1.04	0.99	0.96	0.5057	0.7022	0.7943	0.6841	0.5375	0.5321
7-dehydrocholesterol	0.71	2.36	2.48	0.1749	0.3912	0.0027	0.0971	0.0017	0.1652
7-alpha-hydroxycholesterol	0.98	0.85	0.72	0.9975	0.8799	0.2773	0.5009	0.0698	0.3519
7-beta-hydroxycholesterol	0.88	0.93	0.89	0.6432	0.7718	0.5342	0.6219	0.4058	0.4930
7-ketocholesterol	0.78	1.22	1.03	0.3489	0.5798	0.5617	0.6245	0.9068	0.6287
lanosterol	0.99	1.58	2.86	0.8393	0.8552	0.3233	0.5217	0.1196	0.3852
desmosterol	1.14	1.22	1.32	0.2590	0.4869	0.6296	0.6320	0.4648	0.5018

B)

	1 μg/mL Fullerene	4 μg/mL Fullerene
Statistically Significant (p<0.05)	↑2-oleoylglycerophosphoinositol ↑2-stearoylglycerophosphocholine ↑myo-inositol ↑glycerol ↑1,3-dipalmitoylglycerol ↑4-hydroxybutyrate ↑7-dehydrocholesterol ↑glycerol-3-phosphate ↑propionylcarnitine ↑butyrylcarnitine ↑3-dehydrocarnitine ↑acetyl carnitine ↑glycerophosphorylcholine ↑oleoylglycerol	↑2-oleoylglycerophosphoinositol ↑2-stearoylglycerophosphocholine ↑myo-inositol ↑glycerol ↑1,3-dipalmitoylglycerol ↑4-hydroxybutyrate ↑7-dihydrocholesterol ↑1-myristoglycerol ↑1-palmitoylglycerol ↑1-stearoylglycerol ↑ phosphoethanolamine ↑linolenate (α or γ) ↑myristate ↑palmitoleate ↑10-heptadecenoate
Non-Statistically Significant (0.05<p<0.1)	↑palmitoylcarnitine ↑scyllo-inositol ↑1-palmitoylglycerol ↓docosatrienoate ↓deoxycarnitine	↑glycerol-3-phosphate ↑linoleate ↑dihomolinolenate ↑myristoleate ↑palmitate ↑nonadecanoate ↑15-methylpalmitate ↑inositol-1-phosphate ↑1-palmitoylglycerophosphoinositol ↓7-dehydrocholesterol ↓choline phosphate

C)

	1 µg/mL Fullerene	4 µg/mL Fullerene
B-oxidation	↑propionylcarnitine ↑butyrylcarnitine ↑3-dehydrocarnitine ↑acetyl carnitine ↑palmitoylcarnitine ↓deoxycarnitine ↓docosatrienoate	↑myristate ↑palmitoleate ↑10-heptadecenoate ↑myristoleate ↑palmitate ↑nonadecanoate
Membrane Dynamics	↑myo-inositol ↑1, 3-dipalmitoylglycerol ↑glycerol-3-phosphate ↑glycerophosphorylcholine ↑scyllo-inositol	↑myo-inositol ↑1,3-dipalmitoylglycerol ↑ phosphoethanolamine ↑glycerol-3-phosphate ↑inositol-1-phosphate ↓choline phosphate
Hydrolysis of Triglycerides	↑glycerol ↑oleoylglycerol ↑1-palmitoylglycerol	↑1-myristoglycerol ↑1-palmitoylglycerol ↑1-stearoylglycerol
Cholesterol Synthesis	↑7-dehydrocholesterol	↓7-dehydrocholesterol
Eicosanoid Precursor		↑linolenate (α or γ) ↑linoleate ↑dihomolinolenate
Lipid Turnover	↑2-oleoylglycerophosphoinositol ↑2-stearoylglycerophosphocholine	↑2-oleoylglycerophosphoinositol ↑2-stearoylglycerophosphocholine ↑1-palmitoylglycerophosphoinositol

D)

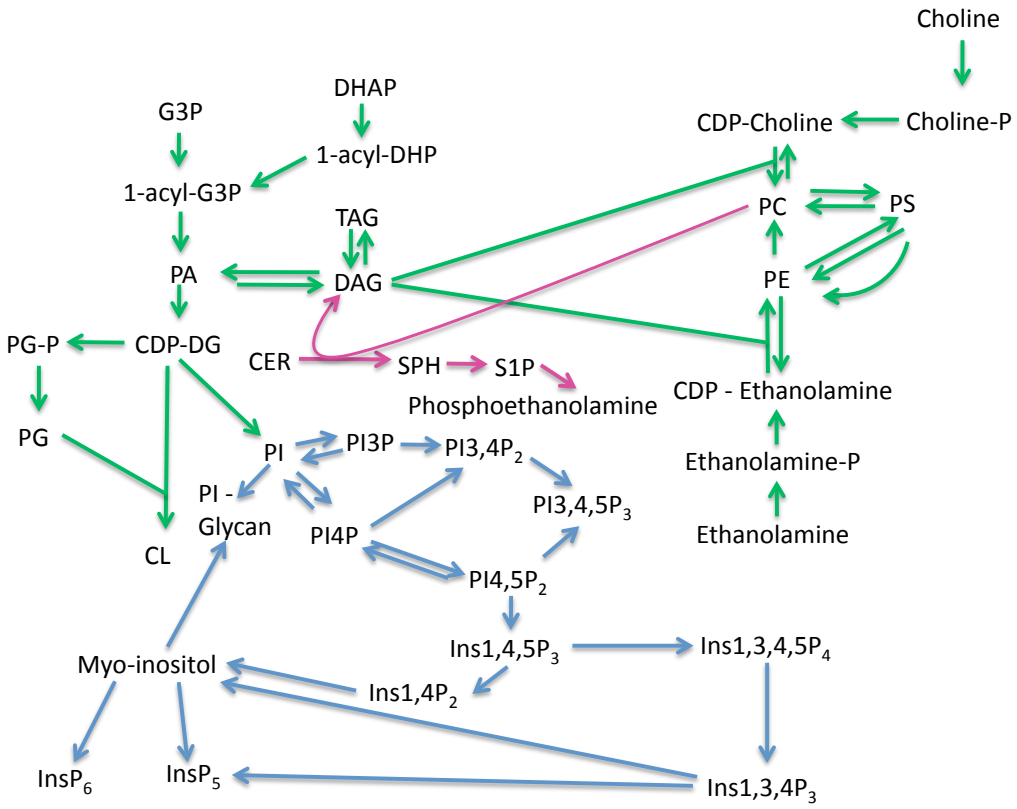
Choline
DHAP
G3P
CDP-Choline
Choline-P
1-acyl-DHP
1-acyl-G3P
PC
PS
TAG
PA
DAG
PE
PG-P
CDP-DG
CER
SPH
S1P
CDP - Ethanolamine
Phosphoethanolamine
PG
PI
PI3P
PI3,4P2
Ethanolamine-P
PI -
Glycan
PI3,4,5P3
PI4P
Ethanolamine
CL
PI4,5P2
Ins1,4,5P3
Ins1,3,4,5P4
Myo-inositol
Ins1,4P2
InsP6
InsP5
Ins1,3,4P3

E)

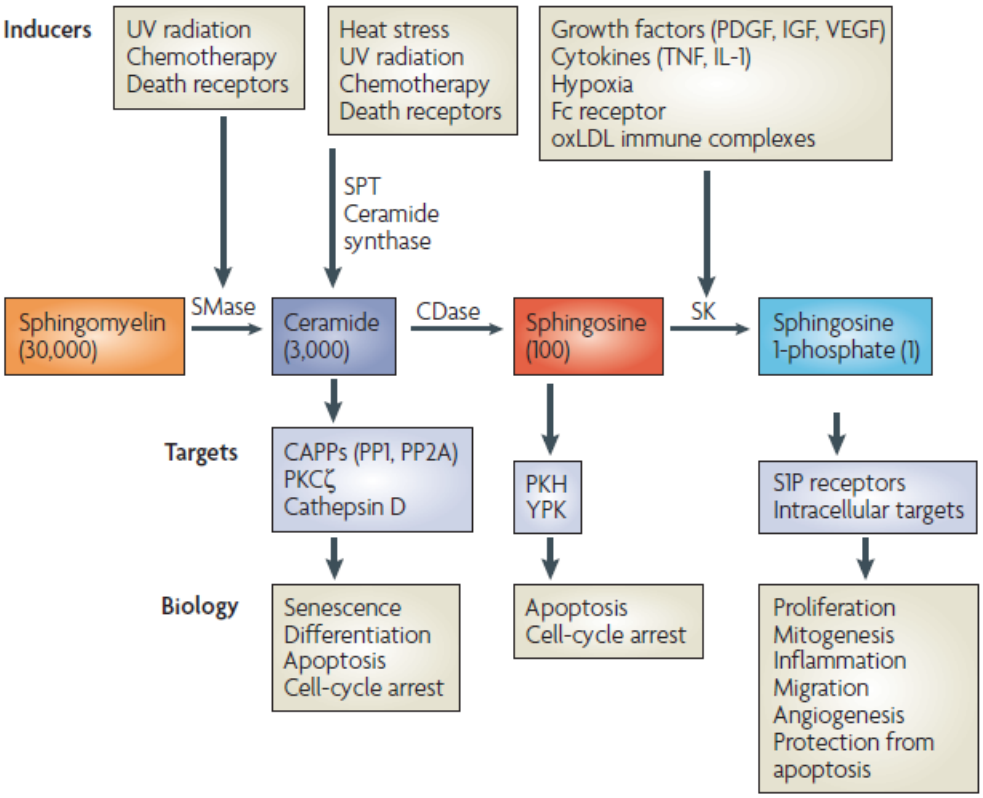
Inducers
UV radiation
Chemotherapy
Death receptors
Heat stress
UV radiation
Chemotherapy
Death receptors
Growth factors (PDGF, IGF, VEGF)
Cytokines (TNF, IL-1)
Hypoxia
Fc receptor
oxLDL immune complexes
SPT
Ceramide
synthase
Sphingomyelin
(30,000)
SMase
Ceramide
(3,000)
CDase
Sphingosine
(100)
SK
Sphingosine
1-phosphate (1)
Targets
CAPPs (PP1, PP2A)
PKCζ
Cathepsin D
PKH
YPK
S1P receptors
Intracellular targets
Biology
Senescence
Differentiation
Apoptosis
Cell-cycle arrest
Apoptosis
Cell-cycle arrest
Proliferation
Mitogenesis
Inflammation
Migration
Angiogenesis
Protection from
apoptosis

F)

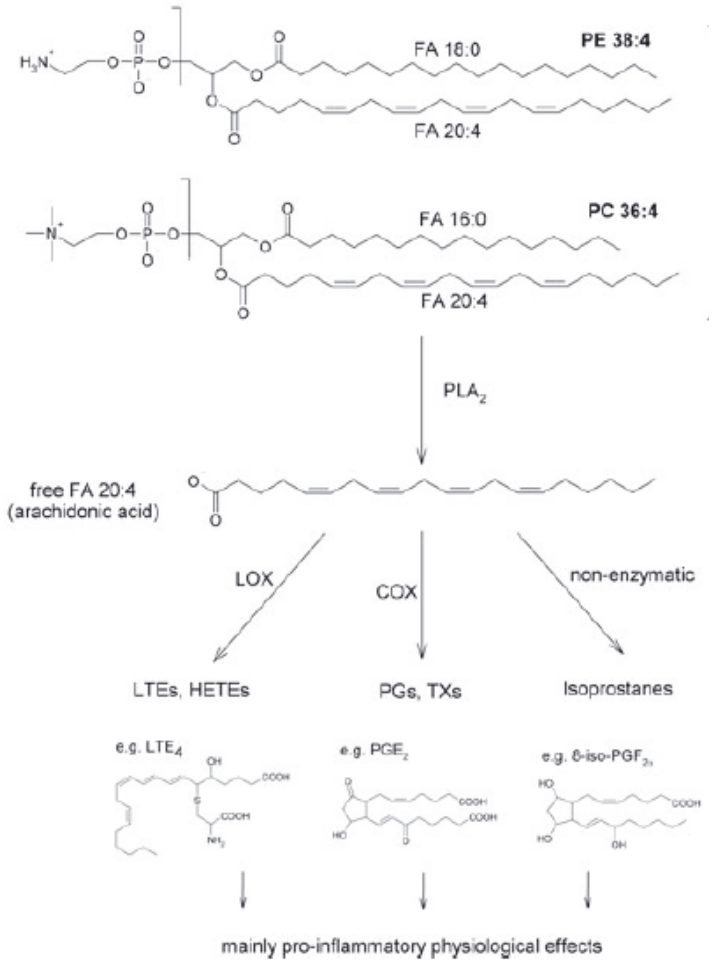

Figure 5.4: Alterations to Lipid Metabolism A) Lipid Metabolism Data (n=6) B) Statistical Significance within Lipid Metabolism Pathway organized by the dose the change was seen in and whether the change in the metabolite is statistically significant or almost statistically significant (0.05<p>0.1). C) Alterations in signaling catagorized by function D) GPL synthesis pathway Ddagram which shows the synthesis of the major membrane structural and signaling lipids [Adapted from 7, 11] E) Ceramide pathway and outcome diagram which shows the possible changes in signaling that may occur as a result of the increase in phosphoethanolamine seen in fullerene exposure. [8] F) Eicosanoid production by lipid metabolism [9].

References

[1] Fulda, S; Gorman, A. M.; Hori, O.; Samali, A. Cellular Stress Responses: Cell Survival and Cell Death. *Int J of Cell Bio.* **2010**: 214074-97; 2010.

[2] Vander Heiden, M. G.; Lunt, S. Y.; Dayton, T. L.; Fiske, B. P.; Israelsen, W. J.; Mattaini, K. R.; Vokes, N. I.; Stephanopoulos, G.; Cantley, L. C.; Metallo, C. M.; Locasale, J. W. Metabolic Pathway Alterations that Support Cell Proliferation. *Cold Spring Harb Symp Quant Biol.* **76**: 325-334; 2011

[3] Zhao, X.; Striolo, A; Cummings, P. T. C_{60} Binds to and Deforms Nucleotides. *Biophysical Journal.* **89**: 3856-3862: 2005.

[4] Xu, X; Wang, X; Li, Y; Yang, L. A large-scale association study for nanoparticle C60 uncovers mechanisms of nanotoxicity disrupting the native conformations of DNA/RNA. *Nucleic Acids Research.* **40 (16)**: 7622-7632; 2012.

[5] Hellsten, Y.; Svensson, M.; Sjodin, B.; Smith, S.; Christensen, A.; Richter, E. A.; Bangbo, J. Allantoin Formation and Urate and Glutathione Exchange in Human Muscle During Submaximal Exercise. *Free Radical Bio Med.* **31 (11)**: 1313-1322; 2001.

[6] Becker, B. F. Towards the Physiological Function of Uric Acid. *Free Radical Bio Med* .**14**: 615-631; 1993.

[7] Hermansson, M.; Hokynar, K.; Somerharju, P. Mechanisms of glycerophospholipid homeostasis in mammalian cells. *Prog Lipid Res.* **50**: 240-257; 2011.

[8] Hannun, Y. A.; Obeid, L. M. Principles of bioactive lipid signaling: lessons from sphingolipids. *Nature.* **9:** 139- 150; 2008.

[9] Ecker, J. Profiling Eicosanoids and Phospholipids using LC- MS/MS: Principles and Recent Applications. *J Sep Sci.* **35**: 1227-1235; 2012.

[10] Galli, C.; Marangoni, F.; Galella, G. Modulation of Lipid Derived mediators by Polyunsatureated Fatty Acids. *Prostag Leukotr Ess.* **48**: 51-55; 1993.

[11] Downes, C. P.; Macphee, C. H. Myo-Inositol: metabolites as cellular signals. *Eur J Biochem.* **193**: 1-18; 1990.

Chapter VI

Conclusion

Throughout the literature there are studies of fullerenes in multiple cell lines, most commonly C6 glioma, fibrosarcoma, and keratinocytes [1, 2, 3]. In these studies the fullerenes have been dissolved in THF, dissolved by solvent exchange utilizing THF, or dissolved in water via sonication for 4 weeks [1, 2, 3, 4]. Perhaps the most interesting of these studies compared the results of fullerenes dissolved by the solvent exchange credited to Fortner et al. (2005) and fullerenes dissolved via stirring in water for 4 weeks [5]. The comparison by Markovic et al. (2007) showed that residual THF may confound the cytotoxicity testing of fullerenes dissolved via the Fornter et al. (2005) method and certainly in the previous papers that utilized previous solvent to water methods [2, 5].

The method used to prepare fullerenes in the current study employed THF to water exchange with the additional wash steps that were shown to eliminate the harmful breakdown products of THF by Spohn et al. (2009) method that has been shown to eliminate to the limits of detection all known by-products [6]. Another notable difference between the current study and those available in the literature is that the current study uses vehicle controls that contain the highest amount of water found in the largest concentration of fullerenes received by cells in culture. In contrast, most of the literature report control cells that are untreated.

Macrophages are the specialized immune cells utilized by the body to defend itself against foreign materials or bacteria. These specialized cells are able to phagocytose the foreign materials and attempt to destroy them with bursts of ROS generated in the vicinity of and within the endocytotic vesicles. The toxicity of fullerenes to immune cells has major health, hazard identification and risk assessment implications for the future use of fullerenes as a drug delivery device due to the proclivity of nanomaterials to coalesce into sizes that are readily recognized by immune cells. This study addresses the ability of immune cells to respond to the presence of fullerenes and probes the ability of aggregates to gain access to important intracellular compartments.

Cells have three major intracellular compartments: the plasma membrane, the cyotsol (with its own subdivisions of the smooth/rough endoplasmic reticulum, mitochondria, Golgi body, cytoskeleton, etc., that form a complex hydrogel), and the nucleus. The nucleus can be considered to have two compartments since the nuclear membrane is very similar in structure to the lipid membrane. Each compartment has unique characteristics that influence the ability of nanomaterials to interact within them.

The lipid membrane is composed of hydrophilic heads that make direct contact with the more hydrophilic extracellular space and the cytosol whereas the hydrophobic tails are protected within the hydrophobic core of membrane. The nuclear membrane is similar with lipid heads contacting the hydrophilic cytosol and the nuclear space while the hydrophobic tails are inside the membrane core. The phospholipids in both the plasma membrane and the nuclear membrane maintain the structure of the membranes and are utilized for cellular signaling. In phagocytic cells, such as immune cells, the plasma membrane is able to reorganize

foreign materials and engulf them, whereas the nuclear membrane contains pores that allow entry of materials from the cytosol. The ability of nanomaterials to interact with the various components of the plasma and nuclear membrane- and to potentially stimulate unscheduled secondary signaling cascades- may be (in part) dictated by the hydrophobic or hydrophilic characteristics of the nanomaterial.

In their native state, C_{60} fullerenes are highly hydrophobic. Therefore, they may interact directly with the hydrophobic tails at the core of the lipid membrane. The results of this study show that the fullerene aggregates appear to decrease in size as they near the plasma membrane and are able to reside in the membrane space as determined by freeze fracture-TEM. Unpublished computational studies conducted by Paolo Elvati showed that while small aggregates appear to diffuse through the plasma membrane larger aggregates tend to insert into the membrane and are stabilized [26].

TEM imaging showed membrane bound vesicles containing fullerene aggregates and inhibition studies revealed that fullerene aggregates are endocytosed by the cell via clathrin mediated endocytosis and caveolae mediated endocytosis. In addition, fullerenes were found unbound in the cytosol. This may be due to an ability to move through the plasma membrane or through the lipid membrane surrounding the vesicle after endocytosis, which would allow the fullerenes access to the cytosolic components, and potentially result in cellular damage. Other nanomaterials, e.g., silver nanoparticles, utilize scavenger receptors to gain entry into the cell. This method of entry results in entry of nanoparticles unbound by vesicles to the cytsolic compartment [21]. Due to the observation of unbound aggregates in the cytosolic compartment, additional studies should focus on the role of scavenger receptors like MARCO in

permitting fullerenes not contained within a biological membrane to gain access to the cytosol. Additional experiments should attempt to quantify the fraction of the extracellular particulate load that gains access to the cytosol through diffusion. Appropriate use of combinations of pharmacological inhibitors of endocytosis such as those used in this thesis, as well as inhibitors of scavenger receptors, will provide a comprehensive picture of the degree to which transmembrane diffusion plays a major role. Unfortunately, due to the potency of of these agents, it may not be possible to stop one hundred percent of all endocytosis and scavenger receptor related uptake and this may bias the results obtained in these studies. Moreover, if diffusion through the membrane is not a major contributor to intracellular particle loads, it may be difficult to visualize/quantify the number, localization and concentration of aggregates with the fluorescently labeled antibodies that sufficiently differentiate the aggregate from any background cellular/tissue fluorescence.

The data collected in this study showed, in addition to interactions with the plasma membrane, fullerenes also interact with nuclear membranes. TEM images show fullerene aggregates passing through the nuclear membrane into the nucleus. The nuclear envelope consists of similar lipids that comprise the plasma membrane. Since it appears that the fullerenes are able to slip through the plasma membrane or through the lipids comprising the endocytotic vesicles, it is logical to consider that this may be the method of entry into the nucleus. The fullerene aggregates may also be entering the nucleus through nuclear pores. However, nuclear pores are 30-40 nm in size, which is smaller than the average aggregate size determined via the Nanosight and Zetasizer [7] (Figure 6.2). It is possible that, as seen in the

freeze fracture images, the aggregate size could decrease as it approaches the membrane. In either case, future studies need to be conducted to determine the exact route of entry.

Regardless of the route of entry, TEM images in this study clearly show fullerene aggregates entering the nucleus. The entry of the fullerenes into the nucleus raises the question of direct fullerene interactions with DNA and its outcome in immune cells. Computational studies discussed in Chapter V have shown that non-aggregated fullerenes are able to interact with the minor grooves of double stranded DNA and force the strands apart. Additionally, these computational studies showed that an individual fullerene would be able to bind to single stranded DNA and distort the nucleotides [8, 9]. This study assessed changes to nucleotide catabolism. At 4 μg/mL fullerene exposure, there was a statistically significant increase in CMP, adenine, urate, and allantoin. As previously discussed the increase in urate and allantoin indicates that oxidative stress may potentially be occurring as nucleotide catabolism of xanthine to urate, an antioxidant, is increased upon exposure to C_{60} fullerenes. These metabolites cannot be recycled and depletes ATP in the system. However, there were also non-statistically significant increases in AMP, uridine, cytidine, AMP and GMP that are indicative of increased nucleotide catabolism when the pathway is looked at as a whole. It is possible that fullerenes are disrupting DNA strands, which may result in the increase in catabolism seen in this study; however, future studies to confirm the exact role of C_{60} fullerene's interaction with DNA and DNA damage should be performed.

The decrease in cellular proliferation seen in RAW 264.7 macrophages could also be linked to potential DNA damage. Quiescence is a regulated growth arrest. This mechanism is utilized by the cell in unfavorable situations, such as disregulated metabolism or in cells with

DNA damage to remove the cell from the normal cell cycle. Quiescence is a reversible alteration to the normal cycle of the cell [10, 11]. In this study it was determined that exposed cells have altered metabolism pathways as well as indirect signs that DNA damage may have occurred; therefore a future direction may be to determine if the cells enter a state of quiescence or senescence. RAW 264.7 cells as previously discussed are an appropriate cell line for most experiments; however, because they have been immortalized they are not a proper cell line to test the occurrence of senescence because immortalization results in altered cellular aging profiles. In future studies, primary monocytes may need to be utilized to look at senescence as an endpoint.

At 24 hours the cell is responding to the stress of fullerene exposure by utilizing repair options for DNA damage and oxidative stress. Increase in production of taurine, a radical scavenger, urate, an antioxidant, as well as a mild change in GSH:GSSG ratio is indicative of potential oxidative stress within the cell; however, direct assays for these endpoints must be completed in the future to determine that these endpoints are occurring at 24 hours. Altered lipid pathways indicate that ceramide pathways, which are known for making cell survival or death decisions, have altered metabolism as well. In addition, altered proliferation was seen in RAW 264.7 macrophages exposed to 1 and 4 μg/mL fullerenes. This altered proliferation could result from the alterations in metabolism of the ceramide pathway or potentially utilized DNA damage repair mechanisms.

The cytosol contains cellular organelles and is the site of protein and nucleotide synthesis. The ability of fullerene aggregates to remain in the cytosol unbound by vesicles requires further investigation to determine whether or not fullerene aggregates or free

fullerenes (that as yet are difficult to track in solution) are able to have direct interactions with proteins and nucleotides. Work completed as part of this thesis elucidated alterations in nucleotide catabolism, glutathione synthesis, and lipid metabolism upon fullerene exposure of RAW 264.7 immortalized macrophages to C_{60} fullerenes at 24 hours.

Nontargeted metabolic studies were utilized in this thesis to observe changes in the glutathione synthesis, nucleotide catabolism, and lipid synthesis pathways. Nontargeted metabolic studies result in the ability to amass large sets of data on biological alterations via comparison of ionized molecules of biological origin as determined by an accumulated library of ion standards [22, 23]. Metabolomics studies that are nontargeted are only able to quantitate the amount of metabolite relative to control samples; however, alterations in fold change seen in metabolic studies have been validated by independent studies in the literature analyzing the metabolites quantitatively. Sarcosine and adenosine exhibited fold changes in nontargeted metabolomics studies for prostate cancer and sickle cell disease respectively and quantitative measurment in biological fluids showed that the change was conserved as well as important in the role of the disease [24, 25].

In this study, relatively early metabolic changes found prior to the onset of cellular death leads to a conclusion that the final biochemical *decision* as to cellular survival or death at 24 hours is yet to occur (Figure 6.1). Li et al. (2008) suggests an oxidative stress paradigm that classifies the results of this study to be a mild cellular stress that may be repairable (Figure 1.2) [12]. Precursors to inflammatory eicosanoids can be seen in the lipid metabolism of linolenate, linoleate, and dihomolinolenate at non-significant but higher than normal levels ($0.05<p< 0.1$). Also, PCR arrays showed gene expression changes in chemokines and inflammatory cytokines

(MyD88, CX3CR1, IL10ra, CCL4) some of which would result in decreased inflammation and others that result in increased inflammation. The lack of inflammatory response suggests that the cell has yet to integrate the biochemical signals that determine whether the damage is irreparable at 24 hours; thus the exposure paradigm used in these studies should be considered as a mild cellular stressor. Consistent with these conclusions is the lack of evidence that the cells are in early or late apoptosis or undergoing necrosis. Future studies utilizing bioinformatic metabolic pathway analysis will be performed using the metabolic data in order to gain more insight to the metabolic alterations seen in this study. Moreover, future studies should include a quantitative analysis of GSH and GSSG as well as cysteine and cystine redox pairs to allow calculation of redox potential changes resulting from C_{60} fullerene exposure.

In the present study immune cells were represented by RAW 264.7 immortalized murine macrophages. This cell line has been utilized in the study of many other types of nanomaterials and the immune response elicited from the exposure of these cells to the nanomaterials [13, 14, 15, 16, 17, 18, 19]. The most relevant of these studies are that of Kovochich et al. (2009) that examined fullerenes using the solvent to water method with additional filtration steps by Fortner et al. (2005) [5, 19]. This study utilized a much higher dose of fullerenes, 20 µg/mL, and looked at earlier time points of 4 or 16 hours. Kovochich et al. (2009) showed increased hydrogen peroxide production at 4 hours, and increased intracellular and mitochondrial calcium concentrations as well as an increase in necrotic cells at 16 hours [19]. In comparison, the current study showed no signs of increased necrosis at 24 hours. This may be due to the difference in preparation method, but may be due to the more environmentally relevant lower dose of C_{60} fullerenes.

Another comparison of interest is multiwalled carbon nanotubes (MWCNT) and single walled carbon nanotubes (SWCNT) [18]. Comparing the current study of fullerenes to that of Di Girogio et al. (2011) allows an excellent comparison of the effect of shape on interactions with immune cells as both studies were conducted in RAW 264.7 cells [18]. MWCNT and SWCNT are rolled sheets of graphene that have large aspect ratios and vary in length. SWCNT are one sheet of graphene with a diameter of 1-2 nm while MWCNT are any number of rolled graphene sheets with a diameter between 2 and 100 nm depending on the amount of rolled sheets that comprise the nanotube [20]. Di Giorgio et al. (2011) showed that MWCNTs were endocytosed, able to escape the vesicles (as shown by vesicles that had been perforated), and able to interact with the nucleus. 5 hours and 24 hours exposure to MWCNT and SWCNT increased ROS production over controls; however, the level of ROS did not vary significantly between the two timepoints when the cells were exposed to 50 μg/mL MWCNT and SWCNT [18]. In this fullerene study, at 24 hours antioxidant and radical scavenging metabolites were increased, an indication of potentially increased oxidative stress in the cell. At 24 hours, their study showed that MWCNT and SWCNT were able to cause DNA damage at low and high concentrations respectively. Chromosomal defects and micronuclei formation were observed at 48 hours and at 72 hours [18]. At 24 hours in this fullerene study, there was increased nucleotide catabolism that may be an indication of DNA damage. Also, SWCNT showed signs of apoptosis at 50 μg/mL and MWCNT showed signs of necreosis and apoptosis at the same concentration at 24 hours. Signs of apoptosis were observed in SWCNT at 50 μg/mL and 72 hours as well [18]. This fullerene study showed no apoptosis or necrosis at 24 hours. The most marked decrease in cell proliferation was observed at high doses in both nanotubes but could be observed throughout

the 24-72 hour exposures [18]. This fullerene study showed a decrease in cell proliferation at 24 hours in 1 and 4 μg/mL. The comparison of the fullerenes to CNT elucidates the difference that aspect ratio makes in the cytotoxicity of nanomaterials. C_{60} fullerenes are composed of all carbons just like the MWCNT and SWCNTs, yet the MWCNT and SWCNT resulted in major DNA and chromosomal damage and ultimately in cell death suggesting that these nanomaterials are much more cytotoxic to the RAW 264.7 macrophages as compared to the C_{60} fullerenes. In the oxidative stress paradigm proposed by Li et al. (2008) the MWCNT and SWCNTs would likely fall into the category of cytotoxic tier 3 whereas the data in this fullerene study indicate that fullerenes would fall into tier 1 where damage repair was occurring rather than cellular death (Figure 1.2).

In summary, the findings reported in this thesis show that C_{60} fullerenes are able to reside in multiple comparments of the cell. They are able to enter the plasma membrane, reside free in the cytosol, and enter the nucleus. C_{60} fullerenes appear to be a mild cellular stressor at 24 hours. Exposure to fullerenes for 24 hours results in alterations to glutathione synthesis, DNA catabolism, and lipid synthesis in RAW 264.7 immortalized macrophages. The most sensitive target of C_{60} fullerenes is DNA, which resides in a cellular compartment to which the fullerenes have access. The aggregates of fullerenes unbound in the cytosol may potentially produce oxidative stress, which may result in injury to cellular components that also reside in the cytosol such as proteins. These alterations are not accompanied by signs of cell death, but are accompanied by a decrease in cellular proliferation, which is observed at 1 and 4 μg/mL C_{60} exposure. The decrease in cell proliferation may be a result of DNA damage or pathways

involved in cell survival or death decisions. At this 24 hour time point, the cell appears to have made no biochemical *decision* as to cellular survival or death.

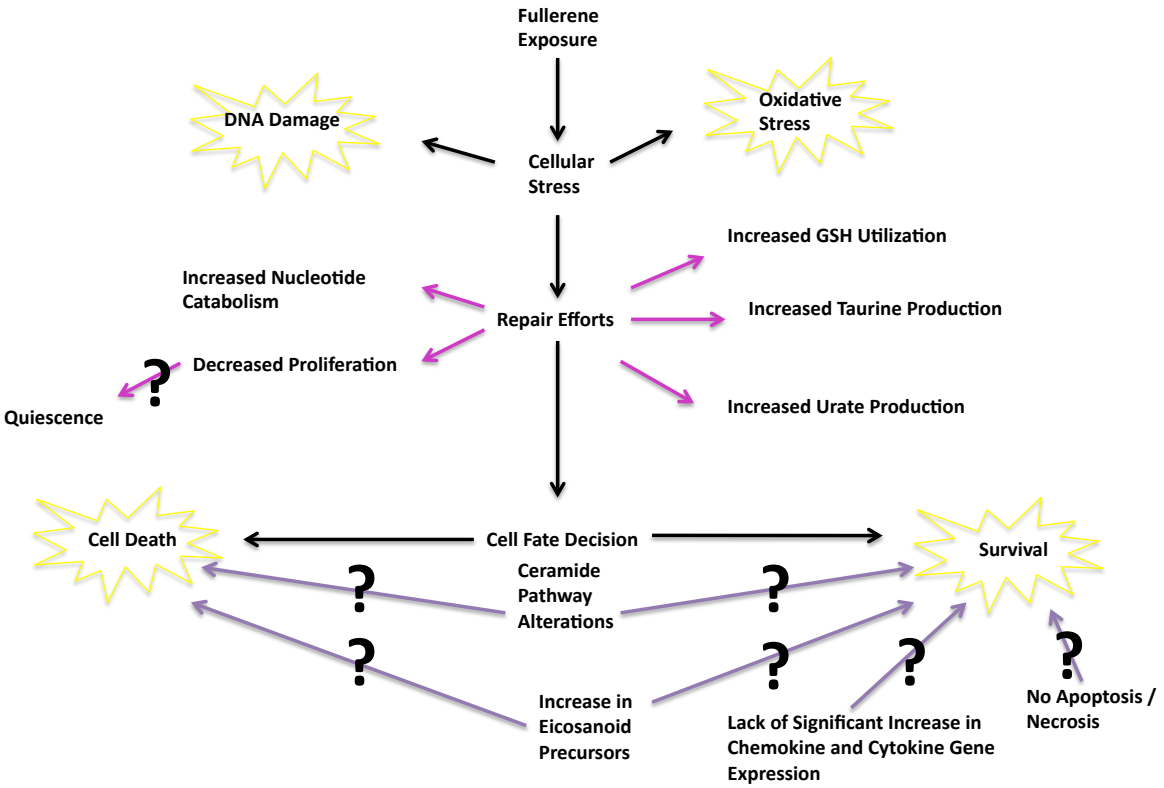

Figure 6.1: Fullerenes as a Cellular Stressor and Cellular Response: Exposure of RAW 264.7 immortalized macrophages to C_{60} fullerenes for 24 hours resulted in signs that the cell has increased the presence of repair mechanisms for oxidative stress (GSH utilization, taurine production, and urate production). Additionally decreased proliferation and increased nucleotide catabolism were observed which point to potential DNA damage. However, no apoptosis or necrosis were observed at 24 hours suggesting along with the increase in eicosanoid precursors and lack of significant inflammatory gene expression changes that there has not yet been a biochemical *decision* to cellular fate.

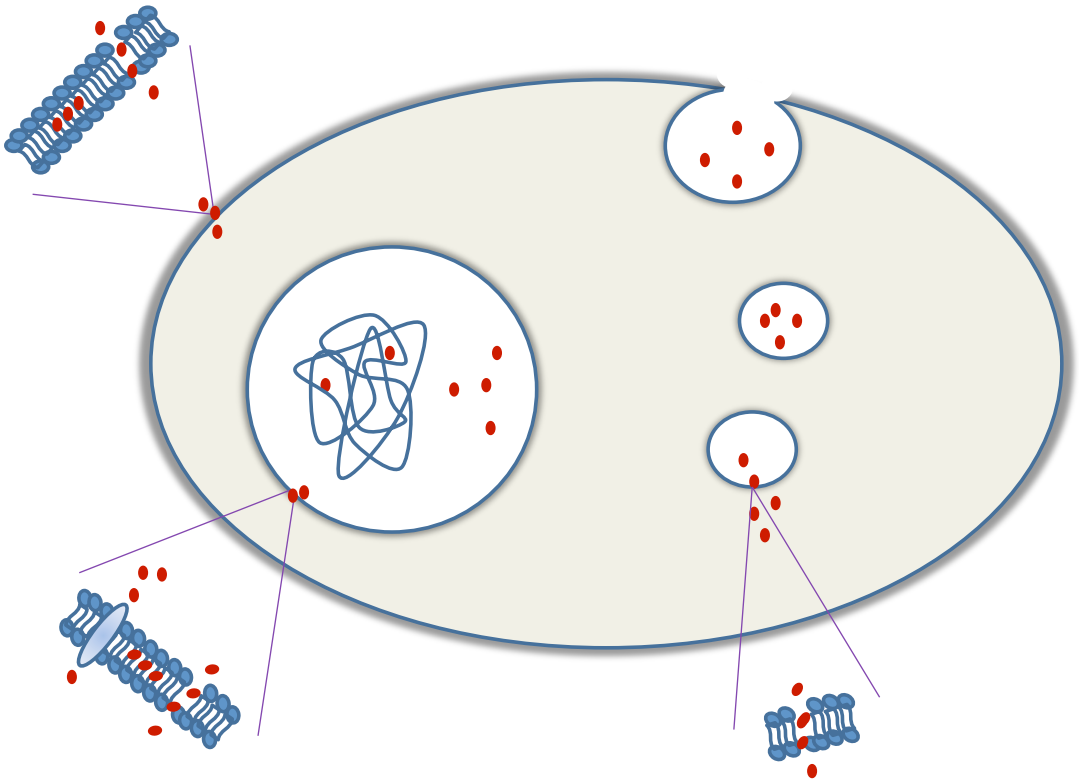

Figure 6.2: Diagram of C_{60} fullerene interactions in RAW 264.7 macrophages: This diagram shows the locations of fullerenes in the cell observed in this thesis and potential mechanisms by which the fullerenes entered the compartments: endocytosis, diffusion through the membrane (vesicle membrane or plasma membrane) that results in fullerene aggregates unbound by vesicles in the cytosol) and entry into the nucleus (by nuclear pore or diffusion through the nuclear membrane) with particles potentially interacting with the DNA. Also, in agreement with the freeze fracture TEM data, there are fullerenes in the membrane space.

References

[1] Sayes, C.M.; Fortner, J.D.; Guo, W.; Lyon, D.; Boyd, A.M.; Ausman, K.D.; Tao, Y.J.; Sitharaman, B.; Wilson, L.J.; Hughes, J.B.; West, J.L.; Colvin, V.L. The Differential Cytotoxicity of Water-Soluble Fullerenes. *Nano Lett.* **4(10)**: 1881-1887; 2004.

[2] Markovic, Z.; Todorovic-Markovic, B.; Kleut, D.; Nikolic, N.; Vranjes-Djuric, S.; Misirkic, M.; Vucicevic, L.; Janjetovic, K.; Isakovic, A.; Harhaji, L.; Babic-Stojic, B.; Dramicanin, M.; Trajkovic, V. The mechanism of cell-damaging reasctive oxygen generation by colloidal fullerenes. *Biomaterials.* **28**: 5437-5448; 2007.

[3] Isakovic, A.; Markovic, Z.; Tordorovic-Markovic, B.; Nikolic, N.; Vranjes-Djuric, S.; Mirkovic, M.; Dramicanin, M.; Harhaji, L.; Raicevic, N.; Nicolic, Z.; Trajkovic, V. Distinct Cytotoxic Mechanisms of Pristine versus Hydroxylated Fullerene. *Tox. Sci.* **91(1):** 173-183; 2006.

[4] Porter, E.P.; Muller, K.; Skepper, J.; Midgley, P.; Welland, Mark. Uptake of C60 by human monocyte macrophages, its localization and implications for toxicity: Studied by high resolution electron microscopy and electron tomography. *Acta Biomaterialia*. **2**: 409-419; 2006.

[5] Fortner, J.D.; Lyon, D.Y.; Sayes, C.M.; Boyd, A.M.; Falkner, J.C.; Hotze, E.M.; Alemany, L.B.; Tao, Y.J.; Guo, W.; Ausman, K.D.; Colvin, V.L.; Hughes, J.B. C60 in Water: Nanocrystal Formation and Microbial Response. *Environ. Sci. Technol*. **39:** 4307-4316; 2005.

[6] Spohn, P.; Hirsch, C.; Hasler, F.; Bruinink, A.; Krug, H.F.; Wick, P. C_{60} fullerene: A powerful antioxidant or a damaging agent? The importance of an in-depth material characterization prior to toxicity assays. *Environmental Pollution.* **157 (4)**:134-1139; 2009.

[7] Jang, H.; Ryoo, S-R.; Kostarelos, K.; Han, S. W.; Min, D-H. The effective nuclear delivery of doxorubicin from dextran-coated gold nanoparticles larger than nuclear pores. *Biomaterials.* **34**: 3503-3510; 2013.

[8] Xu, X; Wang, X; Li, Y; Yang, L. A large-scale association study for nanoparticle C60 uncovers mechanisms of nanotoxicity disrupting the native conformations of DNA/RNA. *Nucleic Acids Research.* **40 (16)**: 7622-7632; 2012.

[9] Zhao, X.; Striolo, A; Cummings, P. T. C_{60} Binds to and Deforms Nucleotides. *Biophysical Journal.* **89**: 3856-3862: 2005.

[10] Valcourt, J. R.; Lemons, J. M. S.; Haley, E. M.; Kojima, M.; Demuren, O. O.; Coller, H. A. Staying alive Metabolic adaptions to quiescence. *Cell Cycle*. **11(9)**: 1680-1696; 2012.

[11] Fulda, S; Gorman, A. M.; Hori, O.; Samali, A. Cellular Stress Responses: Cell Survival and Cell Death. *Int. J. of Cell Bio.* **2010**: 214074-97; 2010.

[12] Li, N.; Xia, T.; Nel, A. The role of oxidative stress in ambient particulate matter-induced lung diseases and its implications in the toxicity of engineered nanoparticles. *Free Radical Bio. Med.* **44**:1689-1699; 2008.

[13] Wang, W.; Luo, M.; Fu, Y.; Wang, S.; Efferth, T.; Zu,Y.Glycyrrhizic acid nanoparticles inhibit LPS-induced inflammatory mediators in 264.7 mouse macrophages compared with unprocessed glycyrrhizic acid. *Int. J. Nanomedicine.* **8:** 1377-83; 2013.

[14] Di Bucchianico, S.; Fabbrizi, M. R.; Misra, S. K.; Valsami-Jones, E.; Derhanu, D.; Reip, P.; Bergamaschi, E.; Migliore, L. Multiple cytotoxic and genotoxic effects induced in vitro by differently shaped copper oxide nanomaterials. *Mutagenesis*. **28(3)**: 287-99; 2013.

[15] Xia, W.; Song, H. M.; Wei, Q.; Wei, A. Differential response of macrophages to core-shell Fe3O4@Au nanoparticles and nanostars. *Nanoscale.* **4(22)**: 7143-8; 2012.

[16] Rehman, M. U.; Yoshihisa, Y.; Miyamoto, Y.; Shimizu, T. The anti-inflammatory effects of platinum particles on the lipopolysaccharide- induced inflammatory response in RAW 264.7 macrophages. *Inflamm. Res.* **61(11)**: 1177-85; 2012.

[17] Nishanth, R. P.; Jyotsna, R. G.; Schlager, J. J.; Hussain, S. M.; Reddanna, P. Inflammatory responses of RAW 264.7 macrophages upon exposure to nanoparticles: role of ROS NF-κB signaling pathway. *Nanotoxicology*. **5(4)**: 502-16; 2011.

[18] Di Giorgio, M. L.; Di Bucchianico, S.; Ragnelli, A. M.; Aimola, P.; Santucci, S.; Poma, A. Effects of single and multi walled carbon nanotubes on macrophages: Cyto and genotoxicity and electron microscopy. *Mutat. Res.* **722**: 20-31; 2011.

[19] Kovochich, M.; Espinasse, B.; Auffan, M.; Hotze, E. M.; Wessel, L.; Xia, T.; Nel, A. E.; Wiesner, M. R. Comparative toxicity of C_{60} aggregates toward mammalian cells: Role of tetrahydrofuran (THF) decomposition. *Environ. Sci*. *Technol.* **43**: 6378-6384; 2009.

[20] NIOSH. Occupational Exposure to Carbon Nanotubes and Nanofibers. *Current Intelligence Bulletin* **65**: 1-184; 2013.

[21] Singh, R. P.; Ramarao, P. Cellular uptake, intracellular trafficking and cytotoxicity of silver nanoparticles. *Toxicol. Lett.* **213:** 249-259; 2012.

[22] Evans, A. M.; DeHaven, C. D.; Barrett, T.; Mitchell, M.; Milgram, E. Integrated, Nontargeted Ultrahigh Performance Liquid Chromatography/Electrospray Ionization Tandem Mass Spectrometry Platform for the Identification and Rlative Quantification of the Small-Molecule Complement of Biological Systems. *Anal. Chem.* **81:** 6656-6667; 2009.

[23] Evan, A. M.; Mitchell, M. W.; Dai, H.; DeHaven, C. D. Categorizing Ion- Features in Liquid Chromatography/Mass Spectrometry Metabolomics Data. *Metabolomics.* **2 (3):** 1-8; 2012.

[24] Sreekumar, A.; Poisson, L. M.; Rajendiran, T. M.; Khan, A. P.; Cao, Q.; Yu, J.; Laxman, B.; Mehra, R.; Lonigro, R. J.; Li, Y.; Nyati, M. K.; Ahsan, A.; Kalyana-Sundaram, S.; Han, B.; Cao, X.; Byun, J.; Omenn, G. S.; Ghosh, D.; Pennathur, S.; Alexander, D. C.; Berger, A.; Shuster, J. R.; Wei, J. T.; Varambally, S., Beecher, C.; Chinnaiyan, A. M. Metabolomic profilesdelineate potential role for sarcosine in prostate cancer progression. *Nature Letters.* **457**:910- 915; 2009.

[25] Zhang, Y.; Dai, Y.; Wen, J.; Zhang, W.; Grenz, A.; Sun, H.; Tao, L.; Lu, G.; Alexander, D. C.; Milburn, M. V.; Carter-Dawson, L.; Lewis, D. E.; Zhang, W.; Eltzschig, H. K.; Kellems, R. E.; Blackburn, M. R.; Juneja, H. S.; Xia, Y. Detrimental effects of adenosine signaling in sickle cell disease. *Nature Medicine.* **17 (1):** 79-87. 2011.

[26] Elvati, P. Unpublished Data. Personal Conversation. 2012.